



Imię i nazwisko autora rozprawy: Agnieszka Rymarczyk  
Dyscyplina naukowa: Automatyka, elektronika, elektrotechnika i technologie kosmiczne

## **ROZPRAWA DOKTORSKA**

Tytuł rozprawy w języku polskim: Prognozowanie zdolności statku do dynamicznego pozycjonowania

Tytuł rozprawy w języku angielskim: Ship dynamic positioning capability prognosis

Promotor	Drugi promotor
<i>podpis</i>	<i>podpis</i>
Dr hab. Anna Witkowska	
Promotor pomocniczy	Kopromotor
<i>podpis</i>	<i>podpis</i>
Dr Inż. Tomasz Zubowicz	

## OŚWIADCZENIE

Autor rozprawy doktorskiej: Agnieszka Rymarczyk

Ja, niżej podpisana, oświadczam, iż jestem świadoma, że zgodnie z przepisem art. 27 ust. 1 i 2 ustawy z dnia 4 lutego 1994 r. o prawie autorskim i prawach pokrewnych (t.j. Dz.U. z 2021 poz. 1062), uczelnia może korzystać z mojej rozprawy doktorskiej zatytułowanej:

Prognozowanie zdolności statku do dynamicznego pozycjonowania  
do prowadzenia badań naukowych lub w celach dydaktycznych.<sup>1</sup>

Świadoma odpowiedzialności karnej z tytułu naruszenia przepisów ustawy z dnia 4 lutego 1994 r. o prawie autorskim i prawach pokrewnych i konsekwencji dyscyplinarnych określonych w ustawie Prawo o szkolnictwie wyższym i nauce (Dz.U.2021.478 t.j.), a także odpowiedzialności cywilno-prawnej oświadczam, że przedkładana rozprawa doktorska została napisana przeze mnie samodzielnie.

Oświadczam, że treść rozprawy opracowana została na podstawie wyników badań prowadzonych pod kierunkiem i w ścisłej współpracy z promotorem Dr hab. Anną Witkowską, promotorem pomocniczym Dr Inż. Tomaszem Zubowiczem.

Niniejsza rozprawa doktorska nie była wcześniej podstawą żadnej innej urzędowej procedury związanej z nadaniem stopnia doktora.

Wszystkie informacje umieszczone w ww. rozprawie uzyskane ze źródeł pisanych i elektronicznych, zostały udokumentowane w wykazie literatury odpowiednimi odnośnikami, zgodnie z przepisem art. 34 ustawy o prawie autorskim i prawach pokrewnych.

Potwierdzam zgodność niniejszej wersji pracy doktorskiej z załączoną wersją elektroniczną.

Gdańsk, dnia .....  
*podpis doktoranta*

Ja, niżej podpisana, wyrażam zgodę na umieszczenie ww. rozprawy doktorskiej w wersji elektronicznej w otwartym, cyfrowym repozytorium instytucjonalnym Politechniki Gdańskiej.

Gdańsk, dnia .....  
*podpis doktoranta*

---

<sup>1</sup> Art. 27. 1. Instytucje oświatowe oraz podmioty, o których mowa w art. 7 ust. 1 pkt 1, 2 i 4–8 ustawy z dnia 20 lipca 2018 r. – Prawo o szkolnictwie wyższym i nauce, mogą na potrzeby zilustrowania treści przekazywanych w celach dydaktycznych lub w celu prowadzenia działalności naukowej korzystać z rozpowszechnionych utworów w oryginale i w tłumaczeniu oraz zwielokrotniać w tym celu rozpowszechnione drobne utwory lub fragmenty większych utworów.  
2. W przypadku publicznego udostępniania utworów w taki sposób, aby każdy mógł mieć do nich dostęp w miejscu i czasie przez siebie wybranym korzystanie, o którym mowa w ust. 1, jest dozwolone wyłącznie dla ograniczonego kręgu osób uczących się, nauczających lub prowadzących badania naukowe, zidentyfikowanych przez podmioty wymienione w ust. 1.

## OPIS ROZPRAWY DOKTORSKIEJ

**Autor rozprawy doktorskiej:** Agnieszka Rymarczyk

**Tytuł rozprawy doktorskiej w języku polskim:** Prognozowanie zdolności statku do dynamicznego pozycjonowania

**Tytuł rozprawy w języku angielskim:** Ship dynamic positioning capability prognosis

**Język rozprawy doktorskiej:** Angielski

**Promotor rozprawy doktorskiej:** Dr hab. Anna Witkowska

**Promotor pomocniczy rozprawy doktorskiej:** Dr Inż. Tomasz Zubowicz

**Data obrony:**

**Słowa kluczowe rozprawy doktorskiej w języku polskim:** dynamiczne pozycjonowanie, alokacja naporów, identyfikacja statku, symulator dynamicznego pozycjonowania

**Słowa kluczowe rozprawy doktorskiej w języku angielskim:** dynamic positioning, thrust allocation, ship identification, dynamic positioning simulator

**Streszczenie rozprawy w języku polskim:**

Badania przedstawione w niniejszej rozprawie doktorskiej dotyczą zagadnień związanych z inżynierią systemów sterowania, koncentrując się na projektowaniu i analizie struktur sterowania oraz algorytmów istotnych dla stabilizacji systemów dynamicznych, przeciwdziałających zakłóceniom zewnętrznym. Badania te w szczególności dotyczą projektowania systemu dynamicznego pozycjonowania (DP) statku oraz oceny zdolności statku do DP.

Efektem pracy jest prototyp systemu wspomagania decyzji dla inżyniera projektanta, który obejmuje algorytm alokacji naporów, parametryczną identyfikację modeli matematycznych kadłuba i pędników oraz projekt systemu dynamicznego pozycjonowania. Wdrożenie wszystkich tych komponentów do narzędzia oceny zdolności statku do DP umożliwia prognozowanie w szerokim zakresie warunków pogodowych, zgodnie z wymaganiami towarzystwa klasyfikacyjnego DNV.

Wykorzystując wyniki badań na fizycznym modelu statku Multi Service Vessel (MSV) w skali 1:36 dla prądu, fali krótkiej i długiej, przeprowadzono walidację symulatora DP dla tych przypadków. Następnie, określono współczynnik dynamiczny uwzględniający dodatkową dynamikę w celu korekty metod statycznych w oparciu o symulacje numeryczne. Zastosowanie współczynnika dynamicznego umożliwia dokładniejsze prognozowanie na podstawie metod statycznych wspierając decyzje na wczesnym etapie projektowania.

**Streszczenie rozprawy w języku angielskim:**

The research presented in this dissertation addresses issues related to control systems engineering, focusing on the design and analysis of control structures and algorithms relevant to stabilizing dynamic systems in presence of external disturbances. In particular, the research concerns the design of a ship's dynamic positioning (DP) system and the evaluation of the ship's DP capability.

The study results in a prototype of a decision support system for the design engineer, which includes a thrust allocation algorithm, parametric identification of mathematical models of the hull and thrusters, and design of the dynamic positioning system. Implementing all of these components into a DP capability assessment tool allows a ship's DP capability prognosis in a wide range of weather conditions, and according to the DNV classification society.

Using the results of experiments on a physical model of a Multi Service Vessel (MSV) in scale 1:36, for current, short wave and long wave, the DP simulator was validated for these cases. Subsequently, a dynamic factor was determined to account for additional dynamics and for correction of static methods based on numerical simulations. The application of the dynamic factor allows more accurate predictions based on static methods supporting decisions at an early design stage.

# Ship dynamic positioning capability prognosis

*For Engineers, like my beloved husband*

# Contents

<b>1</b>	<b>Introduction</b>	<b>18</b>
1.1	Background . . . . .	19
1.2	Problem statement . . . . .	28
1.3	Purpose and significance of the study . . . . .	31
1.4	Thesis and research objectives . . . . .	32
1.5	Methods, theoretical framework and scope . . . . .	34
1.6	Assumptions and limitations . . . . .	36
1.7	Work outline . . . . .	40
<b>2</b>	<b>Dynamic positioning capability assessment</b>	<b>41</b>
2.1	DP capability levels . . . . .	41
2.2	Static DP capability calculation . . . . .	46
2.3	Dynamic DP capability analysis . . . . .	51
2.4	Thrust allocation . . . . .	52
2.5	Collation of different methods of DP capability assessment . .	53
<b>3</b>	<b>Modeling and identification of DP ship</b>	<b>55</b>
3.1	Physical model of a ship . . . . .	56
3.2	Mathematical model of a ship . . . . .	58
3.2.1	Hull utility model . . . . .	61
3.2.2	Thruster utility model . . . . .	63
3.3	Ship mathematical model numerical identification . . . . .	66
3.3.1	Numerical tools . . . . .	69
3.3.2	Hull model parametric identification . . . . .	69
3.3.3	Thrusters models parametrical identification . . . . .	76
3.4	Modeling disturbances . . . . .	78
3.4.1	Current . . . . .	79
3.4.2	Wind . . . . .	79

3.4.3	Waves . . . . .	80
<b>4</b>	<b>Static DP capability calculation</b>	<b>84</b>
4.1	Optimal thrust allocation . . . . .	84
4.2	An approach based on quadratic programming . . . . .	85
4.2.1	Decision variables . . . . .	86
4.2.2	Inequality constraints . . . . .	86
4.2.3	Equality Constraints . . . . .	90
4.2.4	Objective function . . . . .	91
4.2.5	Optimization task decomposition . . . . .	91
4.2.6	TA algorithm . . . . .	92
4.2.7	Case study . . . . .	95
4.3	An approach based on nonlinear programming . . . . .	96
4.3.1	Decision variables . . . . .	97
4.3.2	Constraints . . . . .	97
4.3.3	Objective functions . . . . .	98
4.3.4	Optimization task decomposition . . . . .	98
4.3.5	TA algorithm . . . . .	98
4.4	Results . . . . .	100
4.5	Summary . . . . .	104
<b>5</b>	<b>Dynamic DP capability analysis</b>	<b>105</b>
5.1	DPS components . . . . .	106
5.2	State observer . . . . .	107
5.3	DP controller . . . . .	110
5.3.1	PID . . . . .	111
5.3.2	Model Predictive Control . . . . .	111
5.4	Thrust allocation . . . . .	113
<b>6</b>	<b>Numerical experiments</b>	<b>115</b>
6.1	Methods and tools . . . . .	115
6.2	Results and discussion . . . . .	117
6.3	Summary . . . . .	125
<b>7</b>	<b>Physical model experiments</b>	<b>126</b>
7.1	Setup . . . . .	126
7.2	DPS incorporation . . . . .	129
7.3	Results and discussion . . . . .	130

7.4	Summary . . . . .	136
<b>8</b>	<b>Comparative analysis of numerical and physical experiments</b>	<b>137</b>
8.1	Quality indicators . . . . .	139
8.2	Summary and discussion . . . . .	146
<b>9</b>	<b>Conclusions and future research</b>	<b>150</b>
9.1	Comparative analyses . . . . .	150
9.2	Summary and conclusions . . . . .	151
9.3	Recommendation for future research . . . . .	155
<b>A</b>	<b>Data of analyzed ships</b>	<b>156</b>
<b>B</b>	<b>Numerical identification of thrusters losses</b>	<b>164</b>
<b>C</b>	<b>Experimental setup specification and results</b>	<b>169</b>
C.1	Specification of MSV physical model DPS . . . . .	169
C.2	Remaining results . . . . .	175

# List of Figures

1.1	DP capability prognosis impact on the ship design . . . . .	21
1.2	Problem of overactuated system . . . . .	23
1.3	DPS concept . . . . .	26
1.4	Concept of decision support system in a typical design office .	29
2.1	Wave force models comparison at sway motion for level 1 and 2	43
2.2	DP ship footprint . . . . .	43
2.3	Coordinate system (x, y), environmental angle and thrusters orientation convention . . . . .	45
2.4	Exemplary DP capability plot . . . . .	46
2.5	Environmental forces with DNV level 1 method - exemplary case . . . . .	48
2.6	Thrust regions of different types of thrusters . . . . .	50
3.1	MSV model in scale 1:36 . . . . .	57
3.2	MSV model in scale 1:36 - azimuth thrusters . . . . .	57
3.3	MSV model in scale 1:36 - tunnel thrusters . . . . .	57
3.4	Concept of a ship hull model as mass-spring-damper system .	59
3.5	Concept of mass distribution . . . . .	62
3.6	Added mass meaning concept . . . . .	62
3.7	Concept of damping model . . . . .	63
3.8	Exemplary thrusters models in scale 1:36 . . . . .	65
3.9	Thruster - hull interactions concept . . . . .	65
3.10	Thruster - thruster interactions concept . . . . .	66
3.11	Mesning of the hull surface of MSV in <i>Ansys Aqwa</i> . . . . .	70
3.12	Added mass resulting from the potential flow numerical simulation compared to the values resulting from the experiments	71
3.13	Computational mesh on the free surface in surge, sway and yaw	72

3.14	Numerical identification of viscous damping in yaw motion by CFD simulation . . . . .	73
3.15	Damping force and moment resulting from the numerical simulation with fitted model in comparison to the model of parameters determined by experiment . . . . .	75
3.16	Numerical mesh on the MSV ship azimuth thruster . . . . .	77
3.17	Results of bollard pull tests . . . . .	78
3.18	Numerical results error relative to the experimental results . .	78
3.19	Wave loads at $H_S = 4$ cm, in scale 1:36 . . . . .	83
4.1	Linearization of a typical azimuth thruster saturation region .	87
4.2	Definition of a $j$ th polygon, Eq. 4.3, within zone III, IV . . . .	88
4.3	Definition of $j$ th polygon, Eq. (4.4) within zone I, II . . . . .	89
4.4	Linearization of the propeller with rudder constraints . . . . .	90
4.5	Flowchart of DP capability assessment program with QP algorithm utilization . . . . .	94
4.6	Thrusters layout - exemplary case . . . . .	95
4.7	Flowchart of DP capability assessment program with NSGAII algorithm utilization . . . . .	99
4.8	DP capability plots of a RV with QP and NSGAII algorithms	101
4.9	Power utilization in DP operations of a RV with QP and NS-GAII algorithms . . . . .	101
4.10	Thrust allocation of RV (QP) . . . . .	102
4.11	Thrust allocation of RV (NSGAII) . . . . .	102
4.12	DP capability plots of a RV for intact and failure cases . . .	103
4.13	Power utilization in DP operations of RV for intact and failure cases for a DP number 3 . . . . .	104
5.1	DP simulator main components . . . . .	105
5.2	DP Control system concept . . . . .	106
6.1	Introduction of the tool . . . . .	116
6.2	Ship model footprint: current . . . . .	119
6.3	Thrusters settings: current . . . . .	120
6.4	Ship model footprint: short waves . . . . .	121
6.5	Thrusters settings: short waves . . . . .	122
6.6	Ship model footprint: long waves . . . . .	123
6.7	Thrusters settings: long waves . . . . .	124

7.1	The test stand carriage at the offshore towing tank in CTO S.A.	127
7.2	The flap type wave maker at the offshore towing tank in CTO S.A. . . . .	128
7.3	Theoretical wave spectra for short and long wave - model scale	129
7.4	Footprint of the physical ship model in dynamic positioning under current conditions - test 21 . . . . .	133
7.5	Revolutions of the propellers recorded during test 21 . . . . .	133
7.6	Footprint of the physical ship model in dynamic positioning under short wave conditions - test 29 . . . . .	134
7.7	Revolutions of the propellers recorded during test 29 . . . . .	134
7.8	Footprint of the physical ship model in dynamic positioning under long wave condition - test 30 . . . . .	135
7.9	Revolutions of the propellers recorded during test 30 . . . . .	135
8.1	All methods: Current . . . . .	144
8.2	All methods: Short wave . . . . .	145
8.3	All methods: Long wave . . . . .	146
9.1	Decision support system prototype . . . . .	154
A.1	Vessel geometrical parameters for wave drift. $X_{Los}$ has a neg- ative value in this case . . . . .	157
A.2	Bow <sub>angle</sub> definition . . . . .	158
A.3	Rescue Vessel thruster layout . . . . .	161
A.4	MSV ship thrusters layout . . . . .	163
B.1	Thruster efficiency depending on thruster direction . . . . .	165
B.2	Thruster interaction with the hull with numerical simulation as pressure distribution . . . . .	165
B.3	Thrust divination from its original set direction with numerical simulation . . . . .	166
B.4	Thruster interaction with another working thruster in numer- ical simulation as speed field . . . . .	167
B.5	Thrusters interaction with each other . . . . .	168
C.1	DP tests stand structure . . . . .	169
C.2	Control computer with ACS . . . . .	173
C.3	Ship physical model stern view - stern azimuth thrusters mo- tors and controllers . . . . .	174

C.4	Footprint of the physical ship model in dynamic positioning under environmental disturbances - test 22 . . . . .	175
C.5	Footprint of the physical ship model in dynamic positioning under environmental disturbances - test 23 . . . . .	176
C.6	Footprint of the physical ship model in dynamic positioning under environmental disturbances - test 24 . . . . .	177
C.7	Footprint of the physical ship model in dynamic positioning under environmental disturbances - test 25 . . . . .	178
C.8	Footprint of the physical ship model in dynamic positioning under environmental disturbances - test 27 . . . . .	179
C.9	Footprint of the physical ship model in dynamic positioning under environmental disturbances - test 28 . . . . .	180

# List of Tables

2.1	Environmental conditions according to (DNV, 2021) . . . . .	44
2.2	Comparison of different methods of DP capability assessment . . . . .	54
3.1	MSV model main particulars in scale 1:36 . . . . .	56
3.2	Added mass inertia of MSV in model scale . . . . .	70
3.3	CFD analysis set-up . . . . .	72
3.4	Damping coefficients resulting from the polynomial curve fitting into the numerical results for MSV in model scale . . . . .	74
4.1	Boundary constraints . . . . .	97
7.1	DP model tests conditions . . . . .	128
7.2	Model tests runs . . . . .	131
7.3	Dynamic positioning limits and realization according to DNV standard (DNV, 2021) . . . . .	132
7.4	Summary of the DP experiments results . . . . .	132
8.1	Static and dynamic methods distinction . . . . .	139
8.2	Dynamic positioning capability results with all tested methods	142
8.3	Dynamic factor based on thrust utilization . . . . .	143
8.4	RMS of radius and heading relative values variations . . . . .	143
A.1	Wind, wave, current forces calculation ship input data. . . . .	157
A.2	Thruster data . . . . .	158
A.3	Hull data of the Rescue Vessel and Multi-Service Vessel (MSV)	159
A.4	Thrusters data - Rescue Vessel . . . . .	160
A.5	Thrusters data - Multi-Service Vessel . . . . .	162
C.1	DP system components . . . . .	170
C.2	Measured values and measuring devices . . . . .	172

# List of symbols

$f_{\text{dyn}}$	dynamic factor
$T_{\text{stat}}$	total thrust utilization from static method
$T_{\text{dyn}}$	total mean thrust utilization from dynamic method
$F_{\text{stat}}$	static environmental force or moment
$F_{\text{dyn}}$	environmental force or moment corrected with dynamic factor $f_{\text{dyn}}$ .
$x$	surge - ships' motion at x axis
$y$	sway - ships' motion at y axis
$z$	heave - ships' motion at z axis
$\phi$	roll - ships' motion about x axis
$\theta$	pitch - ships' motion about y axis
$\psi$	yaw - ships' motion about z axis
$r_{\text{max}}$	maximum radius of deviation from reference position
$x_{\text{max}}$	maximum deviation along x axis from reference position
$y_{\text{max}}$	maximum deviation along y axis from reference position
$x$	notation of x axis
$y$	notation of y axis
$z$	notation of z axis

$F_{xy}$ wind/current	generalized force due to wind or current at x or y axis
$M_z$ wind/current	generalized moment due to wind or current at x or y axis
$F_x$ waves	static wave force along x axis
$F_y$ waves	static wave force along y axis
$M_z$ waves	static wave moment around z axis
$\rho_{w/a}$	generalized density (water or air)
$v_{w/a}$	speed of the medium (water or air)
$A$	projected area of above water part or underwater part of the ship in reference to a wind or current direction respectively
$C_{DNV}$	nondimensional coefficient given by the DNV standard for wind and current forces calculations
$\alpha$	angle of environmental disturbances
$L_{pp}$	ships' length between perpendiculars
$x_L$	center of projected longitudinal area above water or underwater
$\rho_{\text{water}}$	water density
$H_s$	significant wave height
$T_p$	wave peak period
$g$	gravitational acceleration
$B$	ships' maximum breadth at the waterline
$\text{Bow}_{\text{angle}}$	angle between the vessel x-axis and a line drawn from the foremost point in the water line to the point at $y = B/4$ (ahead of $L_{pp}/2$ ) on the water line
$L_{os}$	longitudinal distance between the foremost and aftmost point underwater
$T_{\text{nom}}$	nominal thrust of the thruster
$D$	thruster propeller diameter

$P$	power delivered to the propeller
$\eta_{\text{DNV}}$	thruster efficiency factor defined by the DNV standard and dependent on the thruster type
$\beta_{\text{relative}}$	thrust vector angle relative to the position of the obstacle
$\beta_{\text{vent}}$	thrust loss due to ventilation
$x_{\text{thr}}$	position of the thruster in x axis is body fixed frame
$y_{\text{thr}}$	position of the thruster in y axis is body fixed frame
$z_{\text{thr}}$	position of the thruster in z axis is body fixed frame
$i$	identification notation of each thruster
$N$	total number of thrusters
$T_{x_i}$	force at x produced by $i$ th thruster
$T_{y_i}$	force at y produced by $i$ th thruster
$F_{x \text{ env}}$	environmental force at x axis
$F_{y \text{ env}}$	environmental force at y axis
$M_{z \text{ env}}$	environmental moment about x axis
$F_{x \text{ ctrl}}$	control force at x axis
$F_{y \text{ ctrl}}$	control force at y axis
$M_{z \text{ ctrl}}$	control moment about x axis
$\boldsymbol{\eta}$	position vector of the ship in global reference frame
$\boldsymbol{\nu}$	ship velocity vector in body fixed frame
$u$	ship velocity is surge
$v$	ship velocity in sway
$r$	ship velocity in yaw
$\boldsymbol{\nu}_c$	current velocity vector in body fixed frame
$\boldsymbol{\nu}_r$	relative velocity vector of the ship in body fixed frame

$M_{RB}$	rigid body mass matrix
$M_A$	added mass matrix
$M$	total mass matrix (rigid body and added)
$D_L$	linear damping matrix
$D_{NL}$	nonlinear damping matrix
$D$	total damping matrix
$C_{RB}$	rigid body inertial Coriolis matrix
$C_A$	added mass inertial Coriolis matrix
$\tau_{\text{env}}$	environmental forces vector
$\tau_{\text{wind}}$	wind forces vector
$\tau_{\text{waves}}$	waves forces vector
$\tau_{\text{thr}}$	thruster forces vector
$R$	rotation matrix from body fixed frame to global reference frame
m	mass of the ship
$I_z$	ship moment of inertia
$\omega$	angular frequency of the regular wave
$A_{11}$	frequency dependent added mass on x axis
$A_{22}$	frequency dependent added mass on y axis
$A_{66}$	frequency dependent added mass on z axis
$A_{26}, A_{62}$	frequency dependent added mass on $y$ axis due to motion about z axis
$A_{62}$	frequency dependent added mass about z axis due to motion in y axis
$X_u$	hydrodynamic linear coefficient on x axis
$Y_v$	hydrodynamic linear coefficient on y axis

$N_r$	hydrodynamic linear coefficient in yaw motion
$Y_r$	hydrodynamic linear coefficient on y axis due to yaw motion
$N_v$	hydrodynamic linear coefficient about z axis due to sway motion
$X_{ u u}$	hydrodynamic quadratic coefficient on x axis
$Y_{ v v}$	hydrodynamic quadratic coefficient on y axis
$N_{ r r}$	hydrodynamic quadratic coefficient at $\psi$ motion
$Y_{ r r}$	hydrodynamic quadratic coefficient on y axis due to yaw motion
$N_{ v v}$	hydrodynamic quadratic coefficient at yaw motion due to sway motion
$Y_{ r v}, Y_{ v r}$	hydrodynamic quadratic coefficient on y axis due to coupled sway and yaw motion
$N_{ r v}, N_{ v r}$	hydrodynamic quadratic coefficient at yaw motion due to coupled yaw and sway motion
$T_{\text{eff}}$	effective thrust
$n$	propeller revolutions
$\beta$	thruster angle
$a_{\text{thr}}$	nondimentianal coefficient of thrust polynomial
$n_{\text{set}}$	set value of thruster propeller revolutions
$\beta_{\text{set}}$	set value of azimuth thruster angle
$T_{\text{const.}n}$	time constant of revolutions rate of change
$T_{\text{const.}\beta}$	time constant of azimuth angle rate of change
$F_u$	force at x axis due to ship model surge motion
$F_v$	force at y axis due to ship model sway motion
$F_r$	force at y axis due to ship model yaw motion
$N_v$	moment about z axis due to ship model sway motion

$N_r$	moment about z axis due to ship model yaw motion
$F_{\text{wave Iorder}}$	1st order wave induced forces
$F_{\text{wave IIorder}}$	2nd order wave induced forces (wave drift forces)
$S_{\text{wave}}$	wave spectrum
$A_{\text{rao Iorder}}$	response amplitude operators
$A_{\text{rao IIorder}}$	quadratic transfer functions
$\mathbf{u}$	vector of decision variables
$T_{x_i}$	thrust of the $i$ th thruster at x axis
$T_{y_i}$	thrust of the $i$ th thruster at y axis
$\beta_{\text{start } z_i}$	angle at which the convex $z$ th zone of $i$ th thruster of the constraint starts
$\beta_{\text{end } z_i}$	angle at which the convex $z$ th zone of $i$ th thruster of the constraint ends
$z$	identification of the convex zone within the non-convex constraint
$Z_i$	total number of convex zones in $i$ th thruster
$J_{z_i}$	total number of polygons in $z$ th zone of the $i$ th thruster
$\varphi_{j z_i}$	identification of the angle of the $j$ th polygon within the convex $z$ th zone of the $i$ th thruster
$r_i$	maximum thrust without losses, within the polygon of the $i$ th thruster
$x_k$	x position of the point at the outline of the polygon describing a spoiled zone in a thruster reference frame
$y_k$	y position of the point at the outline of the polygon describing a spoiled zone in a thruster reference frame
$T_{\max i}$	maximum thrust of the reverse mode of the propeller or of the tunnel thruster
$P_{\text{total}}$	total utilized power in dynamic positioning operations

$\mathbf{W}_l$	weight matrix
$\mathbf{A}_l$	matrix of coefficients of equality constraints in quadratic programming $l$ th problem
$\mathbf{b}_l$	vector of equality constraints in quadratic programming $l$ th problem
$\mathbf{G}_l$	matrix of coefficients of inequality constraints in quadratic programming $l$ th problem
$\mathbf{h}_l$	vector of equality constraints in quadratic programming $l$ th problem
$L$	total number of convex subproblem in quadratic programming optimization of thrust allocation
$P_{\max}$	maximum power boundary in non-dominated sorting genetic algorithm
$e$	static balance error
$J_e$	quadratic objective function of balance error in non-dominated sorting genetic algorithm
$\mathbf{u}_{\min}$	lower decision variable boundaries
$\mathbf{u}_{\max}$	upper decision variable boundaries
$\mathbf{K}_{11}, \mathbf{K}_{12}$	observer gains matrices concerning 1st order wave motion estimation
$\mathbf{K}_2, \mathbf{K}_3, \mathbf{K}_4$	observer gains matrices for velocity estimation
$\mathbf{K}_P, \mathbf{K}_I, \mathbf{K}_D$	PID controller gains matrices
$x_j^{ref}$	reference trajectory response at $j$ th prediction step in MPC
$x_j^{pred}$	predicted trajectory at $j$ th prediction step in MPC
$\lambda_{\text{MPC}}$	weight coefficient to account for control signal change
$\Delta T_{x_i}$	thrust increase/decrease between previous and current simulation time at $x$ axis

$\Delta T_{y_i}$	thrust increase/decrease between previous and current simulation time at y axis
$v_c$	current speed
$\gamma$	wave spectrum coefficient
<b><math>L</math></b>	location matrix
$r$	maximum position radius variations from reference position based on dynamic analyses and all samples
$\Delta_\psi$	heading variation from reference heading based on dynamic analyses and all samples
$RMS$	root mean square
$P_{\max \text{total}}$	maximum available propulsion power on the ship
$T_{\text{total}}$	sum of mean thrust utilization of each thruster in dynamic methods and total thrust utilization in static methods

# Chapter 1

## Introduction

The research presented in this dissertation contributes to the field of control systems engineering. The work focuses on the identification of objects of control and the design of control structures and algorithms essential for the desired performance of the dynamic positioning system (DPS) launch. This research, in particular, addresses the dynamic positioning (DP) capability assessment of a ship at its design stage, comprising DP prognosis which also relates to the field of marine engineering. The aim is to provide a high quality, verified decision support tool capable of assisting a regular engineer during the design phase and contributing to the reduction of ship production and operational costs and, above all, ensure primarily assumed ship operability.

The research results presented in this dissertation together with developed methods also included contribute to a proposal of the decision support system for a regular engineer to use in a design office. Modification of the static method of DP prognosis and an approach to utilizing static, dynamic, and experimental methods for the assessment of the DP capability are emphasized. An important advantage of the proposed solutions is that the approach is developed in alignment with the commonly used DNV-ST-0111 standard, (DNV, 2021).

The tangible result is a software prototype designed to analyze the DP capability of a marine vessel. It was developed for use at the Maritime Advanced Research Centre (CTO S.A.), in a hydromechanics division. The facility's primary objective is to perform research mainly for supporting ship design for clients all over the world. This tool supports analysts by allowing prediction of the ship's behavior during DP operations at sea.

To ensure the legibility of the research results presented in the disserta-

tion, this chapter is divided into seven sections. In Sect. 1.1 a background of the problem is discussed and, consequently, knowledge gaps are identified. In Sect. 1.2 a problem is stated to which a solution would fill those gaps. The justification and importance of the research are discussed in Sect. 1.3. In Sect. 1.4 the thesis and research objectives that are pursued are formulated. In Sect. 1.5 methods and theoretical framework applied are discussed to accomplish the research objectives. The required sets of assumptions are given in Sect. 1.6. Finally, the overall layout of the dissertation is introduced in Sect. 1.7 which completes the chapter.

## 1.1 Background

Dynamic positioning is an operation concerning a free-floating object that uses its thrusters exclusively to maintain its orientation in space, even under varying environmental conditions, within a closed-loop control system. The DP ensures safe and efficient execution of various tasks at a fixed location and a low velocity (close to zero), in accordance with the object's purpose and operational profile.

For ships, these tasks may include offshore construction, transferring goods and personnel to oil rig or wind platform, refueling operations, research such as seabed mapping, drilling, diving, and rescue operations. In the case of surface ships, planar motion (position and heading) is controlled to counteract environmental forces such as currents, waves, and wind. This functionality is commonly referred to as station keeping.

The primary function of the DP system is to balance the environmental load vector acting on the vessel with the thrust vector generated by the thrusters. This process, known as disturbance rejection, ensures that the vessel maintains its position under the influence of environmental forces.

Dynamic positioning is enabled by the application of the DPS. The system components include the propulsion system as the executive actuators, position and heading measurement devices, and a control system comprising a controller supported by an observer and a thrust allocation (TA) module, which generates control inputs for the actuators. A typical DPS structure is described in (Johansen and Fossen, 2013; Smierzchalski, 2016; Fu et al., 2019; Witkowska et al., 2020; Fossen, 2021; Deng et al., 2024). System design offers a wide range of choices, and innovations in this field are continually emerging. For example, papers such as (Li et al., 2020; Ya-nan et al., 2020;

Wen et al., 2023) propose advances in observer design, while (Zheng et al., 2020; Chen et al., 2021; Cheng et al., 2023; Wang et al., 2024; Yu and Du, 2024) focuses on controllers, and works such as (Ding et al., 2021; Lu et al., 2021; Tuo et al., 2021; Raghunathan et al., 2023; Wei et al., 2024) address the thrust allocation problem.

The ship is considered capable of dynamic positioning when the heading and position variations in reference to the set values remain within defined margins. These margins are dictated by the type of operation, but can also be adopted based on specific standards, such as those proposed by (DNV, 2021). The latter not only allows the vessel to receive a class notation (granted by this ship classification society), but also serves as benchmarks for future designs, enabling comparative analyses.

DP capability is assessed, analyzed, or evaluated in the design stage of the ship, both in the preliminary and advanced phases. It provides fundamental knowledge that guides design-altering decisions. Such decisions primarily influence the selection of thrusters and total power demand, but in some cases may also affect the hull and superstructure shape, ultimately also impacting the DPS design. Assessment involves a prognosis, also called a prediction or estimate, of DP capability.

Based on (DNV, 2021), two primary approaches to DP capability assessment are identified: the static approach and dynamic simulation. The static approach is suitable for the early design stage when only limited data is available and also serves as the basis for classification. In contrast, dynamic simulation requires detailed knowledge of thruster and hull dynamics, as well as the control system. In addition, a sophisticated identification procedure for these elements is essential. Another dynamic method involves model tests, which, although highly accurate, are extremely time-consuming and expensive. These tests are typically used to validate other methods or provide the most accurate final predictions. In addition, full-scale trials can be conducted, providing data for ultimate validation.

Figure 1.1 illustrates the influence of each method on the design process, highlighting static calculations (I) as fundamental and most critical in terms of shaping the design. Dynamic simulation (II) is typically performed at a more advanced stage of the design process. Although simulation results can still influence the design, the extent of their impact is limited, as the ship is usually contracted at this stage and pricing is set. However, in some cases, designers may opt to implement changes based on simulation results. The same applies to model tests (III), although these are rarely performed and are

usually reserved for validation purposes. During sea trials (IV), significant design flaws can also be discovered. In such cases, the vessel may require substantial modifications or even be partially rebuilt.

The more advanced the design stage, the more expensive any changes become. Therefore, achieving an accurate prognosis in the early stage of ship design using static methods that are the cheapest, easiest, and fastest approach makes the quality of these methods critically important.

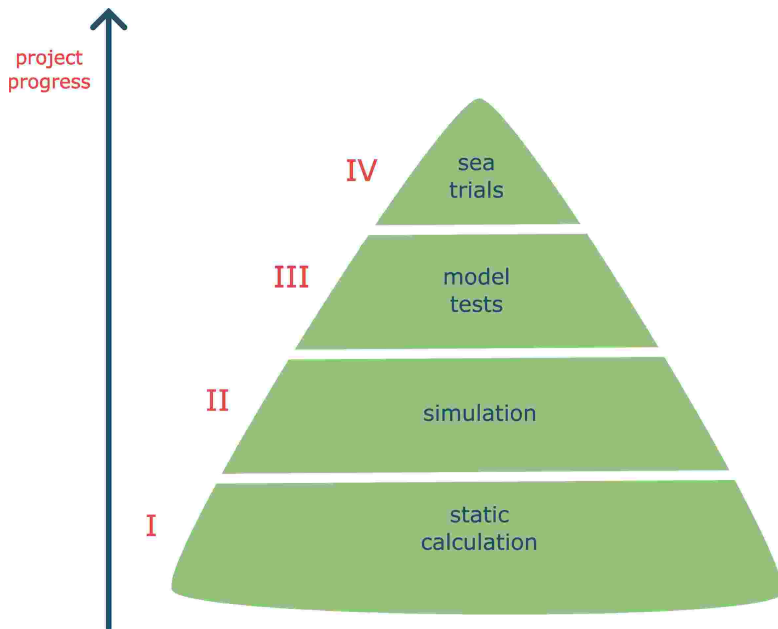


Figure 1.1: DP capability prognosis impact on the ship design

Classification societies, such as Det Norske Veritas (DNV) and the American Bureau of Shipping (ABS), offer simplified methods to support static analyses of dynamic positioning (DP) systems (ABS, 2021; DNV, 2021). These methods include empirical models for both thrusters and environmental forces. Thruster models are typically based on key characteristics, such as thruster type, diameter, and available power, while environmental models depend on the vessel's main dimensions, including length, breadth, draft, and other relevant parameters. Furthermore, the International Marine Contractors Association (IMCA) provides a more general approach to static analysis (IMCA, 2017). A detailed comparison of these guidelines is available in (Hasan, 2018).

Static methods are used to determine whether a vessel is able to maintain its position by balancing the environmental loads with the forces generated by the thrusters. In this context, the concept of "margins" discussed earlier is not applicable. The vessel either successfully maintains its position or fails.

To assess DP capability, thrust allocation must be applied. Through specific algorithms, thrust allocation calculates the amount of thrust each thruster must generate to effectively achieve balance between the environmental forces and keep the vessel's position. Thrust allocation is crucial in both static and dynamic analyses, as it directly impacts the overall performance of the DP system (Kalikatzarakis et al., 2022).

In the case of overactuated systems, as DP ships typically are, thrust allocation becomes an optimization problem. Although a DP ship is limited to three degrees of freedom (surge, sway, and yaw), the number of thrust components to allocate exceeds three due to the redundancy criteria these vessels are designed to fulfill. For each axis (surge - x, sway - y, and yaw -  $\psi$ , rotation - around z), three static equilibrium equations can be constructed. However, these equations involve more than three unknowns (the thrust components along x and y for each thruster), as illustrated in Fig. 1.2. The figure represents environmental forces and moments with blue arrows and thrust force components generated by thrusters with red arrows. The thrusters counteract environmental forces to maintain position and heading, effectively rejecting disturbances. The challenge lies in determining the individual thrust components required to achieve this balance in an efficient way. Then a suitable optimization algorithm is applied to solve the thrust allocation problem.

The thrust allocation algorithm is not addressed by any of the known standards, leaving the solution to a potential designer. This is the reason why most design offices outsource static DP capability analyses instead of in-house implementation. Over the years, two main approaches have been applied, gradient-based methods and metaheuristic methods. The first comprises solutions based on Lagrangian multipliers, quadratic programming (QP), or sequential quadratic programming (SQP) presented in (de Wit, 2009; Ruth, 2008; Wang et al., 2018; Valčić, 2020). Both approaches assume that the objective function and constraints are smooth, and they guarantee reaching a global minimum. In turn, the second group of methods consists of the so-called nongradient (derivative-free) methods such as particle swarm optimization (PSO) (Kalikatzarakis et al., 2022), colony-based algorithms (Wu et al., 2016; Wang and Wei, 2021), genetic algorithms (GA) or evolutionary

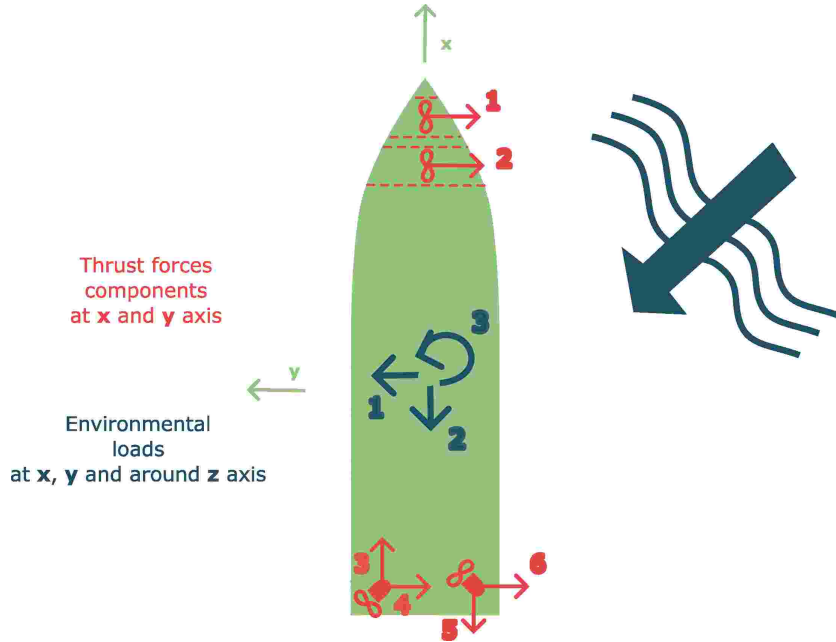


Figure 1.2: Problem of overactuated system

algorithms (EA) as presented in (Deb et al., 2002; Gao et al., 2019; Kalikatzarakis et al., 2022) and recent Drosophila algorithm applications (Jiao and Wang, 2024), to name a few.

In (Ruth, 2008; de Wit, 2009; Wang et al., 2018; Valčić, 2020) a comprehensive description of the application of QP to DP capability analyzes in an early design stage is given. The method shows high applicability to the thrust allocation problem, high compliance with the validation tools, and relatively simple implementation. Moreover, the sequential QP method allows for the solution of highly non-linear problems by solving subproblems with the QP optimization algorithm in an iterative process as shown by (Johansen et al., 2004; Tang et al., 2021).

As for the metaheuristic methods, the application of the PSO and GA to the minimization of fuel consumption is proposed in (Kalikatzarakis et al., 2022). The authors state that the solution is achieved in near-real time. The same conclusion is given in (Gao et al., 2019), where a non-dominated sorting genetic algorithm (NSGAII) was applied. In (Gao et al., 2019) SQP is also compared with NSGAII in application to DP simulations, with the conclusion that the latter ensures lower thruster force and orientation (angle) variations.

In (Ding et al., 2020) the improved differential evolutionary (IDE) algorithm is proposed and shows better performance than the standard DE. In addition, (Wu et al., 2016) proposes the algorithm based on the artificial bee colony (ABC) and (Wang and Wei, 2021) introduces the Cuckoo algorithm of the bird colony showing improved TA in both cases. An improved sparrow search algorithm (ADGSSA) based on multi-strategy fusion is introduced in (Wei et al., 2024) and compared to the Coati optimization algorithm (COA), the whale optimization algorithm (WOA), and the sparrow search algorithm (SSA), showing significant improvements. The neural network approach also found its application in the optimal thrust allocation problem as presented in (Liu and Zhang, 2020; Raghunathan et al., 2023). Specifically, a deep reinforcement learning (DRL) based algorithm was implemented in (Øvereng et al., 2021) and compared to QP.

In (Valčić, 2020), based on a comparison of SQP and direct search methods - generating set search (GSS), and mesh adaptive direct search (MADS) - it is concluded that SQP applies for a simplified definition of the problem and converges faster than the listed derivative-free algorithms.

In addition, hybrid approaches were proposed in (Zhao and Roh, 2015), where GA and SQP were applied together, resulting in slightly lower power consumption compared to the intelligently tuned harmony search algorithm (ITHS). Also, multiagent strategy using QP methods is applied in (Lu et al., 2021), resulting in a reliable and efficient TA with multiple criteria.

From a broader perspective, neither gradient-based methods nor metaheuristic approaches can be universally superior. The choice between these methods depends on the specific characteristics of the problem at hand and the utilization of TA either in operation or for prognosis. A wide range of solutions is available, most of which are tailored for application on operational ships. However, the focus of this dissertation is on early-stage prognosis, which directly impacts the design process.

To address this specific challenge, a detailed study of the available methods must be performed to identify the most suitable approach under the given conditions. The key factors influencing this choice include time efficiency, accuracy, applicability across different types of ship, and simplicity of implementation.

Building on the guidance provided in (Piekło et al., 2023b,a) and extended in this dissertation, with additional support from (de Wit, 2009; Zalewski, 2016, 2017; Wang et al., 2018; Valčić, 2020), a method based on quadratic programming is proposed and implemented for thrust allocation. Further-

more, an alternative optimization approach utilizing a genetic algorithm is also explored and compared, as detailed in (Piekło et al., 2022). Specifically, the non-dominated sorting genetic algorithm II, as described in (Gao et al., 2019), is employed for this purpose. Comparison of performance and results of application of both algorithms allows verification and justifies the choice of a more suitable candidate.

Quadratic programming offers a favorable compromise among the listed factors, as demonstrated by the literature review and aligned with the problem specifications outlined in the DNV standard DNV-ST-0111 (DNV, 2021). Given that this standard is the most widely adopted worldwide for the prognosis of DP capability, the application of QP to this framework addresses a significant gap in the field of static DP analysis, providing verified and reliable results.

Thrust allocation is crucial not only in static methods but also as an integral part of dynamic positioning simulators, where it works alongside the observer and the controller (Fig. 1.3). In static methods, TA focuses on balancing predefined environmental forces. However, in dynamic methods, including model tests and real-world operations, TA must account for system dynamics. It distributes the control forces, calculated by the controller, among the thrusters' set controls. Some TA algorithms, as discussed in (Xia et al., 2019b; Deng et al., 2024), are adaptable to dynamic environments. The dynamics of thruster control inputs directly depend on the selected TA algorithm, which is also influenced by the performance of the controller, which in turn uses the observer output signals - vessel estimated state. Hence, DPS needs to be designed complexly to perform synergically.

In dynamic positioning systems, an observer is used to estimate hard-to-measure system states, such as velocities or accelerations. This enables more accurate control, improving the stability and precision of DP. The observer also helps filter out wave-induced disturbances, correct control errors, and optimize the use of thrusters, avoiding wear and tear. Recent studies on DPS have a great deal of concern for the observer design and its improvement as given in (Liu et al., 2019; Yang et al., 2019; Xia et al., 2019a; Zhang and Xu, 2020). However, more than a decade ago, (Fossen, 2021) proposed a pioneering solution at that time of a nonlinear passive observer that showed improved qualities over a simple extended Kalman filter that was utilized until then. The solution outperformed others due to its robustness and simplified tuning. For the prognosis of DP, it is still considered an efficient and universal approach, while the new solutions discussed in the references are

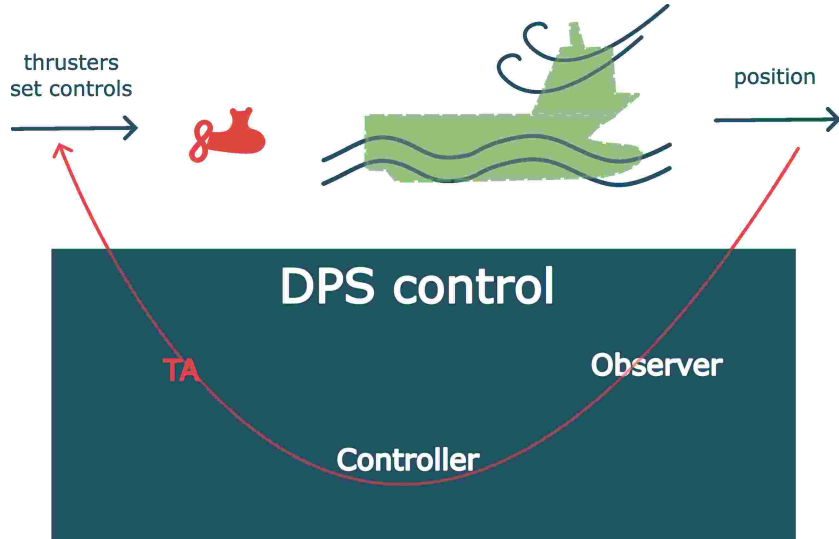


Figure 1.3: DPS concept

more applicable to real-world operations.

The remaining component of the dynamic positioning system is the controller. In advanced stages of ship design, the use of a dedicated controller is beneficial for a more accurate prognosis and is a standard practice. However, a simpler, temporary approach may be adopted initially, assuming that the final solution will be tailored. The most straightforward and widely used solution is the proportional-integral-derivative (PID) controller. Although simple to implement and tune, PID controllers are also often used as a foundation for further enhancements, including hybrid approaches such as fuzzy logic, as discussed in (Qiu, 2022; Liu et al., 2024).

Among the various alternatives, the model predictive controller (MPC) has demonstrated the most promising results and is already widely implemented on DP vessels, as noted by DP control system providers like Kongsberg. When applied to the prediction process in simulations (or model tests), MPC is expected to offer higher accuracy, reflecting real-world operations more closely. Additionally, MPC is relatively easy to tune as it is based on the natural constraints and dynamics of the system. Examples of its application can be found in (Ji et al., 2023; Øveraas et al., 2023; Syntakas and Vlachos, 2023; Hao et al., 2024; Ljungberg et al., 2024).

A nonlinear passive observer combined with a MPC (or PID) controller and QP-based optimal thrust allocation, accounting for system dynamics,

provides a fast and straightforward solution, as proposed in the dissertation. It can be used in the prognosis and for validation with the model tests that mirror similar DPS.

Experiments are typically conducted in towing tanks, which require additional preparation due to their nonstandard nature. A benchmark example of a DP ship model is the Cybership II, in scale 1:70, with multiple validation tests described in (Ihle et al., 2004; Skjetne et al., 2004; Skjetne, 2005; Tomera, 2009; Wondergem et al., 2011). Other examples are found in (Zaman et al., 2019; Li et al., 2024). However, more well-documented validation models are needed as few models are available for further development of DP systems. Introducing additional examples contributes to the advancement of the field of DP ship control, as discussed in the dissertation.

These approaches cover all three methods of prognosis of DP capability. Final verification occurs in real-world operations. A comparison of simulations with full-scale trials is presented in (Donnarumma et al., 2018). Although quantitative comparisons are not always possible, the limits of DP capabilities can be determined, helping to verify the effectiveness of other assessment methods.

Through a comparison of all available methods, including static analysis, simulation, model tests and full-scale trials, it is possible to determine accuracy margins or dynamic factors for the refinement of static methods of DP capability assessment. These refinements can significantly reduce prediction time and improve the accuracy of the early-stage prognosis, thus optimizing the design process.

In (Martelli et al., 2022) the comparison between static and dynamic analysis is presented and based on that it can be concluded that the static methods overestimate the DP performance which can lead to the selection of undersized propulsion. The discrepancies varied for different conditions; however, they were found to not exceed around 15 - 20%. In (Mauro and Gaudiano, 2018) the same tendency was found but up to 30% differences were observed. In (DNV, 2021) a dynamic factor of 1.25 (25%) is proposed to account for environmental forces that vary over time. In (van 't Veer and Gachet, 2011) it was found that the discrepancies are mainly caused by variations in the wave forces over time and a dynamic factor of 2 (100%) was applied to these forces to even the results of the static and dynamic calculations. A method for estimating the accuracy of the static approach using time-domain simulations for an offshore supply vessel is also given in (Serraris and Cozijn, 2017). The problem of uncertainty and sensitivity in

DP calculations in the context of different stages of the design is broadly discussed in (van 't Klooster, 2018).

Regarding the dynamic factor as a correction for static methods, there are few examples in the literature, especially in recent years and with respect to experimental data. New studies would provide better insight into the assessment of static methods and add value to the subject, which is the objective of this dissertation, ultimately achieved through the analysis of a selected case.

In summary, current standards and guidelines from the classification society provide limited details on the application of static and simulation methods. Moreover, their accuracy is not specified, probably due to the incomplete nature of the description. A comprehensive development of these methods, specifically in the context of the DNV-ST-0111 standard, including thrust allocation, mathematical model identification, and control system design, is lacking. Combining insights from various research studies to create a more robust guidance system, with improvements addressing these gaps, would significantly advance the field.

## 1.2 Problem statement

This dissertation addresses the issue of supporting the designer's decision-making process in the prognosis of a vessel's dynamic positioning capabilities under a wide range of weather conditions, regarding classification societies' requirements. The literature review highlights the lack of reliable and experimentally validated tools concerning static methods that enable the prognosis of DP capability at early stages of ship design. To fill this gap, it is proposed to develop a decision support system (DSS) based on a static method, corrected and validated using both simulation and experimental methods. Assessment of a vessel's DP capabilities using the developed system can significantly contribute to minimizing ship production and operational costs through the optimal design, concerning thruster selection, power demand estimation, and hull shape design. A general concept of the proposed decision support system for DP capability assessment is presented in Fig. 1.4.

The DSS is based on knowledge in the form of methods and tools developed by the expert. Following the graph in Fig. 1.4, the expert delivers methods for the dynamic assessment of DP capability with simulation. This comprises ship numerical identification methods and simulator design. The

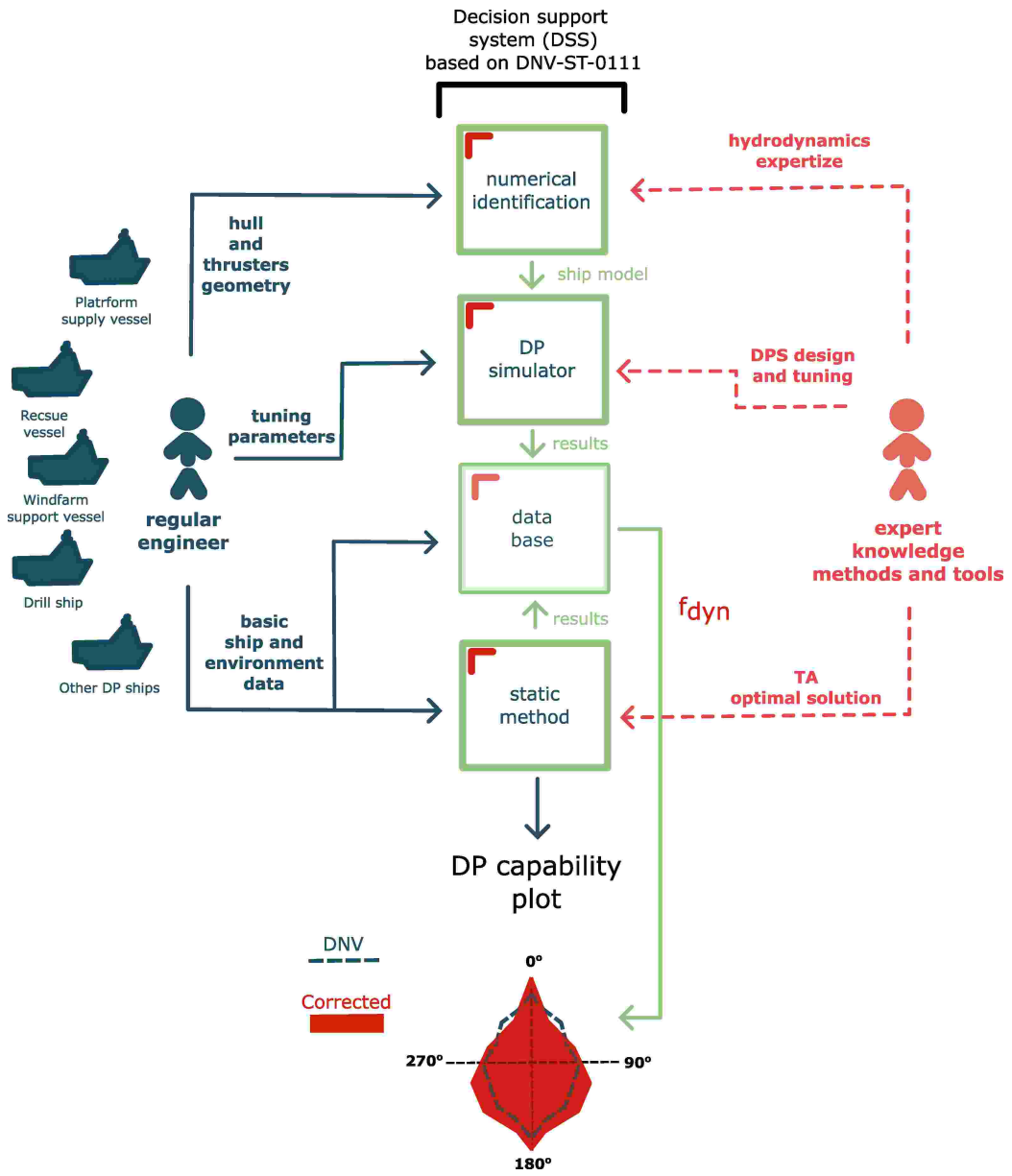


Figure 1.4: Concept of decision support system in a typical design office

latter is provided as a complete tool for a regular engineer to use. For a simpler prognosis, the expert provides methods of solving the thrust allocation problem in a static approach by providing a complete tool for the assessment

of DP capability level 1 or 2 with the output of a DP capability polar plot, (DNV, 2021).

To build the system, the expert needs to present knowledge on DP control system design, including different controllers and observers, comprising also tuning of controller and observer gains. In both static method and dynamic simulations, an expert develops a suitable thrust allocation algorithm accounting for the nonlinear and non-convex nature of the problem. Moreover, expert has thorough knowledge in the field of hydrodynamics, which allows for correct hull, thrusters, and waves modeling. Finally, experts perform a validation of both the simulator and the static method with experiments to ensure verification of the DSS.

On the other hand, a regular engineer can either do a prognosis with static analyses using basic ship data such as length, breadth, propeller diameter, and other easily derived data, or perform more sophisticated analyses, a simulation. In the latter case, the engineer needs to perform parametric identification of the hull and thrusters with provided methods and also tune the controller and observer parameters.

Assessment of dynamic positioning capability with the static method and simulation is fed into the database of all results for different types of ships in various weather conditions. With obtained data, this content allows dynamic factor determination that could be used for static DP prognosis correction for new vessels. The dynamic factor  $f_{dyn}$  is defined and used as follows.

$$f_{dyn} = \frac{T_{dyn}}{T_{stat}}, \quad (1.1)$$

$$F_{dyn} = f_{dyn} F_{stat}, \quad (1.2)$$

where  $T_{stat}$  is the total thrust utilization resulting from the static method;  $T_{dyn}$  is the total mean thrust utilization resulting from the dynamic method;  $F_{stat}$  is the static environmental force or moment (according to the DNV-ST-0111 standard) and  $F_{dyn}$  is the environmental force or moment corrected for with the dynamic factor  $f_{dyn}$ .

The dynamic factor is understood as a factor that, if multiplied by the environmental forces that appear in static analyzes, (DNV, 2021), would result in a more accurate prognosis. The factor is considered dependent on the basic data of the ship, the heading, and the DP number <sup>1</sup>.

---

<sup>1</sup>Standard DNV-ST-0111 defines 11 DP numbers corresponding to a predefined weather conditions (wind, waves, current) that are acting simultaneously and are collinear.

The result of the system would be a plot of DP capability, showing the limits of DP capability depending on the direction and magnitude of the environmental loads, (DNV, 2021). However, the plot would be corrected for with a dynamic factor.

In addition to the DP capability plot, a regular engineer would have access to more results such as thrust and power distribution over thrusters, environmental forces, and in simulation additionally, controller output, thrust allocation output, position, and heading variations in time.

The DSS is a standalone structure that an engineer can use for multiple designs of different types of ship without further guidance from the expert. Furthermore, by utilizing tools and methods provided by the expert, the engineer can not only use the existing database (initiated by the expert) but also feed this database with new content to improve the dynamic factor and subsequently the prognosis.

The DSS presented would allow better decisions at an early stage of ship design by correcting the DP capability plot for level 1 or 2 to get closer to the real-world operations.

### 1.3 Purpose and significance of the study

Well established decision support system as presented in previous section, would serve as an ultimate guidance in the field of DP capability assessment at an early design stage in a ship design office. It follows that the prognosis would be more accurate and faster to conduct. Moreover, system assumes continuous expansion of the database, making the prognosis more trustworthy and the designer more confident within the years of using it. Even though, feeding the database would be time consuming and laborious, in time the efforts would be surpassed by its added value.

In the database of the system, a comparative analysis of static and dynamic methods (simulation and experiments) would be processed to output a range of dynamic factors that are weather scenario and ship type dependent. This field is significantly understudied, as proved in Sec. 1.1. The DSS, in its form at the end of the studies, serves as a prototype.

Developed thrust allocation method for static approach, components of the simulator, controller (PID and MPC), observer, thrust allocation, hull and thrusters dynamic models together with methods of their identification and experimental results are fundamentals of the DSS. Its detailed descrip-

tion would allow any design office to settle an in-house guidance tool on an image of proposed DSS and further development of the database based on new designs.

Methods and tools are to be an in-house development of the author in Maritime Advanced Research Centre (CTO S.A.). Furthermore, it would establish the Polish maritime industry on a higher level of know-how, concerning mainly DP simulations and experiments. Since the model testing is slowly displaced by numerical methods, a complete DP prognosis tool (with static method and simulator) is an obvious direction.

From an economical perspective, as already mentioned in Sec. 1.2, exploitation, maintenance, purchasing, and production costs could be reduced with more accurate prognosis. On the other hand, reduced operability due to poor design decisions would lead to lower efficiency of a wind farm, oil rig, construction, etc., generating more costs.

Accurate DP capability prediction is also a form of guarantee of safety of goods and people. This concerns transfer of people onto a wind turbine platform or oil rig, diving operations, construction or rescue operations. In other words, accurate estimation of the DP capability is a form of assurance that the operation could be carried out.

Decision support system and research leading to its development have obvious short term and long term benefits. In the former case, the system can be established relatively fast (within few months if supported by these studies) and serve for further database expansion. In the latter, a significant profit of the system could be visible in the cost of the ship, cost of operations, and operability in many years forward.

## 1.4 Thesis and research objectives

Despite advancements in simulation and static tools, there remains a significant gap that the decision support systems for designers would facilitate with the assessment of DP capabilities at various stages of the design process. More effective tools could enable designers to simulate and compare different scenarios and DP system configurations, thereby improving the accuracy with which vessels are tailored to operational requirements.

Given the uncertainty inherent in DP prognosis based on static methods, there is a pressing need for more accurate prediction methods. These methods should be capable of verifying their reliability under operational

conditions that closely resemble real-world scenarios, such as model tests. The development of such methods would provide valuable support in the design decision-making process and enable optimization of vessel design even before engaging in dynamic simulations.

Filling those gaps, in the context of DP ship design, would be realized through justifying the following theses.

1. It is possible to develop a decision support system for predicting a ship's dynamic positioning capabilities, using static and dynamic methods synergically and incorporating classification societies standards.
2. The developed system allows for a more accurate dynamic positioning assessment and prognosis based on static approach supported with database containing the results of dynamic methods, for a ship under various weather conditions. Subsequently, it would enable support for designer decisions at different stages of ship design.

Verification of the theses would be realized through meeting the following objectives.

1. Development and implementation of the static method of DP capability assessment based on selected nonlinear thrust allocation algorithms and according to the standard DNV-ST-0111, (DNV, 2021).
2. Parametric identification of hull and thruster mathematical models using numerical techniques.
3. Development and implementation of the dynamic method (simulation) of DP capability assessment according to the standard DNV-ST-0111, (DNV, 2021).
4. Case study validation of the simulator with DP model tests results and subsequently validation of the static tool with the simulator to define a dynamic factor.

Justifying the theses through realizing the above milestones would result in a complete software and range of methods comprising a decision support system with an initiated database for further expansion.

## 1.5 Methods, theoretical framework and scope

Methods that are used to solve the stated problem and that lead to the achievement of set objectives are within the scope of the control engineering field. However, also a subject of hydrodynamics is addressed concerning hull, thrusters, and wave loads models identification. Nevertheless, especially optimization methods, mathematical modeling, and design of the DP system, including the MPC controller, are studied.

To achieve the first objective (development and implementation of the static method of DP capability assessment based on selected nonlinear thrust allocation algorithms and according to the standard DNV-ST-0111) a thrust allocation problem that ensures static balance of thrust and environmental forces is solved. The problem turns out to be a multi-objective, nonlinear and non-convex optimization. It is solved with two proposed methods - quadratic programming based on (de Wit, 2009; Valčić, 2020; Piekło et al., 2023a) and genetic algorithm based on (Gao et al., 2019; Deb et al., 2002; Piekło et al., 2022). However, the problem is adapted to allow the implementation of those methods to the DNV-ST-0111 standard.

In QP, problem is reduced to a single quadratic objective function with linear constraints. This procedure introduces some simplifications that have an effect on the final results. On the other hand, even though the problem is applied in its original form in GA, the random nature of that algorithm also results in some level of inaccuracy. Moreover, those two applied methods differ drastically in computation time. Quadratic programming is much faster; hence, it is also applied in simulation studies, however extended to account for thruster dynamics.

Developed TA method is applied to the static and later also dynamic methods and is independent of the ship type, propulsion system, and environmental conditions. In other words, the method is made universal by accounting for different types of propulsion selection (including forbidden zones and decreased efficiency zones of azimuth thrusters).

Second milestone of the study (parametric identification of hull and thruster mathematical models using numerical techniques) is possible to achieve through the development of methods based on (Maciel et al., 2013; Koop et al., 2017; Liu and Zhang, 2020; Fossen, 2021; Piekło et al., 2023; Piekło et al., 2024) and utilizing commercial numerical software *STAR CCM+* and *Ansys Aqwa*. Mainly, a nonlinear hull damping model depending on the ship's speed and a thrust model depending on propeller revolutions is determined. Analyses

are carried out in model scale for fair validation with available results from model tests.

Additionally, a method for the definition of interactions between two azimuth thrusters is presented and supported with (Bosland et al., 2009; Zhou and Zhao, 2020). The efficiency of the thrusters due to interactions with the hull is determined for a full range of thruster operation angles. The implementation of the azimuth thrusters' losses directly to the simulator is, however, omitted within the studies due to limited time. Nevertheless, the procedure is valid and may serve for future applications. Instead, in the dissertation, losses are calculated according to DNV level 1 and applied to all levels (static and dynamic analyses).

To achieve the third objective (development and implementation of the dynamic method of DP capability assessment according to the standard DNV-ST-0111) DP system is designed comprising PID, MPC controller and observer parameters selection and implementation, thrust allocation development and implementation, hull and thrusters dynamic models application, and wave loads modeling, based on (Xia et al., 2015; Veksler et al., 2016; Mehrzadi et al., 2020; Fossen, 2021).

Controllers are selected based on literature, with PID as the most common, simple, and verified approach and MPC as the most accurate based on recent studies as given in (Alagili et al., 2020) and also due to its popularity in application on DP ships. MPC is designed based on a nonlinear ship hull model, as is the nonlinear passive observer which is structured as given in (Fossen, 2021). Thrust allocation and hull and thrusters models are implemented as resulted from first and second thesis objectives, and wave loads model based on (Fossen, 2021) and numerical analysis with *Ansys Aqwa* is adopted.

A complete simulator is delivered with the application of existing methods and their development by the author as mentioned. Test runs of simulation studies as initiation of the decision support system are performed on a ship model in scale to allow validation with experiments on the corresponding model.

Fourth objective (case study validation of the simulator with DP model test results and subsequently validation of the static tool with the simulator to define a dynamic factor) is possible to achieve with utilization of results obtained in physical model experiments in CTO S.A. towing tank. The tests were conducted prior to the doctoral studies. As a case, a Multi Purpose Vessel (MPV) equipped with a DP system including two stern azimuth thrusters

and two bow tunnel thrusters was selected. Choice of the ship was dictated by the availability as well as the ship type perfectly matching DP ships series. A model of the ship in scale 1:36 included a DP system - position and heading measurement system, observer, PID, simple TA based on pseudo inverse matrix and thrusters with propellers. The system allowed automatic maintenance of the physical model position and heading, recordings of the position (and heading) and thruster settings such as propeller revolutions in time. It was possible to simulate current by enforcing ship model motion along the tank and also wave modeling with utilization of the wave maker installed at the end of the tank.

In the towing tank, one MPV physical model in three weather conditions - current, short wave, and long wave was tested at one ship's heading of 90°. Due to limited towing tank time window and enormous preparation expenditure, the experiments are treated as an initiation of such tests, allowing for a more efficient process of conducting them in the future.

With the use of the static and dynamic (simulation and experiments) results, a comparative analysis and validation study is carried out. Above all, the tests serve to feed the decision support system database with a dynamic factor, Eq. (1.1) that would correct the static prognosis with DNV level 1. A limited amount of three cases allows for a prototype DSS development.

The DSS gathers all developed and adopted methods through achievement of the objectives in a form of dedicated software and this dissertation. The software is developed in *Python 3.8* programming environment and constitutes a stand-alone tool for DP capability assessment with all DNV levels (1, 2, 2-site, 3, 3-site). The tool includes a graphical user interface which adds a user-friendly feature and allows for a non-expert user group to utilize it.

## 1.6 Assumptions and limitations

Throughout the applied methods of evaluation of the dynamic positioning capability, both static and dynamic, a range of assumptions are adopted to achieve the objectives of the thesis. The developed methods are highly based on the DNV classification society standard DNV-ST-0111, (DNV, 2021) and the related literature, of which the most utilized is (Fossen, 2021).

**Assumption 1** *Considering ship motion in 3DOF: surge, sway, and yaw is sufficient for DP capability assessment, (Fossen, 2021; DNV, 2021).*

The ship is free in six degrees: surge ( $x$ ), sway ( $y$ ), heave ( $z$ ), roll ( $\phi$ ), pitch ( $\theta$ ) and yaw ( $\psi$ ). In dynamic positioning, however, the DP capability of ships is assessed only on the basis of three of those: surge, sway, and yaw. Dynamic positioning is a component of ships' operability, which is a broader term. In other words, for instance, crane operations may be possible in terms of DP accuracy, but, due to significant roll and heave motions, the conditions may exclude the ship from operations anyway. However, the dissertation focuses on DP performance, and it is assumed, based on (Fossen, 2021; IMCA, 2017; DNV, 2021) that the other three motions have a negligible impact on surge, sway, and yaw, as they do not generate forces in the direction of  $x$ ,  $y$ , and  $\psi$ .

**Assumption 2** *The DP capability considered in a static analysis is achieved under given operational conditions whenever the static balance of forces and moments in 3DOF holds.*

For simplicity, static methods were introduced by (IMCA, 2017), (DNV, 2021), and other classification societies. Those methods do not allow for accounting for hull, thrusters, and environment dynamics to reduce the number of input data, allowing for DP capability assessment at an early stage of ship design. Hence, based on 1st Newton's law, the ship in a balance between thrust forces vector and environmental forces vector is fixed in position or remains in motion at a constant velocity. Except that the second part of the law is neglected in that case.

To account for the dynamics of the DP vessel, the DNV-ST-0111 standard proposes a dynamic factor of 1.25 that the environmental forces are multiplied by in static analyses.

**Assumption 3** *The relation between power and thrust can be expressed as a quadratic function with satisfactory accuracy in the problem of thrust allocation, (Ruth, 2008; Valčić, 2020; de Wit, 2009).*

The above assumption is created for the purpose of QP implementation to optimal TA and is considered sufficient for optimization algorithm performance.

**Assumption 4** *The thrust constraints imposed by their physical limits, such as propulsion configuration and available power, can be approximated by a set of convex polygons.*

In QP, by definition, the constraints must be linear. Division of a non-linear constraint that could be imagined as circular regions (in the case of azimuth thrusters) into a significant amount of polygons that can be defined with linear equations is considered accurate enough. The accuracy can be increased with more polygons and the calculation time can be improved with fewer polygons.

**Assumption 5** *A vessel operating in DP mode is maneuvering at relatively low speeds (around 2 m/s) as stated in Skjetne et al. (2004); Skjetne (2005); Fossen (2021).*

The DP ship on site is considered stationary and therefore its speed is significantly below 2 m/s as explained in (Faltinsen, 1990; Fossen, 2021). The minimum speed at which the DP ship damping model is valid should include the current speed that is less than 1 m/s as proposed in (DNV, 2021). Moreover, thruster efficiency is significantly influenced by the relative speed of the water above the specified value. Concerning DP dynamic analysis, the speed suggested above gives unfeasible results.

**Assumption 6** *The position of the vessel operating in the presence of waves can be computed based on the composition of the wave-induced high-frequency and low-frequency motion, Faltinsen (1990); DNV (2021); Fossen (2021).*

In DPS only low-frequency motions are controlled. By filtering high-frequency motions in the observer, efficient DP control is possible. Moreover, while modeling wave loads in simulation, they are divided into 1st order wave (high) frequency loads, and 2nd order drift forces following the assumption. While the latter are approximately constant, the former have an oscillating character.

**Assumption 7** *A ship is considered to keep position if heading variation from set direction is within +/- 3° and footprint radius<sup>2</sup> is within 5 m, over a 3-hour window, (DNV, 2021).*

Each operation has its specific constraints concerning station keeping. Since developed methods and tools are meant to serve as a basis for database

---

<sup>2</sup>Maximum deviation radius,  $r_{\max}$  from original position ( $x = y = 0$ ), based on position  $x, y$  record over time, where  $r_{\max} = \sqrt{x_{\max}^2 + y_{\max}^2}$

expansion and to provide guidelines on DP assessment, the above assumption is adopted for the sake of conformity. Thus, when evaluating the DP capability with dynamic methods (simulation and experiments) and subsequently deriving a dynamic factor, this assumption serves as a definition of the DP capability.

**Assumption 8** *Thruster losses defined with DNV level 1 can be adopted to the remaining levels in the TA module.*

This assumption is based on the theory that the TA would be driven by DNV level 1 defined losses in a similar way as it would be by the actual losses. Hence, also assume that the DNV-ST-0111 standard gives a sufficiently accurate losses definition. The above is not justified in the literature. Expansion and further development of the decision support system would provide that proof. However, for the sake of research within the dissertation and with limited time, this assumption allows to simplify the validation procedure.

**Assumption 9** *During static and dynamic methods, only one weather scenario is analyzed at a time, as stated in (DNV, 2021).*

To assess DP capability, the most obvious approach is to analyze constant conditions and use them for comparison over all methods. This also has its reflection in real operations, as weather conditions usually change slowly, which allows the DP system to adjust. Hence, the assessment in an operation scenario will be valid independently of the changing nature of the real environment.

**Assumption 10** *Analyzing the influence of waves and currents on a ship as environmental disturbances is sufficient to evaluate the control system design and perform simulator validation.*

Since it was not feasible to perform model tests in a towing tank facility in the presence of wind, the study was carried out only for cases with current and waves. Since current and wind forces are correlated to fluid mechanics, they impact in a similar way. However, the latter are dependent on air velocity, which is usually much higher than the current and is also highly disturbed and noisy.

**Assumption 11** *The wave-induced ship motion is proportional to the sinusoidal wave amplitude, and the force acting on a hull due to second-order wave drift forces is quadratically proportional to the sinusoidal wave amplitude.*

The above is associated with a physical relation and parameters describing the fluid according to (Lloyd, 1998; Fossen, 2021).

## 1.7 Work outline

In the following pages, Dynamic Positioning Capability assessment is defined and methods of DP prognosis types are listed in Ch. 2. Subsequently, in Ch. 3, one can find a description of modeling of DP ships, such as disturbances modeling and hull and thrusters identification. Static and dynamic methods of DP assessment are explained in detail in Ch. 4 and Ch. 5 respectively. The approach to the problem of thrust allocation is presented in both cases with a full description. Mainly, quadratic programming is implemented; however, results are shown also for the application of NSGAII. Static results are presented in Ch. 4 with a comparison of both strategies to TA. In Ch. 5 all components of the DP control system are listed and discussed, comprising the observer, controller, and TA. All methods and results are presented in Ch. 6 and Ch. 7 where one can find dynamic analysis results and descriptions of applied methods. Moreover, in Ch. 7 a physical model in scale that was utilized in experiments is described together with the DP system used. Finally, all methods of DP Capability assessment and prognosis are compared in Ch. 8 with the final conclusions in Ch. 9.

# Chapter 2

## Dynamic positioning capability assessment

For the purpose of DP capability assessment in this study, the guidelines provided in the DNV-ST-0111 standard (DNV, 2021) are utilized. This approach is widely adopted by many design offices globally and is particularly specific in terms of the methods and empirical formulas it provides. However, the methods and tools developed by the author within the dissertation can also be applied to other standards, such as those outlined by (IMCA, 2017; ABS, 2021).

In the following sections, a brief summary of the DNV standard is given. Definition of different levels of prognosis is presented in Sect. 2.1. Sect. 2.2 and 2.3 describe static and dynamic approaches according to the standard. In Sect. 2.4 the problem of thrust allocation concerning all DNV levels is outlined. Finally, in Sect. 2.5 the DNV method is compared to other aforementioned methods (IMCA and ABS).

### 2.1 DP capability levels

According to (DNV, 2021), the evaluation of the DP capability is divided into three main levels. The higher the level, the more data is required and less guidance is given on its acquisition. Lower levels may be used in the preliminary stage of ship design (level 1, level 2), while level 3 is used in the advanced stage. The first two levels reduce to a problem of fulfilling (or not) a static balance between all forces (environmental and produced by

thrusters) answering if the ship will (or will not) keep position. Level 3, on the other hand, concerns the simulation in the time domain, where the ship is in a dynamic balance due to a dynamically changing environment and the dynamic response of a ship.

Level 1 is the most used among other levels and is a basis for class notation. As the procedure for calculating thrusters and environmental forces based on basic ship data is given explicitly in the standard (except for thrust allocation), this is the easiest way to predict the DP performance. Moreover, it allows for a fair comparison between designs.

DP capability analysis with DNV standard is also used to assess DP performance after a failure of a component of the propulsion system, especially for level 1. It could be a failure of the single thruster or generator, fire, or flooding of an entire section of the ship. Comparative analyses of those failure cases and the intact case are crucial information for the designer and are a decisive factor. This is also very often a classification society requirement in the case of a DP class ship to report DP capability under various failures.

Level 2 enables the introduction of more specific vessel data. In this level, the empirical formulas given in level 1 can be ignored and replaced by models of environmental and thruster forces determined with experimental or numerical methods. For example, wind forces are usually obtained through model tests in the wind tunnel or by using computational fluid dynamics (CFD) software. In some cases, data for a similar kind of ship can be used. A comparison between level 1 and level 2 wave models for a chosen ship is presented in Fig. 2.1. For that particular case, DNV provided a method for level 1 that shows high compliance with the numerical method of wave forces estimation.

The two aforementioned levels assume static balance between thruster forces and environmental forces. Whenever the balance holds, the ship is considered capable of DP. Level 3, on the other hand, concerning time domain simulation, accounts for thrusters, hull, environment, and DP system dynamics. Since in the remaining levels this is not included, DNV proposes a dynamic factor of 1.25 to account for the dynamics in levels 1 and 2 calculations.

In level 3, a judgment of the DP capability of the ship is made by the time record of the vessel position and heading, which can be plotted as presented in Fig. 2.2. The plot is called a vessel footprint and if it is within margins for a specified period of time, the ship is considered capable of DP (Asm. 7). Footprint shows the vessel's motions during a selected exposure

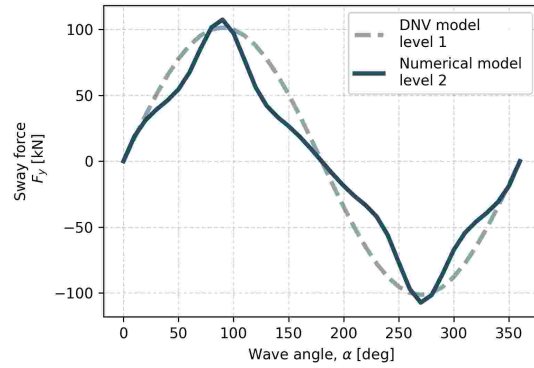


Figure 2.1: Wave force models comparison at sway motion for level 1 and 2

period. Based on the graph, position and heading variations can be measured and verified against the set DP limits (5 m radius of the footprint and 3°maximum heading variation), (DNV, 2021).

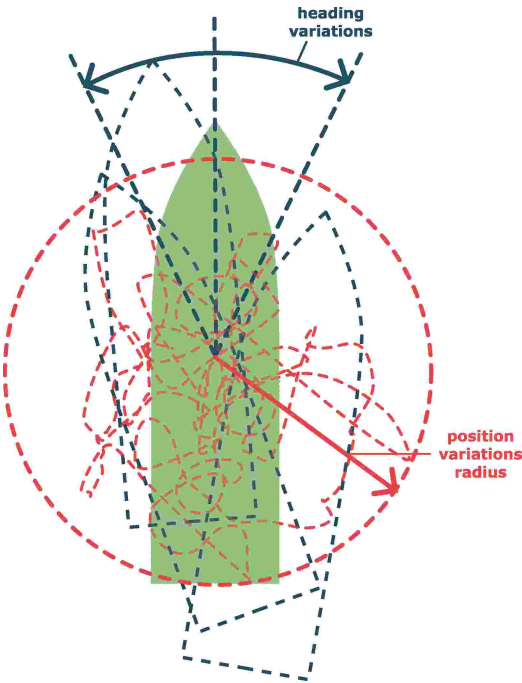


Figure 2.2: DP ship footprint

In level 3, designers have the freedom to propose the DPS and thrusters and hull models, which makes the prognosis dependent on many factors and harder to compare between designs, unlike in level 1. However, it allows valuable insight into vessel performance, which is closer to real operations. Moreover, it is considered more accurate since the prognosis is based on verified data, such as hull models identified numerically, for instance, rather than being defined with empirical formulas.

Analysis on all DP capability levels corresponds to predefined environmental conditions denoted with DP capability numbers (DP number), as given in Tab. 2.1. Those conditions are based on the Beaufort scale. Moreover, it is assumed that wind, current, and waves occur simultaneously and are coming from the same direction.

Table 2.1: Environmental conditions according to (DNV, 2021).

DP capability number	Beaufort description	Wind speed [m/s] *	Significant wave height [m]	Peak wave period [s]	Current speed [m/s]
0	Calm	0	0	NA	0
1	Light air	1.5	0.1	3.5	0.25
2	Light breeze	3.4	0.4	4.5	0.50
3	Gentle breeze	5.4	0.8	5.5	0.75
4	Moderate breeze	7.9	1.3	6.5	0.75
5	Fresh breeze	10.7	2.1	7.5	0.75
6	Strong breeze	13.8	3.1	8.5	0.75
7	Moderate gale	17.1	4.2	9.0	0.75
8	Gale	20.7	5.7	10.0	0.75
9	Strong gale	24.4	7.4	10.5	0.75
10	Storm	28.4	9.5	11.5	0.75
11	Violent storm	32.6	12.1	12	0.75
NA	Hurricane force	NA	NA	NA	NA

\* The wind speed is the upper limit of the mean wind speed 10 m above sea level for the given DP capability number. The given peak wave periods represent the 95% confidence interval found from the world wide scatter diagram.

For the purpose of conformity, the following coordinate system is adopted as depicted in Fig. 2.3, (DNV, 2021) and used throughout the dissertation.

The result of analysis with levels 1, 2, and 3 is a DP capability plot as presented in Fig. 2.4. The plot informs whether the ship maintained position at a given angle and DP number. All conditions inside the envelope plot (col-

ored in blue) as well as its outline are considered to fulfill the station keeping requirements. The prediction is performed for 36 environmental angles and 11 DP capability numbers, giving 396 cases in total. For static analyses, it will be proved that it is not computationally demanding; however, simulations will be much more time-consuming. Thus, in general, only selected cases are analyzed with level 3.

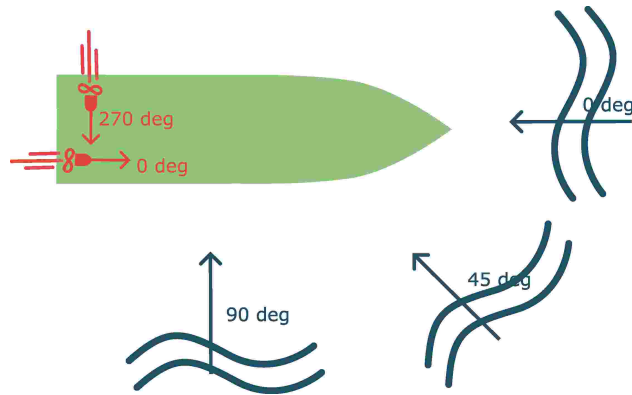


Figure 2.3: Coordinate system ( $x$ ,  $y$ ), environmental angle and thrusters orientation convention

DNV also specifies site condition levels (level 2 - site and level 3 - site) which allow ignoring predefined conditions (Tab. 2.1) and setting a specific environment, with no restrictions.

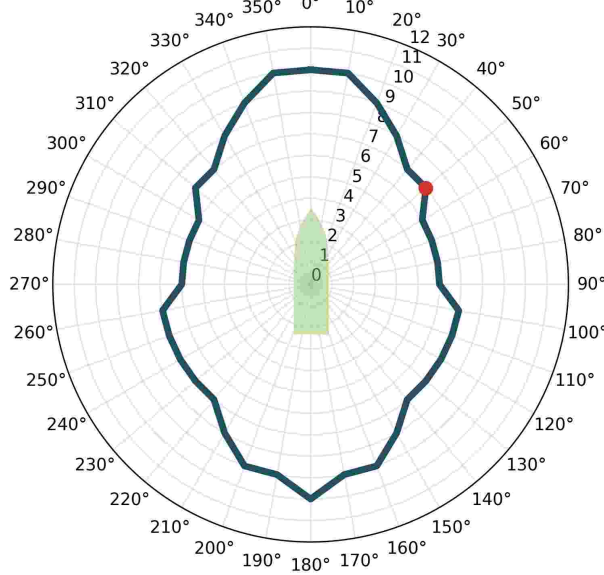


Figure 2.4: Exemplary DP capability plot

## 2.2 Static DP capability calculation

The DNV-ST-0111 standard gives empirical formulas for the calculation of environmental forces, thrust forces, and thruster losses, regarding level 1.

The formulas to calculate wind and current forces and moments are based on kinetic energy and Reynolds number properties (White, 2011) as well as basic ship data, Eq. (2.1),(2.2).

$$F_{x,y, \text{wind/current}} = \frac{1}{2} \rho_{w/a} v_{w/c}^2 A \cdot C_{\text{DNV}} \quad (2.1)$$

$$M_z, \text{wind/current} = f(F_{y,\text{wind/current}}, \alpha, L_{pp}, x_L) \quad (2.2)$$

where  $\rho_{w/a}$  - density of the medium (water or air) [ $\text{kg/m}^3$ ];  $v_{w/c}$  - speed of the medium (wind or current speed) [ $\text{m/s}$ ];  $A$  - projected area [ $\text{m}^2$ ] (in this case, a cross-section) of the considered body;  $C_{\text{DNV}}$  - nondimensional coefficient given by the DNV standard;  $L_{pp}$  - length of the ship between perpendiculars [m];  $x_L$  - center of projected longitudinal area above water or underwater [m].

In the representative Eq. (2.1) the  $C_{\text{DNV}}$  is an empirical formula dependent on the environmental angle,  $\alpha$  [ $^\circ$ ].

In case of waves, fairly complicated empirical formulas are given where the forces and moments depend on significant wave height,  $H_S$ , wave peak period  $T_P$ , gravitational acceleration,  $g$ , and dimensions and characteristics of the ship hull as given in Eq. (2.4) - (2.5).

$$F_x \text{ waves} = f(\rho_{\text{water}}, H_S, g, B, \alpha, \text{bow\_angle}, C_{\text{WLaf}}, T_P, L_{\text{pp}}) \quad (2.3)$$

$$F_y \text{ waves} = f(\rho_{\text{water}}, H_S, g, L_{\text{os}}, \alpha, T_P, L_{\text{pp}}) \quad (2.4)$$

$$M_z \text{ waves} = f(F_y \text{ waves}, X_{\text{Los}}, L_{\text{os}}, \alpha) \quad (2.5)$$

where  $B$  is the ship's breadth at waterline [m];  $\text{bow\_angle}$  is the angle between the vessel x-axis and a line drawn from the foremost point in the waterline to the point at  $y = B/4$  (ahead of  $L_{\text{pp}}/2$ ) on the waterline [ $^\circ$ ];  $C_{\text{WLaf}}$  is the water plane area coefficient behind mid-ship [-];  $L_{\text{os}}$  is the longitudinal distance between the foremost and aftmost points underwater [m] and  $X_{\text{Los}}$  is the longitudinal position of  $L_{\text{os}}/2$  [m]. For a selected ship case and DP number 6 (strong breeze), a set of plots of the environmental forces and moments is shown in Fig. 2.5. All plots have a sinusoidal character that is typical for a smooth and elongated object such as a ship. The thrust force as given in Eq. (2.6), diameter of the thruster propeller, and the corresponding coefficients defined by the DNV standard depending on the thruster type. The force calculated in that way is valid for the bollard pull conditions. Those are the conditions where the ship's speed is equal to zero.

$$T_{\text{nom}} = \eta_{\text{DNV}} (D \cdot P)^{\frac{2}{3}} \quad (2.6)$$

where  $T_{\text{nom}}$  is the nominal thrust [N];  $\eta_{\text{DNV}}$  is the thruster efficiency factor defined by the DNV standard and dependent on the thruster type [-];  $D$  is the diameter of the propeller [m] and  $P$  is the power delivered to the propeller [kW]. Fig. 2.6 presents saturation regions for different thruster types in a horizontal plane ( $x, y$  plane). The regions are possible thrust vector coverage. The azimuth thrusters and pods can rotate  $360^\circ$ . However, their saturation region is additionally limited by possible losses due to interactions with the hull or another thruster. Hence, the maximum thrust is limited more in selected zones. DNV standard distinguishes and defines azimuth thruster interactions such as thruster-thruster, hull-thruster, and thruster-dead thruster (switched off thrusters) interactions. The first type causes regions excluded from operation, forbidden zones, whereas the other two create losses and result in lowered efficiency zones, spoiled zones. DNV standard defines zones

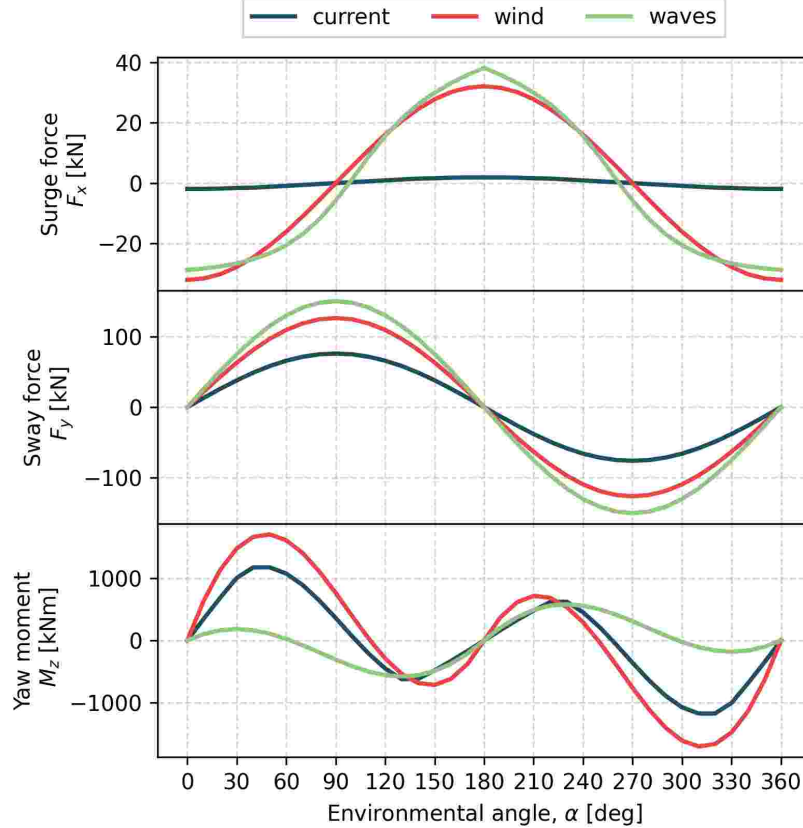


Figure 2.5: Environmental forces with DNV level 1 method - exemplary case

as dependent on the diameter of the thruster propeller,  $D$ , the distance to the obstacle (thruster or skeg),  $s$  and the thrust angle relative to the position of the obstacle,  $\beta_{\text{relative}}$ . The conventional propeller, on the other hand, is fixed (cannot rotate like the azimuth thruster). Hence, it has very limited possibilities of generating side force. Rudder enables side force; however, at zero speed, its efficiency is relatively low. Tunnel thruster regions are most restricted as this type of thruster can only produce a side force (in one direction). Nevertheless, those thrusters are very important in DP operations and greatly improve operability at low speeds as they generate a significant

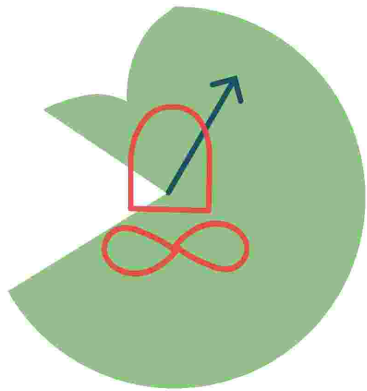
counter moment that balances the stern thrusters while producing a side force that is greatly desired in operation. Additionally, the DNV standard proposes ventilation losses of the thrusters due to propeller emergence above water caused by ship motion in the presence of waves. The empirical formula depends on the state of the sea and the propeller loading (thrust-to-propeller diameter ratio).

$$\beta_{\text{vent}} = f(D, T_{\text{nom}}, L_{\text{pp}}, T, z_{\text{thr}}, H_S, T_P) \quad (2.7)$$

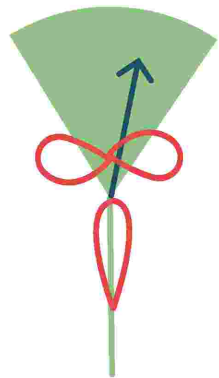
where  $\beta_{\text{vent}}$  is thrust loss due to ventilation [–];  $D$  is propeller diameter [m];  $T$  is draft and  $z_{\text{thr}}$  is the vertical position of the thruster [m].

According to the standard, level 2 and level 2-site can be based on other methods of determining forces in DP (experimental or numerical), but a hybrid approach could also be applied. For instance, thrusters' forbidden zones and spoiled zones could be estimated with the level 1 method, but environmental forces could be determined with numerical methods or model tests. Nevertheless, the approach is the same for both levels; static balance needs to be achieved to consider the ship to keep its position.

Azimuth thruster



Propeller with rudder



Tunnel thruster

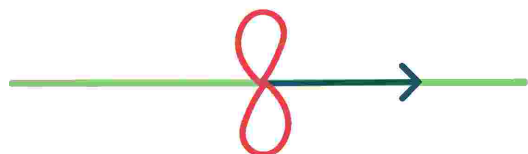


Figure 2.6: Thrust regions of different types of thrusters

## 2.3 Dynamic DP capability analysis

Level 3 and 3-site is realized with the time domain simulations. Simulations provide more information about the station keeping performance than the other DP capability levels, such as recordings of the vessel position, heading, speed, thrust, environmental forces, and many others.

According to DNV standard, DP capability level 3 is to assess the effect of dynamics on the DP performance including relevant dynamics of vessel, environment, actuators/thrusters, and DP control system.

According to the standard, DP control system may or may not be the same as it would be on the designed ship. However, it should include at least a control module, thrust allocation, and wave filter or state observer. Vessel motion shall be described by the equations of motion, including at least the following: vessel mass and inertia; frequency dependent added mass; frequency dependent potential damping; wind forces; current forces; wave forces and thruster forces.

Environmental forces (generated by wind, current, waves) are defined either through model testing or with numerical methods.

The standard states that as a minimum the wave forces shall include slowly-varying drift forces, Froude-Kriloff forces and diffraction forces (Faltinsen, 1990). Slowly-varying wave drift forces may be modeled employing quadratic transfer functions (QTF). In accordance with Asm. 6, simulation of the ship's position in time due to low-frequency wave excitation forces in presence of waves is to be considered. To account for the motion due to first-order wave forces one has to determine motion based Response Amplitude Operators (RAO's) experimentally or using potential theory respective software, transform to the time-domain and apply superposition as shown in Fossen (2021); Faltinsen (1990). A comprehensive guideline on modeling wind, current and wave loads can be based on (DNV, 2010).

Thruster models (including losses) should be defined either through model testing or numerical methods. They should also include the effects from propeller and motor dynamics and angular rate limits for azimuth thrusters and rudders.

## 2.4 Thrust allocation

The task of dynamic positioning comes down to achieving the balance between the environmental forces and thruster forces. In an ideal, so-called static situation, this would be enough for the vessel to keep position. In a dynamic, real environment where disturbances fluctuate in time, this balancing has to be supported with a control system. Nevertheless, in both static and dynamic analyses according to DNV standard, the balance has to be solved to distribute the thrust among the thrusters and set their orientation. Considering a planar motion of the ship according to Asm. 1, the balance equations are as follows.

$$\begin{aligned} \sum_{i=1}^N T_{xi} &= F_x \\ \sum_{i=1}^N T_{yi} &= F_y \\ \sum_{i=1}^N (-T_{xi} y_{thri} + T_{yi} x_{thri}) &= M_z \end{aligned} \quad (2.8)$$

where  $i$  is the identification of a thruster;  $T_{xi}$  and  $T_{yi}$  are unknown thrust vector components of  $i$ th thruster;  $x_{thri}$  and  $y_{thri}$  are  $i$ th thruster's coordinates and  $N$  in a number of thrusters.

Considering static balance  $F_x = -F_{x\text{env}}$ ,  $F_y = -F_{y\text{env}}$  and  $M_z = -M_{z\text{env}}$  are environmental forces and moment calculated based on level 1 and level 2 methods. In dynamic balancing, in level 3,  $F_x = F_{x\text{ctrl}}$ ,  $F_y = F_{y\text{ctrl}}$  and  $M_z = M_{z\text{ctrl}}$  are control forces and moment outputs from the DP controller.

In static calculations, the negative environmental forces need to be distributed among the thrusters. In simulation and real operation, environmental forces are not possible to measure explicitly; hence, control forces that are estimated to reject the environment are to be distributed.

Three equations concerning three degrees of freedom have a unique solution if the unknown parameters are also three, as implemented in (Tomera, 2012, 2014). However, in most cases, this problem has an infinite number of solutions in terms of thruster generated forces  $T_{xi}$  and  $T_{yi}$ ,  $\forall i$  since the DP-capable ships are usually over-actuated. Therefore, instead of solving the equations, the thrust is to be allocated while optimizing the chosen criteria (for instance, total power consumption), taking into account the balance

equation, Eq. (2.8) as one of the equality constraints and thrusters saturation as inequality constraints (as depicted in Fig. 2.6).

## 2.5 Collation of different methods of DP capability assessment

DNV standard (DNV, 2021) is one of the possible approaches to assessing the DP capability. Two other methods considered are those given by IMCA (IMCA, 2007) and ABS (ABS, 2021). All methods require solving the thrust allocation problem, leaving the choice of the algorithm to the user of the guidelines.

In Tab. 2.2 a comparison of different methods is given. The comparison concerns only a static DNV method level 1 based on empirical formulas, as IMCA and ABS do not distinguish levels.

Among the considered methods, ABS offers a comprehensive methodology for the empirical estimation of thrust interactions. It may be taken into account in DNV level 2, where the thruster interactions can be user defined. Both DNV and ABS propose thrust relation to power with an exponent equal to 2/3. For environmental forces calculations, both ABS and IMCA refer to positions in the relatively old literature and define environmental conditions different from those of DNV; therefore, results cannot be directly compared.

Table 2.2: Comparison of different methods of DP capability assessment

Subject	DNV	IMCA	ABS
Environmental conditions	Based on Beaufort scale	IMCA defined for North Sea	Same as IMCA
Wind and current forces	Empirical formula $f(\rho_{w/a}, v_{w/c}, A, \alpha, L_{pp}, x_L)$	Empirical formula $f(\rho_{w/a}, v_{w/c}, A, \alpha, L_{pp}, C_{c/w})$ , $C_{c/w}$ are current or wind coefficients to be defined based on wind tunnel tests, CFD or similar ship	No formula given but a reference to (Benham, 1997)
Wave forces	Empirical formula as given with: Eq.(2.4) - (2.5)	Data for similar vessel is scaled according to the method suggested in (English and Wise, 1975)	Are to be defined based on ship wind tunnel tests, CFD or similar ship
Thruster forces	Empirical formula $f(P \cdot D)^{\frac{2}{3}}$	$f(rpm^2)^*$ in addition thrusters efficiencies are provided	$f(P \cdot D)^{\frac{2}{3}}$
Thruster interactions	$f(s, D, \beta_{relative})$	No guideline given	$f(s, D, \beta_{relative})$ however standard gives comprehensive methodology to account for different kinds of interactions

\* where  $rpm$  are propeller revolutions

# Chapter 3

## Modeling and identification of DP ship

The models of thrusters and environment used in static analyses, DNV level 1, were presented in the previous section in a generic way, only to show dependencies. More detailed definition with empirical formulas is given in the standard DNV-ST-0111. In static analyses (level 1, 2, and 2-site) ship (hull and thrusters) dynamics and environment dynamics are not modeled. When considering simulation (DNV level 3 and 3-site) however, those components need to be taken into account and identified. This is accomplished within the dissertation with numerical methods such as computational fluid dynamics.

The simulation of DP operations can be divided into two key components: the design of the control system and the modeling of the ship and its surrounding environment. This modeling is essential not only for the accurate simulation of real-world conditions but also for providing the identified models necessary for the effective design of the DP control system, controller in case of MPC, and nonlinear passive observer. Model identification is a critical prerequisite for DP simulation and constitutes a fundamental part of the proposed decision support system.

Considering that results from the experiments on a physical model of a ship in scale are utilized, the same ship in scale is also used in the simulator for validation purposes. In other words, simulations are performed on a scaled ship, however the identification procedure and DPS structure is the same, whether it is a full scale ship or a model. Therefore proposed DSS is universal.

In this chapter in Sect. 3.1, first the physical model that is the object

chosen for the purpose of research (and DSS establishment) will be presented. In Sect. 3.2 a simulation mathematical model of the hull and thrusters will be identified, based on literature. The method of parametric identification performed within the dissertation will be shown in Sect. 3.3 together with the results and discussion. Finally, in Sect. 3.4 the method for the identification of disturbances will be briefly discussed.

### 3.1 Physical model of a ship

A Multi-Service Vessel (MSV) model in scale of 1:36 was used in experiments as shown in Fig. 3.1 Main particulars of the model are presented in Tab. 3.1. The model was equipped with two stern azimuth thrusters and two bow tunnel thrusters as presented in Fig. 3.2 and Fig. 3.3. All particulars of the hull and thrusters are given in Apx. A, (Tab. A.3 and A.5), in full scale. In the appendix, the thrusters layout is also shown in Fig. A.4.

Table 3.1: MSV model main particulars in scale 1:36

Input value	Unit	Value in model scale
$L_{pp}$	[m]	2.74
B	[m]	0.65
T	[m]	0.18
m	[kg]	239.1
$I_z$	[kg m <sup>2</sup> ]	132.0
D - azimuth thruster	[mm]	80
D - tunnel thruster	[mm]	76



Figure 3.1: MSV model in scale 1:36



Figure 3.2: MSV model in scale 1:36 - azimuth thrusters

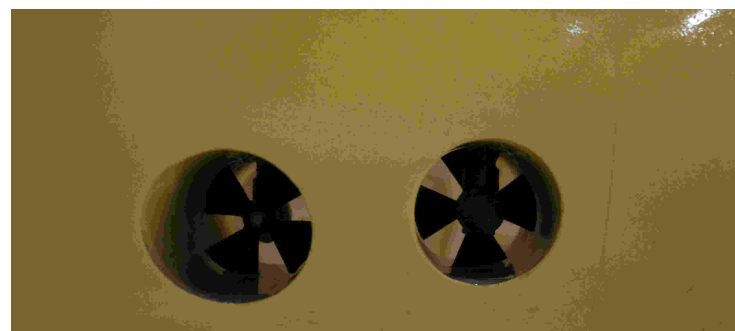


Figure 3.3: MSV model in scale 1:36 - tunnel thrusters

To correctly model the ship, buoyancy and mass distribution on the ship were modeled according to Froude number similarity law. This physical relationship will not be discussed here, the reader may find a comprehensive explanation in (Lloyd, 1998).

For the purpose of nonlinear passive observer design that was implemented in the DPS of the physical model, an identification of hull mathematical model parameters was performed. The identification of the hull by model tests was possible by recording the input signals (thruster propeller revolutions and thruster orientation) and the position of the ship in time. Subsequently, in an iterative process, the mathematical model was fitted using a dedicated simulator developed for this particular purpose. The thruster models were identified in a bollard pull test <sup>1</sup> at the towing tank. Identification procedure with model tests will not be extensively described here. The reader may refer to (Kraskowski and Grymajlo, 2021) and similar procedures given in (Skjetne et al., 2004; Skjetne, 2005) and ITTC procedures. Additionally, for control of the ship motion with thrusters, parameters of their models were identified experimentally.

## 3.2 Mathematical model of a ship

In the DP experiment and simulation, the mathematical model of the ship concerning both hull and thrusters needs to be formulated to proceed with parametric identification. In this section, first the hull model will be discussed and subsequently the thruster model.

The concept of a mathematical model of a ship hull is depicted in Fig. 3.4.

---

<sup>1</sup>Test at zero speed and a set propeller revolutions. In a full-scale ship it is performed by pulling a mooring line attached to the hull on one side and to the pier on the other, with dynamiter in between. Usually predicted for tugs and fishing vessels at low speeds.

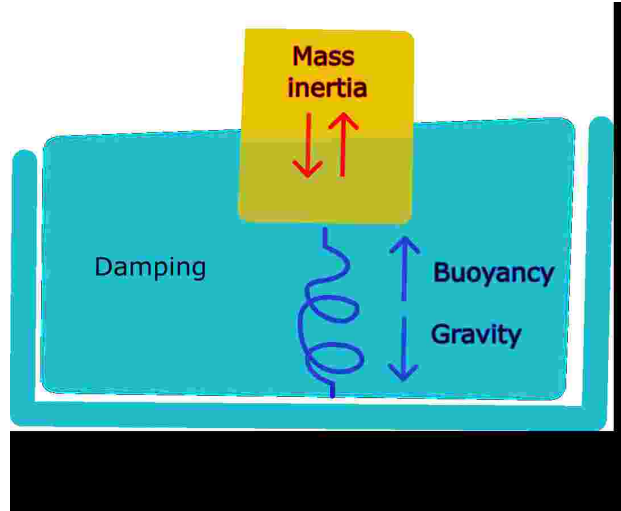


Figure 3.4: Concept of a ship hull model as mass-spring-damper system

The buoyancy and gravity forces work against each other, and whenever the ship is out of equilibrium due to waves, those restoring forces reflect spring behavior. Since the hull is in a liquid environment, the hydrodynamic damping occurs due to the ship motion through water caused by waves, currents, and other disturbances or loads. Naturally, the accelerating and decelerating mass of the hull needs to be accounted for as a second Newton's law force.

The figure only shows heave motion; however, damping also applies to other motions. Considering Asm. 1 the spring effect can be omitted as heave motion is not included in DP analyses within the dissertation. This leaves mass and damping as components of the mathematical models as also given by the following Eq. (3.1).

$$\begin{aligned} \dot{\boldsymbol{\eta}} &= \mathbf{R}(\psi)\boldsymbol{\nu}, \\ \mathbf{M}_{RB}\dot{\boldsymbol{\nu}} + \mathbf{M}_A(\omega)\boldsymbol{\nu}_r + \mathbf{C}_{RB}(\boldsymbol{\nu})\boldsymbol{\nu} + \mathbf{C}_A(\boldsymbol{\nu}_r)\boldsymbol{\nu}_r + \mathbf{D}(\boldsymbol{\nu}_r)\boldsymbol{\nu}_r &= \boldsymbol{\tau}_{thr} + \boldsymbol{\tau}_{env}, \end{aligned} \quad (3.1)$$

where:  $\boldsymbol{\eta} = [x, y, \psi]^T \in R^3$  is the position vector in the global reference frame;  $\boldsymbol{\nu} = [u, v, r]^T \in R^3$  is the velocity vector in the body-fixed reference frame (fixed to the ship);  $u$  is the speed along axis x, [m/s],  $v$  is the speed along axis y, [m/s] and angle  $r$  about axis z, [°/s];  $\boldsymbol{\nu}_r = \boldsymbol{\nu} - \boldsymbol{\nu}_c$ , where  $\boldsymbol{\nu}_c$  is the current velocity vector;  $\mathbf{M}_{RB}$  and  $\mathbf{C}_{RB}$  are the inertial and Coriolis-centripetal

matrices of a rigid body;  $\mathbf{M}_A(\omega)$  and  $\mathbf{C}_A$  are the frequency-dependent added mass inertia and Coriolis-centripetal matrices related to added mass;  $\mathbf{D}$  is the viscous damping matrix containing linear and quadratic damping;  $\boldsymbol{\tau}_{thr}$  is the thruster forces vector;  $\boldsymbol{\tau}_{env} = \boldsymbol{\tau}_{wind} + \boldsymbol{\tau}_{waves} = [F_{x\text{ env}}, F_{y\text{ env}}, M_{z\text{ env}}]^T$  is the environmental disturbances (wind and waves) forces vector at  $x, y$  axis and moment about z axis;  $R(\psi)$  is the rotation matrix from body to global reference frame.

The matrices that appear in Eq. (3.1) are as follows:

$$\mathbf{R}(\psi) = \begin{bmatrix} \cos(\psi) & -\sin(\psi) & 0 \\ \sin(\psi) & \cos(\psi) & 0 \\ 0 & 0 & 1 \end{bmatrix}, \quad (3.2)$$

$$\mathbf{M}_{RB} = \begin{bmatrix} m & 0 & 0 \\ 0 & m & 0 \\ 0 & 0 & I_z \end{bmatrix}, \quad (3.3) \quad \mathbf{M}_A(\omega) = \begin{bmatrix} A_{11}(\omega) & 0 & 0 \\ 0 & A_{22}(\omega) & A_{26}(\omega) \\ 0 & A_{62}(\omega) & A_{66}(\omega) \end{bmatrix}, \quad (3.4)$$

where:  $m$  is the ship's mass [kg] and  $I_z$  is the ship's moment of inertia about z axis [ $\text{kg m}^2$ ];  $A_{11}, A_{22}, A_{66}$  are frequency-dependent added mass coefficients in surge (along x axis), sway (along y axis) and yaw (about z axis) motion, [kg], [ $\text{kg m}^2$ ] respectively;  $A_{26} = A_{62}$  is the frequency-dependent added mass coefficient in sway motion due to rotation about z axis [kg m].

$$\mathbf{C}_{RB}(\nu) = \begin{bmatrix} 0 & 0 & -mv \\ 0 & 0 & mu \\ mv & -mu & 0 \end{bmatrix}, \quad \mathbf{C}_A(\nu) = \begin{bmatrix} 0 & 0 & A_{22}v - A_{26}r \\ 0 & 0 & A_{11}u \\ A_{22}v + A_{26}r & -A_{11}u & 0 \end{bmatrix}, \quad (3.5)$$

$$\mathbf{D}(\nu) = \begin{bmatrix} -X_u - X_{|u|u}|u| & 0 & 0 \\ 0 & -Y_v - Y_{|v|v}|v| - Y_{|r|v}|r| & -Y_r - Y_{|v|r}|v| - Y_{|r|r}|r| \\ 0 & -N_v - N_{|v|v}|v| - N_{|r|v}|r| & -N_r - N_{|v|r}|v| - N_{|r|r}|r| \end{bmatrix}, \quad (3.6)$$

where:  $X_u, Y_v, N_r$  are hydrodynamic linear coefficients components on  $x, y$  and  $\psi$ , [kg/s], [kg/s] and [ $\text{kgm}^2/\text{s}$ ];  $Y_r$  and  $N_v$  are transverse linear coefficients of drag in sway and moment in yaw respectively resulting from the movement in yaw and sway respectively, [ $\text{kgm/s}$ ];  $X_{|u|u}, Y_{|v|v}, N_{|r|r}$  are hydrodynamic

quadratic coefficients components on  $x$ ,  $y$  and  $\psi$ , [kg/m], [kg/m] and [kgm<sup>2</sup>];  $Y_{|r|r}$ ,  $N_{|v|v}$  are transverse quadratic coefficients of drag in sway and moment in yaw respectively resulting from the movement in yaw and sway respectively (coupled motions) [kg m] and [kg]. The terms  $Y_{|r|v}$ ,  $Y_{|v|r}$ ,  $N_{|r|v}$  and  $N_{|v|r}$  are force and moment coefficients due to double coupled motions at both the sway velocity and the yaw rate simultaneously [kg] and [kg m].

Eq. (3.1) assumes the possibility of isolating all three force vectors associated with hull, thrusters, and environment into separate independent loads. The influence between all three is distributed separately on each element. For example, the interactions between thrusters and the hull are credited to the thrusters' models rather than to the hull damping force.

The forces due to motions of the hull, on the other hand, are coupled in some cases (except for mass and inertia forces associated with the rigid body dynamics). This is due to the non-linear character of motion-induced forces in a fluid environment.

The presented ship model, Eq. (3.1) is sufficient for further analysis of DP performance in various environmental conditions and can be applied in the DP simulator for the purpose of DP capability evaluation. However, identification of some parameters, such as coefficients of coupled damping coefficients and consideration of Coriolis matrix components, adds a certain complexity to the problem.

### 3.2.1 Hull utility model

To allow application to a DP simulator for prognosis purposes and to DPS in experiments, the model can be further simplified as given in Eq. (3.7). Considering operations at speeds close to zero, Coriolis forces could be neglected, and only mass, added mass, and damping matrices can be accounted for in the utility model.

$$\begin{aligned}\dot{\boldsymbol{\eta}} &= \mathbf{R}(\psi)\boldsymbol{\nu}, \\ \mathbf{M}_{RB}\dot{\boldsymbol{\nu}} + \mathbf{M}_A(\omega)\boldsymbol{\nu}_r + \mathbf{D}(\boldsymbol{\nu}_r)\boldsymbol{\nu}_r &= \boldsymbol{\tau}_{thr} + \boldsymbol{\tau}_{env},\end{aligned}\tag{3.7}$$

The mass and inertia of the rigid body of the ship is assumed as a known value since the mass and its distribution (Fig. 3.5) can easily be derived in the early stage of the design of the ship. Hence, the parameters  $m$  and  $I_z$  are known.

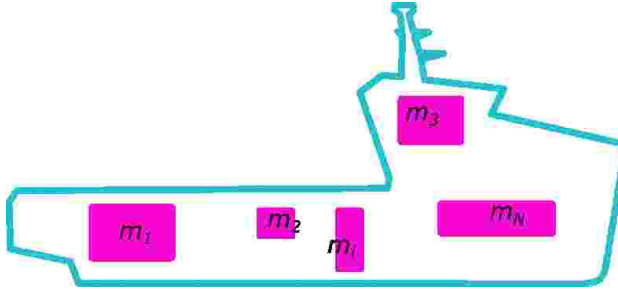


Figure 3.5: Concept of mass distribution

The added mass is defined as a virtual mass that, if it were added to a ship, would justify the additional acceleration or deceleration of it. This can be visualized as in Fig. 3.6, where  $f_1, f_2$  denoted different wave peak frequencies. However, one needs to understand that the added mass is not a physical mass of the displaced water but rather a mass that would correspond to the force due to the hydrodynamic effect caused by accelerating the hull and disturbed fluid around it.

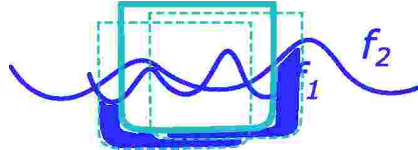


Figure 3.6: Added mass meaning concept

The viscous damping matrix stores coefficients that describe forces induced on the hull due to viscous flow. Those contain both pressure and viscous forces and introduce non-linearity to the mathematical model of the ship.

The damping model given in Eq. (3.6) was reduced based on (Fossen, 2021) and additional studies carried out by the author. In (Fossen, 2021) the author proposes an application of current coefficients instead of the damping coefficients given in Eq. (3.6). The former are derived for only the velocities of the sway ( $v$ ) surge ( $u$ ) and yaw ( $r$ ). That approach implies that the coupled motion of sway and yaw, coefficients  $Y_{|r|v}|r|$ ,  $Y_{|v|r}|v|$ ,  $N_{|r|v}|r|$ , and  $N_{|v|r}|v|$  are not considered and thus neglected. Furthermore, based on the identification of a damping model of a Cybership II benchmark model given in Skjetne et al. (2004); Skjetne (2005), the analysis of the influence of double-coupled motion

damping coefficients can be performed. Such analyses have been performed within the dissertation for a reasonable range of sway and yaw velocities. Based on the analysis, the double coupled motion damping forces are minor compared to isolated motion forces. Based on both references (Fossen, 2021; Skjetne et al., 2004) and the analysis, the damping model can be simplified to the form given in Eq. (3.8) with satisfactory accuracy.

$$D(\nu) = \begin{bmatrix} -X_u - X_{|u|u}|u| & 0 & 0 \\ 0 & -Y_v - Y_{|v|v}|v| & -Y_r - Y_{|r|r}|r| \\ 0 & -N_v - N_{|v|v}|v| & -N_r - N_{|r|r}|r| \end{bmatrix}. \quad (3.8)$$

Fig. 3.7 presents a simple concept of the influence of hull drag in sway motion. As depicted, due to the sway motion with speed  $v$ , a force  $F$  and moment  $N$  are generated on the hull, which shows a coupled character of the phenomena. As can be concluded, no coupling occurs in the  $x$  component of the damping matrix (and the added mass matrix), as the ship is symmetrical at that axis.

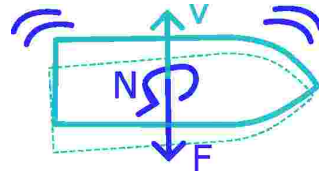


Figure 3.7: Concept of damping model

The hull mathematical model presented in Eq. (3.7) was used in a non-linear passive observer in the experiments and also in the DP simulator for hull dynamics modeling and for MPC design within the dissertation.

### 3.2.2 Thruster utility model

For the purpose of control and thrust allocation in the experiment and DP simulator design, the actuators are modelled. Thrusters' propellers are the generators of the thrust. Propellers for ship industry purposes are designed on the basis of a wing foil theory (White, 2011). The propeller blades are specifically designed and optimized to produce an efficient thrust force induced by the pressure difference between the suction and pressure sides of the propeller blade. The value of this thrust force will depend on the blade

speed (in the case of an aircraft, it will depend on the plane speed) and the propeller pitch.

There are many other geometrical parameters that influence the propeller performance; therefore, for each new propeller, identification needs to be performed for ship design purposes.

The blade speed is a result of the angular speed of the propeller usually expressed as rpm (revolutions per minute). From wing theory and basic hydrodynamic nature dependencies, which can be found in (White, 2011), the thrust force will depend on the square of rpm, Eq. (3.9). The below model is used both in experiments and simulations.

$$T_{\text{eff}} = f(n^2) = a_{\text{thr}} \cdot n^2 \quad (3.9)$$

where  $T_{\text{eff}}$  is effective thrust [N] at the revolutions of the propeller  $n$  [rpm] and  $a_{\text{thr}}$  is the non-dimensional coefficient of the polynomial.

The determination of the coefficient  $a_{\text{thr}}$  is equivalent to the identification of the thruster model for DP purposes.

The value of  $a_{\text{thr}}$  is determined in the so-called bollard pull test (ITTC, 2021), on a ship model in scale equipped with thrusters and at zero speed in a towing tank facility or utilizing numerical, CFD tools, as was done within the dissertation. The bollard pull force is also called the net thrust or the effective thrust.

An exemplary thruster model in the form of a polynomial is shown in Fig. 3.8.

A thruster in DP operation usually suffers some additional losses. Thrusters' losses may occur due to interactions of the thruster with the hull surface or another working thruster. This is depicted in Fig. 3.9 and Fig. 3.10 respectively.

It is possible to identify thruster-hull losses depending on the thruster angle; however, they usually do not fit any mathematical formulation (polynomial or other mathematical representation). They can be applied to a simulation or static analysis, giving ranges where mathematical (usually linear) functions can be applied. Thruster-thruster losses are much more complex and nonlinear. Therefore, the forbidden zone is applied to completely avoid the interaction. Those analyses were carried out within the dissertation; however, it was not used further in the study, assuming its application in the future development of the simulator.

Another important physical quantity that needs to be modeled in DP

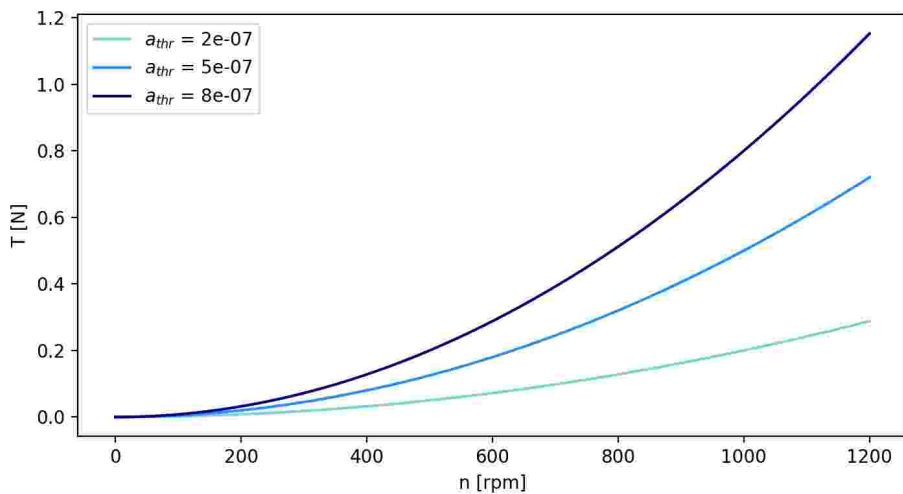


Figure 3.8: Exemplary thrusters models in scale 1:36

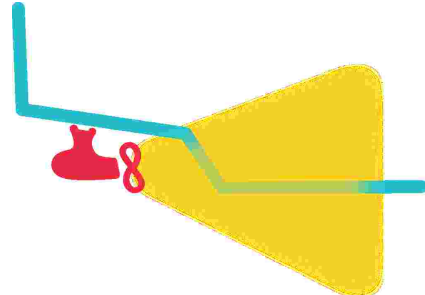


Figure 3.9: Thruster - hull interactions concept

simulation is thruster rate of change of revolutions and azimuth angle change in time.

Both are modeled according to Eq. (3.10) and (3.11) assuming time-domain simulations with a carefully selected time step to capture the dynamics of the whole system (in the case of simulation in model scale, it was 0.05 seconds).

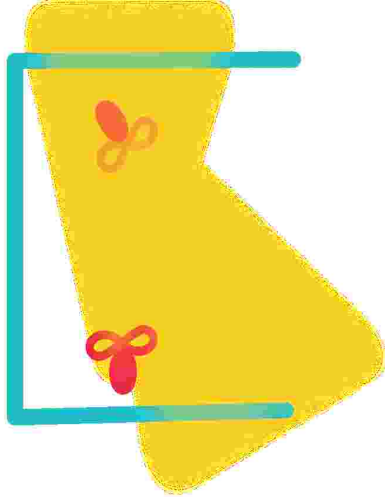


Figure 3.10: Thruster - thruster interactions concept

$$\dot{n} = \frac{n_{\text{set}} - n}{T_{\text{const},n}} \quad (3.10)$$

$$\dot{\beta} = \frac{\beta_{\text{set}} - \beta}{T_{\text{const},\beta}} \quad (3.11)$$

where  $n_{\text{set}}$ ,  $\beta_{\text{set}}$  are the set values of rpm and azimuth thruster angle, respectively, set by the DP control system;  $T_{\text{const},n}$  and  $T_{\text{const},\beta}$  are time constants.

The time constant is the parameter for tuning the rate of the propeller rpm and azimuth thruster angle change. This value is usually known from the thruster supplier and is correlated with mechanical and physical constraints such as the mass inertia of the propeller or azimuth thruster itself, the electrical motor capabilities, or structural strength issues. The values that were adopted in the simulator were selected to match the capabilities of the thrusters in the experiment, for validation purposes.

### 3.3 Ship mathematical model numerical identification

Accurate estimation of the ship's hull mathematical model can be achieved through model tests; however, these tests are often costly and time-consuming.

An alternative approach involves the use of computational fluid dynamics methods. Specifically, employing CFD to determine the hull damping model of a DP vessel has the potential to significantly enhance prediction accuracy compared to traditional empirical methods. This approach, therefore, holds considerable promise for improving the reliability of DP performance predictions in offshore operations and supporting informed decision-making during the ship design phase.

Within the dissertation, a numerical method of parametrical identification of ship's hull damping model and thrusters models was developed and results were compared with experimental identification. This step significantly contributed to the design support system, allowing the running of the DP simulation and potentially ensured a more accurate prognosis. A procedure for identifying the mathematical model of the DP ship is given in (Skjetne et al., 2004; Skjetne, 2005) and it concerns a ship model in scale 1:70. Within the paper, the added mass was determined with analytical formulas, and the sway and surge damping was performed by towing the model at constant speeds. In the case of yaw damping, an adaptive estimate was applied to a free-running model with the propulsion system.

Identification can also be made based on full-scale trials (Meng et al., 2023) maneuvers, recordings, and the use of intelligence optimization algorithms. Another branch of mathematical model determination methods is the estimation method, such as the Kalman filter and its extensions and improvements (Witkowska et al., 2020); this requires a real object where both inputs and outputs can be measured. In case of luck with the model test data or full-scale trials, one has to refer to simplified analytical methods, numerical methods, or use a similar case.

In (Sen and Vinh, 2016) the authors refer to an analytical approach to calculate the added mass based on the equivalent ellipsoid method. The authors also provide a comparison with strip theory (with Lewis transformation mapping) and experiment. The discrepancies compared to the experiment are -10% and -5% for the ellipsoid and strip theory methods, respectively, in the case of sway motion and -30% and -20% in the yaw motion. In surge, only the ellipsoid method was compared with the experiment with a 3% discrepancy. In (Maliky et al., 2019, 2020) the authors introduce added mass estimation with CFD viscous flow tool *Ansys Fluent* and provide a comparison with the ellipsoid method. The discrepancies between the ellipsoid method and the CFD for the added mass in the surge are 7%. In (el Moctar et al., 2022) the authors also use CFD software (*STAR CCM+* and *OpenFOAM*)

for added mass determination and compare it to the analytical approach, showing around 1% differences in surge, swing, and yaw.

In (Fossen, 2021) the author proposes using current coefficients as damping coefficients in the DP ship model. Those are a result of the model tests in the wind tunnel; however, in the literature, an extensive database of those coefficients is also available for different types of ship. In (Fossen, 2021; Skjetne et al., 2004; Lindegaard, 2003) the authors suggest that a linear damping model for DP simulation purposes is sufficient. However, for the purpose of controller design, a non-linear model is more adequate based on (Værnø et al., 2019). In (Maliky et al., 2019, 2020) the authors present results and methodology of viscous damping estimation with CFD tool *Ansys Fluent* of a simple-shaped barge. However, they propose time-efficient 2D analysis and extrapolation to 3D.

A certain gap in the literature is the lack of a description of a comprehensive approach to CFD analysis related to the estimation of the ship's damping model. In addition, comparisons with experimentally obtained data are rarely presented.

The mathematical model of the thrusters can be identified with either experimental and numerical methods, or defined empirical formulas can be used as proposed in (DNV, 2021). From these three, numerical methods, using computational fluid dynamics (CFD), have been proven to combine high accuracy, very detailed insight, and a relatively simple and time-efficient approach (Piekło et al., 2024).

In (Suijkerbuijk, 2013; Zhang and Jaiman, 2019) an extensive description of the setup of CFD computations for a ducted propeller open water analysis is given in comparison to experiments. The procedure for testing the effective thrust on a physical ship model equipped with multiple azimuth thrusters is given by (Arditti and Tannuri, 2012; Arditti et al., 2015). Three different methodologies for modeling thruster-hull interactions using CFD are given in (Koop et al., 2017). In (Maciel et al., 2013) various numerical setups of the CFD simulation in search of thruster-hull interactions were described and tested.

In (Bosland et al., 2009) the authors present a comparison of azimuth thruster interactions with another azimuth thruster using a panel method as a numerical solution, resulting in good compliance with experiments. A broad range of thruster arrangements is tested to find thruster-thruster interactions in (Zhou and Zhao, 2020).

### 3.3.1 Numerical tools

For the purpose of determining the unknown parameters of the mathematical model formulated in Eq. (3.7), numerical tools are employed:

- *Ansys Aqwa* - potential flow simulation software where added mass is determined.
- *STAR CCM+* - viscous flow simulation software where viscous damping and thrust are determined.

In this method, simulation setup, results, and discussion will be presented concerning the identification of added mass elements given in Eq. (3.4), damping coefficients given in Eq. (3.8) and rpm polynomial coefficient, Eq. (3.9).

In the case of viscous flow simulations both for thruster models and damping model parameters identification, a finite volume method was applied as explained below.

### 3.3.2 Hull model parametric identification

For hull, both added mass and viscous damping parameters were identified within the dissertation, with an emphasis on the latter as it included developed methods within the dissertation.

The determination of the added mass elements of the matrix given in Eq. (3.4) was carried out with simulations based on potential theory, in *Ansys Aqwa* software on a full-scale ship.

For hull added mass identification, the default settings were used with 5176 mesh elements in the hull, Fig. 3.11 and a maximum wave frequency of 0.361 Hz. The simulation was performed through a range of wave frequencies. The response of the hull to these sinusoidal waves was calculated, and the added mass was determined for each. The added mass curve is obtained as a function of frequency. By extrapolating to zero frequency,  $\mathbf{M}_A(\omega \approx 0)$  based on (Fossen, 2021) the added mass of the hull is found. The results are scaled down for comparison with the model test results.

The results of the numerical simulations are presented in Fig. 3.12 together with the values obtained from the experimental identification. The quantities are given in Tab. 3.2. Taking into account the total mass (mass of rigid body and added mass), the discrepancies are about 1.0 % and 1.7 % for the surge and sway directions, respectively; however, for the yaw direction,

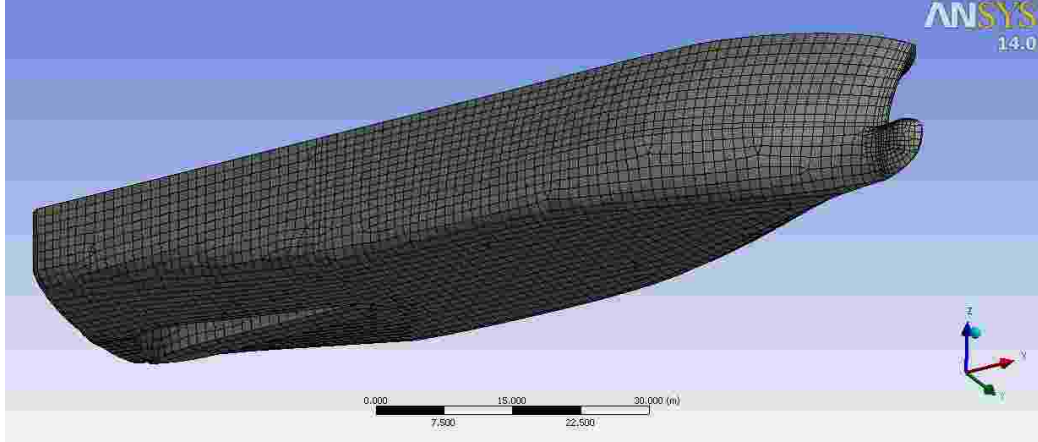


Figure 3.11: Meshing of the hull surface of MSV in *Ansys Aqwa*

the difference is about 30.6 %. In (Sen and Vinh, 2016) the highest discrepancy also resulted for the yaw motion; however, in the opposite direction. This may be caused by inaccurate assumptions during dynamic balancing of the physical model, which may result in slightly different moments of inertia  $I_z$ . Since dynamic balancing of the model in yaw was not possible in the model tests, a value resulting from dynamic pitch balancing was adopted. Although longitudinal mass distributions are dominant on inertia for both pitch and yaw, this approach may not be valid even for a slender ship due to the contribution of the vertical and transverse mass distributions. Moreover, the parameters obtained in experiments may be influenced by the fact that the center of rotation of the model was different during testing than its center of gravity, which ultimately results in a different inertia relative to the gravity point.

Table 3.2: Added mass inertia of MSV in model scale

Coefficient	Potential flow	Model tests	Coefficient	Potential flow	Model tests
$A_{11}$	13	11	$A_{26}$	24	-
$A_{22}$	157	151	$A_{66}$	72	24

The determination of viscous damping elements of the matrix  $\mathbf{D}$  given in Eq. (3.8) was carried out with viscous flow simulations in *STAR CCM+*

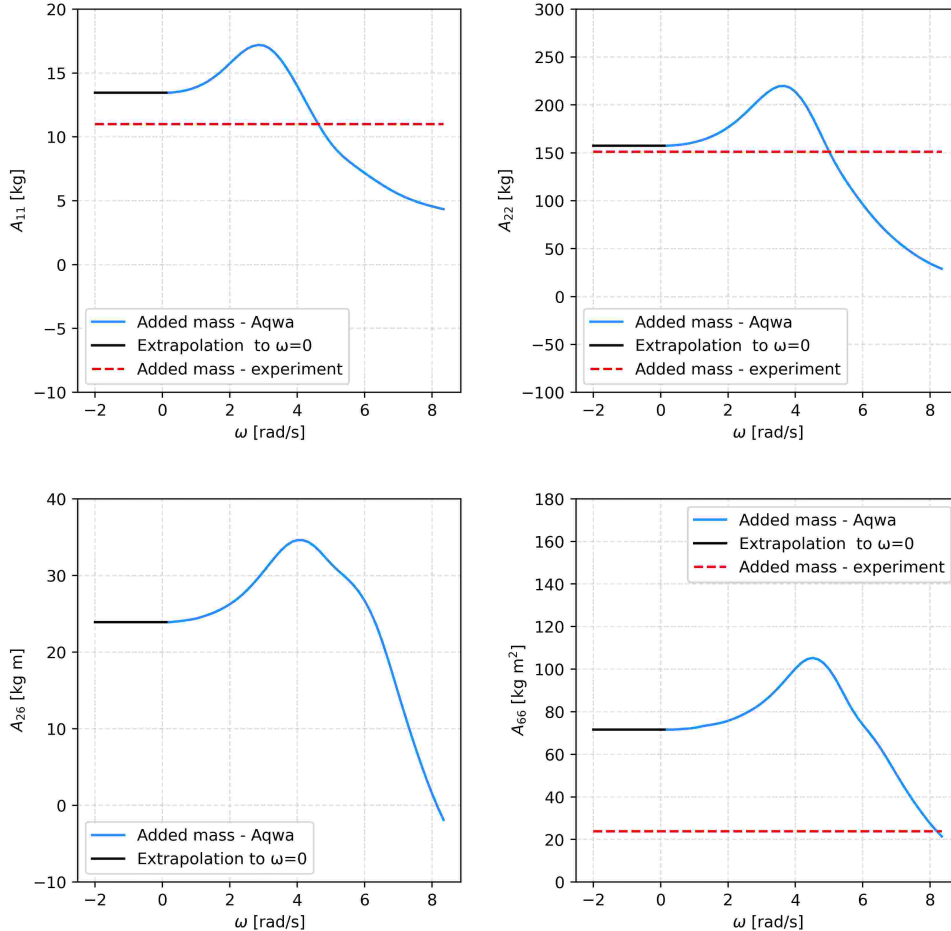


Figure 3.12: Added mass resulting from the potential flow numerical simulation compared to the values resulting from the experiments

software in ship scale of 1:36.

Fig. 3.7 in Sect. 3.2 shows a concept of how the simulation was performed in an exemplary case of sway motion. The hull model was fixed in planar motion, which means that no movement was allowed on the z surface. However, the water was moving in relation to the hull with speed v. In this way, the force (F) and the moment (N) marked in the figure and generated on the

hull due to flow can be calculated. Fig. 3.7 also shows (with a dashed line) what would happen if the hull were released.

With the simplified damping model given by Eq. (3.8) the numerical analyzes reduce to only three kinds of simulation. By conducting simulations for several constant velocities in surge, sway and yaw separately, a nonlinear characteristic (damping curve) results in surge  $F_u$ , sway  $F_v$ ,  $F_r$  and yaw  $M_v$ ,  $M_r$  allowing identification of coefficients given in Eq. (3.8). It has a quadratic character; therefore, it can be further approximated with a quadratic polynomial by the least squares method, which in turn determines the coefficients given in Eq. (3.8).

The simulations were conducted within the dissertation, on an element mesh of around 5 mln (Fig. 3.13) and of turbulence model: realizable  $k-\epsilon$  with boundary layer model: *Two-Layer All  $y+$  Wall Treatment*. Three types of analyses are performed according to Tab. 3.3.

Table 3.3: CFD analysis set-up

Motion	Speed	Range	Degrees of freedom	Measured forces and moments
Surge	$u$	-1 - 1 m/s	pitch, heave	$F_u$ [N]
Sway	$v$	0.1 - 0.42 m/s	roll, heave	$F_v$ [N], $N_v$ [Nm]
Yaw	$r$	9 - 18 deg/s	roll, heave	$F_r$ [N], $N_r$ [Nm]

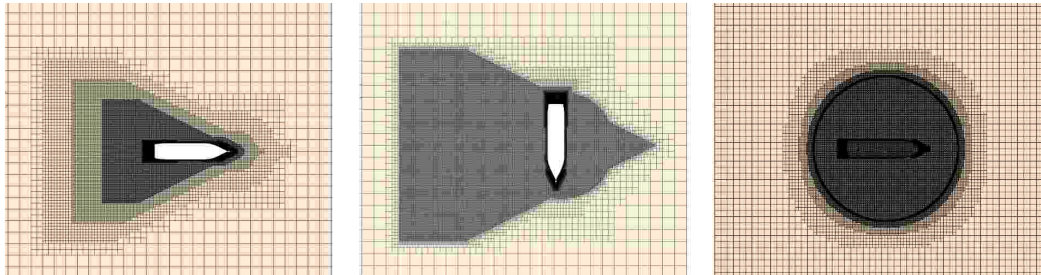


Figure 3.13: Computational mesh on the free surface in surge, sway and yaw

Fig. 3.14 shows the simulation of a yaw motion. In this case, the water rotates anticlockwise, while the hull remains fixed.

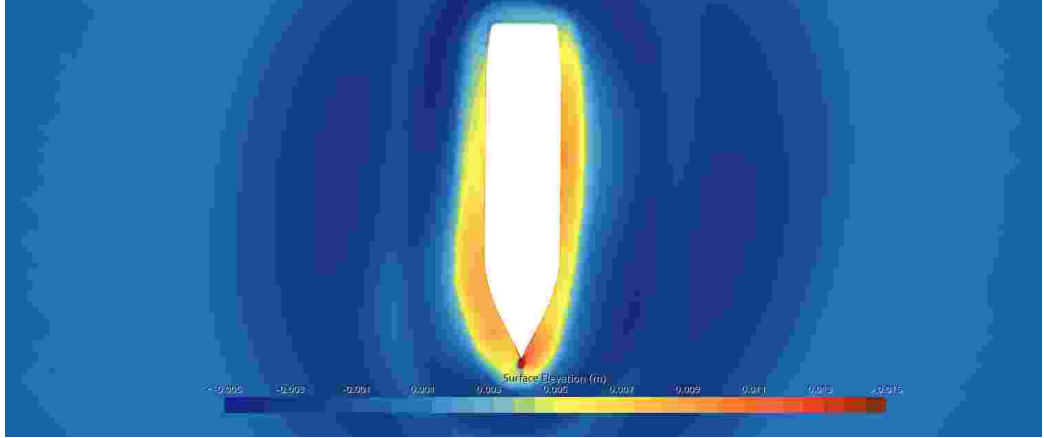


Figure 3.14: Numerical identification of viscous damping in yaw motion by CFD simulation

The viscous damping resulting from the simulation is shown in Fig. 3.15 together with the fitted model and the model obtained from the experimental identification. The parameter quantities are given in the Tab. 3.4. The numerical results for low speeds and force  $F_r(r)$  and moment  $N_v(v)$  give a model curve that double-crosses zero on each side. For better estimation of the model behavior for those cases, analyses within a denser region around zero may improve the results.

The numerical results are in a range higher than the experimental identification for the purpose of the simulator architecture based on (DNV, 2021). However, a typical DP ship will maneuver at maximum speeds around  $u=v=2$  m/s (Fossen, 2021),  $r=3$  °/s corresponding to 0.33 m/s and 18 °/s on model scale (1:36), respectively. In that range, both parameters describe a relatively close model. However, the model obtained through numerical analyzes can only be fairly evaluated on the basis of a DP simulation using both the alternative models and output comparison.

Comparison of each coefficient given in Tab. 3.4 and Tab. 3.2 should be treated carefully since in the experiment the coupled motion coefficient was not determined. Therefore, the coefficients on the main diagonal of the damping matrix in Eq. (3.8) compensate for that in the model determined by experiment.

Table 3.4: Damping coefficients resulting from the polynomial curve fitting into the numerical results for MSV in model scale

Coefficient	Numerical analysis	Experiment	Coefficient	Numerical analysis	Experiment
$X_u$	-1.457	-0.9	$Y_{ r r}$	-0.034	-
$X_{ u u}$	-5.067	-10.1	$N_v$	-4.502	-
$Y_v$	-1.333	-6.2	$N_{ v v}$	67.308	-
$Y_{ v v}$	-145.613	-240.1	$N_r$	-0.061	-0.012
$Y_r$	0.033	-	$N_{ r r}$	-0.067	-0.096

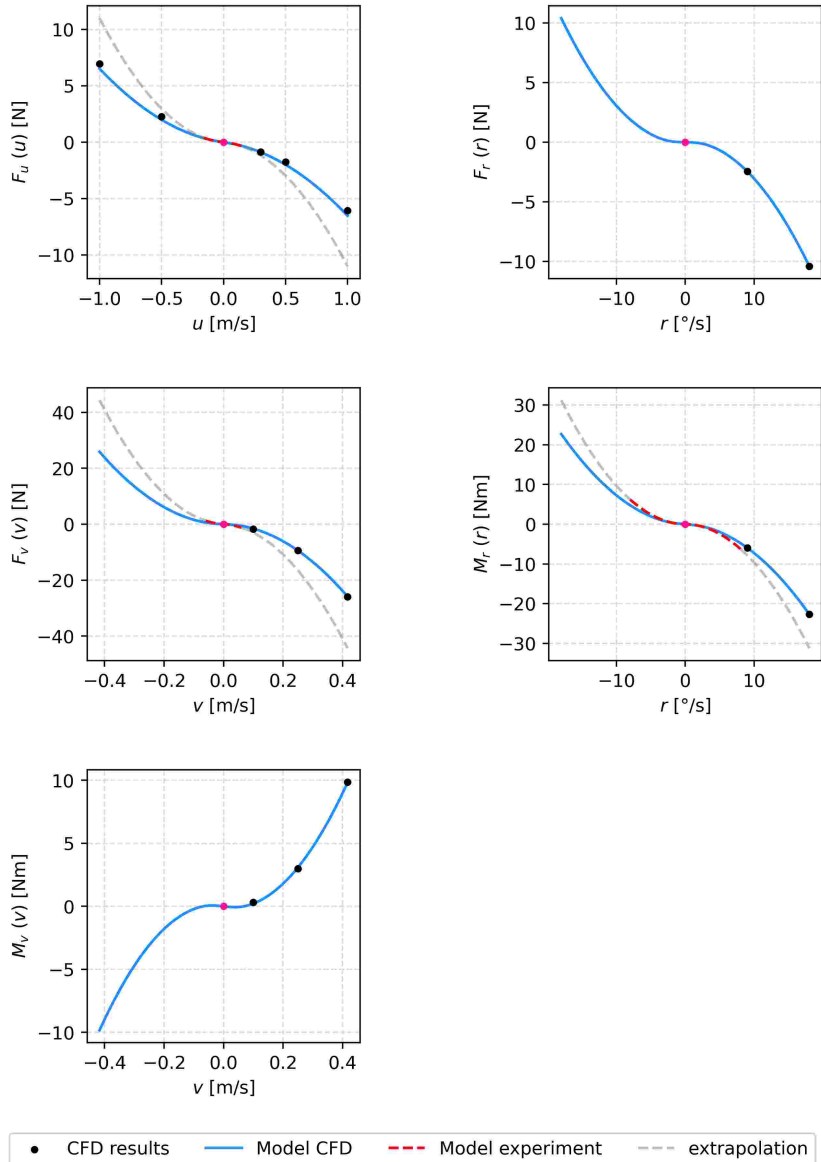


Figure 3.15: Damping force and moment resulting from the numerical simulation with fitted model in comparison to the model of parameters determined by experiment

### 3.3.3 Thrusters models parametrical identification

Added mass can be identified on the basis of ship motion in waves, at different wave frequencies. By extrapolating the resulting added mass function of frequency, the zero-frequency added mass for a ship hull in DP operations is found according to (Fossen, 2021). Parameter  $A_{11}$ ,  $A_{22}$ ,  $A_{26} = A_{62}$  and  $A_{66}$  are to be identified for the wave frequency equal to zero ( $\omega = 0$ ).

The thrusters parameter identification is accomplished within bollard pull conditions. A bollard pull test, either carried out with experiments or computed with numerical simulation, is based on the same method, considering both the procedure of testing and post-processing of the results.

The test and numerical simulations were carried out on a ship model in scale at zero speed, fixed but with the possibility of measuring the force vector on the planar surface (in the  $x$  and  $y$  directions). Both the thrust and the resistance of the hull were measured (in experiment) or calculated (in CFD) within the dissertation. The resultant force value and angle were calculated based on all the measured (in experiment) or simulated (in CFD) forces.

Two azimuth thrusters were installed on the hull model in the  $0^\circ$  orientation (thrust directed forward). Several revolutions were set, and the thrust and force of the propeller on the hull were measured for each setup.

Additionally, in simulation, few other angles of the thrusters were analyzed at a constant rpm to identify thruster losses due to thruster-hull interactions and thruster-thruster interactions. Those, however, were not applied in the DP simulator. However, the results may be of use for a regular engineer in a design office; hence, they will be shown and discussed within the dissertation.

The simulations were conducted on an element mesh of around 45 mln (Fig. 3.16) and of turbulence model: realizable  $k-\epsilon$  with boundary layer model: *Two-Layer All  $y+$  Wall Treatment*.

First, a comparison was made between the numerical analysis and the experimental results Fig. 3.17. The bollard pull condition at forward-directed thrusters was the subject of comparison. Two thrusters were installed on the hull, and a bollard pull force divided by two was taken for further post-processing. A range of revolutions was selected between 500 rpm and 1500 rpm. Since the propeller has a small diameter (80 mm), very high revolutions were required to achieve a sufficient Reynolds number (to fulfill the similarity law). However, the maximum revolutions of the electric motors (installed

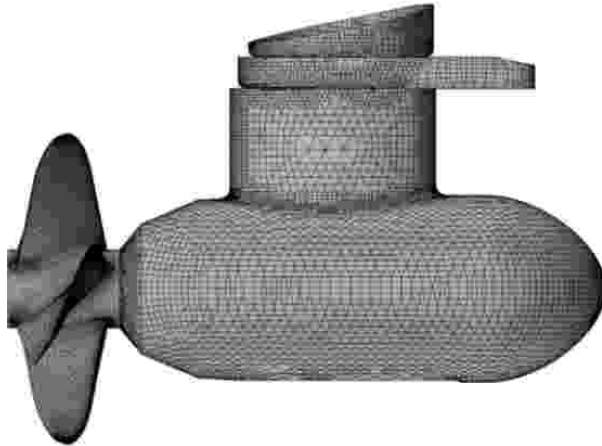


Figure 3.16: Numerical mesh on the MSV ship azimuth thruster

in the model) were 3000 rpm with a 2:1 transition. Hence, the resulting Reynolds number at 500 rpm was  $4.8 \cdot 10^4$ .

Additionally, three higher revolutions were computed in CFD to be used later for interactions analyses. Based on the results, a thruster model can be identified, as shown in Fig. 3.17.

Additionally, Fig. 3.18 presents the relative error between the model identified numerically and the one identified with the bollard pull test. The absolute value of the error is relatively small (2.5% - 6.5%), and decreases with the propeller speed. The values measured in the experiment are significantly low (less than 20 N). Therefore, the accuracy of the measurement (dynamometer) has a greater impact on the results. In addition, a low Reynolds number may cause some overestimation of the results. However, this value of accuracy is considered sufficient for the validation of the CFD method.

Based on the model identified and validated with CFD, the rest of the analyses (losses) continue with CFD methods. Results of identification of thrust losses and thruster interactions are given in Apx. B.

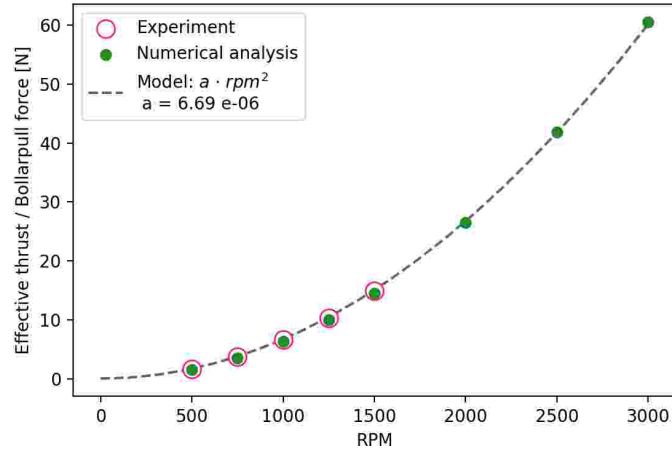


Figure 3.17: Results of bollard pull tests

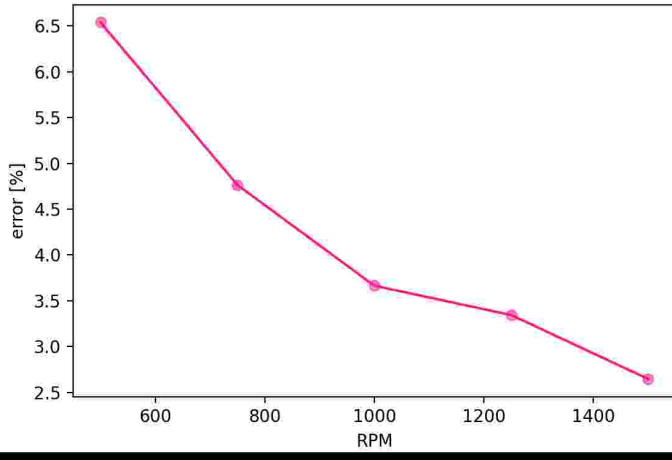


Figure 3.18: Numerical results error relative to the experimental results

### 3.4 Modeling disturbances

Generally, when considering DP operations at sea, three types of disturbances are recognized. Those disturbances are generated by the surrounding environment, water and air. Wind and current influence the above-water part and the underwater part of the ship in the same manner; the only difference is the fluid density between water and air. The force acting on the ship in

both cases is lift and drag. Waves influencing the ship are related to a two-phased fluid, a mixture of water and air, and are accounted differently than the other two disturbances.

Modeling disturbances comprise wind, current, and wave force modeling. In (Aydin et al., 2022) the authors present both empirical and numerical approaches, with validation with experiments for all the types of disturbances mentioned. The paper proves good compliance of the numerical results for the wind and current loads with the experiments. Wave loads, on the other hand, show lower conformity. However, it should be noted that the experimental results are often uncertain to some extent. The general empirical approach proposed by (DNV, 2021) generally shows an overestimation of the forces since it also includes a dynamic factor of 1.25 to them (to account for actuators' dynamics in static analyses).

In (van 't Veer and Gachet, 2011), the authors present a developed dynamic factor for better accuracy in estimating wave loads. In (Yan et al., 2018) one analyses whether different wave spectra (with the same wave height and period) influence DP performance. The authors proved that the discrepancies are significant. This leads to a conclusion that a dynamic factor applied to a static DNV-defined approach should also account for the specific wave spectrum. Both papers use numerical software to calculate wave loads.

### 3.4.1 Current

Changes in current direction and speed over a period of 12 hours. Therefore, current is considered constant in DP operations when designing the DP control system. Hence, DP simulation can be carried out in  $v_c = const.$ . Additionally, in places where DP operations are held, the speed of current is relatively small (maximum 1 - 2 m/s). As given in Eq. (3.7) a reference speed,  $\nu_r$  (relative to water, not to earth) is included in the mathematical model. This means that the current speed is already accounted for in the mathematical model as a damping force and no external loads due to current are introduced in  $\tau_{env}$ .

### 3.4.2 Wind

Unlike the current, the wind has a very noisy character. Wind direction and speed are never constant. However, it may seem stable as multiple measurements of mean speed and direction over a period of a few hours can

be almost the same. This can be noticed by simple observation of the sea surface.

In case wind load models are not available (for example, in an early stage of ship design), coefficients defined by well-recognized (Blendermann, 1994) can be used where empirical formulas for a range of different types of vessels are given.

In general, in DP operations, wind loads are dominant; hence, a feed-forward of those forces is highly valuable and can significantly improve the control. However, within the dissertation, wind loads are not considered in simulation, as they were not modeled in experiments.

Within the dissertation, the wind loads were not modeled in the DP simulator, as it was not possible to perform a DP experiment on a physical model with the wind modeled in the towing tank. Therefore, validation was not possible, and thus no wind was applied according to Asm.10.

### 3.4.3 Waves

In case of modeling loads due to air motion, different scaling laws apply in comparison to a multi-phase liquid. It was not feasible to keep both scaling laws in the physical model in scale. This concerns the preservation of the Froude and Reynolds numbers, (Lloyd, 1998; White, 2011).

Waves result from friction between the moving air and the sea surface. Over a longer period of time (hours to days) and at a sufficient fetch (few to hundred kilometers) waves build up. This developed sea can be described as a spectrum of sinusoidal wave frequencies. In other words, the elevation of the sea surface in time can be defined as a sum of many sinusoidal waves of characteristic periods, amplitudes, directions, and random phases. This spectrum describes an irregular wave. For engineering purposes, the irregular waves are simplified to a unidirectional representation of sea state, which makes predictions more conservative due to the concentration of wave energy in the primary direction.

For DP control purposes, wave loads are generally divided into first-order wave frequency loads and second-order slowly varying loads. The former are characterized by a short (wave) period and high load values as opposed to the latter, which are relatively small with a dominant magnitude of mean drift force, which is treated as a constant in DP analyzes. Formulas for modeling those wave loads in time-domain simulation are presented in Eq. (3.12) = (3.4.3), (Fossen, 2021).

$$F_{\text{wave,Iorder}} = \sum_{k=1}^N A_{\text{rao,Iorder}_k} \sqrt{2S_{\text{wave}_k} \Delta\omega} \cos(\omega_k t + \phi_{\text{rao,Iorder}_k} + \phi_{\text{rand}_k}) \quad (3.12)$$

$$F_{\text{wave,IIorder}} = \sum_{k=1}^N A_{\text{rao,IIorder}_k} 2S_{\text{wave}_k} \Delta\omega \quad (3.13)$$

$$F_{\text{wave}} = F_{\text{wave,Iorder}} + F_{\text{wave,IIorder}} \quad (3.14)$$

where  $N$  is the total number of  $k$  frequencies in a selected range;  $A_{\text{rao,Iorder}_k}$  and  $A_{\text{rao,IIorder}_k}$  are force Response Amplitude Operators (RAO) and force Quadratic Transfer Function (QTF) respectively of a sinusoidal wave of amplitude 1 m at selected frequencies  $\omega_k$  of a given range;  $S_{\text{wave}_k}$  is the wave spectrum in function of frequency;  $\omega_k$  is angular wave frequency;  $\phi_{\text{rao,Iorder}_k}$  is the first order force phase lag at  $\omega_k$ ;  $\phi_{\text{rand}_k}$  is randomly selected phase in the normal distribution from a range between  $-\pi$  to  $\pi$  at  $\omega_k$  and  $t$  is actual simulation time.

The frequency range is carefully selected to cover a range where the response of the ship is significant. Lower and higher frequencies where ship response is minor (close to zero) are neglected as they do not contribute to the total wave force.

In numerical modeling, the above expressions are utilized to calculate the total wave load ( $F_{\text{wave}}$ ). The given formulas are valid for each degree of freedom considered (in the case of DP it is surge, sway, and yaw). The wave spectrum  $S_{\text{wave}}$  of any wave can be modeled using simple formulas recommended by respected ITTC procedures with three input parameters  $H_S$ ,  $T_P$ , and  $\gamma$ , where  $H_S$  is a wave significant height, a mean of 1/3 of the highest waves observed over a period of time, (Faltinsen, 1990),  $T_P$  is the peak period at which the energy spectrum has its peak. A parameter  $\gamma$  defines the wave energy distribution over frequencies. Higher values correspond to a narrower spectrum bandwidth with a dominant modal frequency and are typical for regions with limited area, while lower values describe open ocean waves ( $\gamma = 1$ ) where the distribution of energy over different frequencies is more uniform. For a full explanation on wave mechanics and its modeling, one can refer to (Lloyd, 1998).

Even though a wave over time is always unique in an observation or measurement period in given stable conditions, the spectrum of many such waves will be almost identical. In other words, for the same wave spectrum, an infinite number of different wave runs can be generated that can be characterized by a random seed. In Eq. (3.12) cosine expression with time  $t$ , angular frequency  $\omega$ , and phase allows transformation of the spectrum to a signal in time, which in turn allows one to perform a simulation in the time domain.

The remaining parameters to be identified numerically or experimentally are RAO values of force amplitude and phase ( $A_{\text{rao,Iorder}}$ ,  $\phi_{\text{rao,Iorder}}$ ,  $A_{\text{rao,IIorder}}$ ) as a function of frequency and wave angle.

RAOs are associated with the response of a ship to a sinusoidal wave of a given frequency and wave amplitude equal to 1m. Knowing RAO of a ship is equal to knowing its response to any wave conditions, with respect to Asm. 6. Once RAO is identified as a function of frequency, that RAO can be directly utilized to calculate a response for any given sea spectrum. In other words, knowing RAO allows for analyses of ship responses (motions, velocities, accelerations, forces) in any sea conditions. Therefore, it is important to select frequencies to capture the response of the ship and, at the same time, to cover the wave spectrum. For example, if the peak of response is close to or within the peak of the spectrum, the response force to that wave will be magnified. Analogically, even though the response is significant for some frequencies, some waves (described by wave spectrum) will not affect the ship, causing only a minor response. This has to do with resonance. A very comprehensive explanation of this concept can be found in (Lloyd, 1998; Fossen, 2021).

RAO can be identified experimentally by carrying out multiple test runs at a few (usually around 10) sinusoidal waves of different frequencies and of the same amplitude at chosen wave angles and zero speed. Values of interest are measured (for instance, surge force), and the RAO curve is built as a fraction of the measured value to the regular wave amplitude at the measured frequency range. The numerical experiments are carried out analogously. With the utilization of potential flow software, such analyses can be done in a relatively short time with results of a sufficient compliance with experiments. A matrix of corresponding angles (from  $-180^\circ$  to  $180^\circ$ ) and frequencies is an output of the software or a result of the experiment. By interpolating through that matrix, entering with a current angle (at a current time of the simulation) the wave a RAO in function of frequency is found. That can be

further fed to a DP simulator and post-processed with formulas Eq. (3.12) and Eq. (3.13) to simulate wave loads in time. As already mentioned, magnitudes of II order wave drift forces are much lower than magnitudes of I order wave frequency forces, although the former are assumed constant in time, while the latter oscillate around zero. Therefore, the superposition of wave loads is the first-order harmonic forces with an offset of magnitude of second-order drift force. As an example, Fig. 3.19 shows both the I- and II-order forces for two irregular wave periods applied in the DP simulator (on model scale) within the scope of the dissertation and based on Eq. (3.12)-(3.4.3). In model tests, a physical wave is modeled with the wave-maker. The input signal from the wave-maker control is an inverse Fourier transform of a selected sea spectrum on the model scale with a selected random seed.

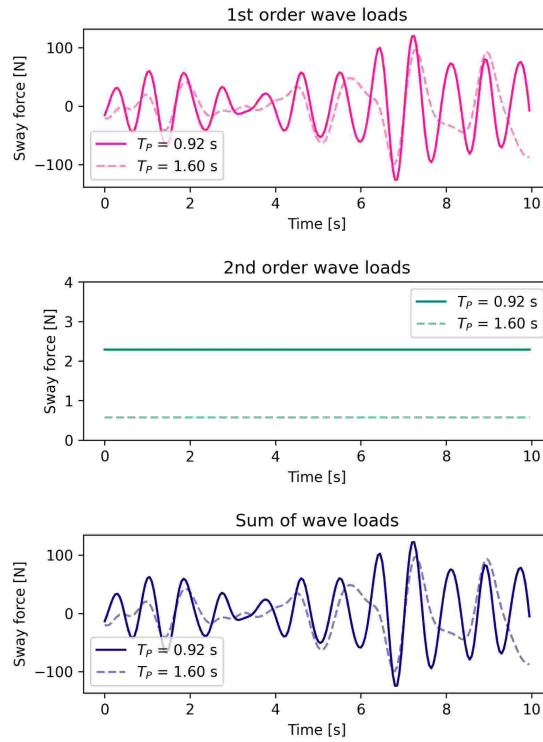


Figure 3.19: Wave loads at  $H_S = 4$  cm, in scale 1:36

# Chapter 4

## Static DP capability calculation

The static analyzes within the dissertation are conducted based on the DNV-ST-0111 standard and considering the level 1, level 2, and level 2-site that it defines. The standard proposes procedures and empirical formulas for calculating environmental forces and thruster-generated forces (as introduced in Ch. 2); however, it does not specify which thrust allocation algorithm should be applied or how to apply it. As the majority of the DP vessels are over-actuated systems, an optimization algorithm to the TA problem needs to be implemented.

Based on the literature review discussed in Sect. 1.1, two optimization algorithms were selected to represent two significantly different approaches to solving the TA problem. The first was quadratic programming, employing a gradient-based approach, and the second was the non-dominated sorting genetic algorithm II, as a metaheuristic method designed for highly nonlinear problems.

In Sect. 4.1, the optimal thrust allocation problem is defined and possible objectives are discussed. Two chosen optimal TA algorithms (QP and NS-GAII) concepts and procedures of application are described in Sect. 4.2 and Sect. 4.3 respectively. Further, results of static DP analyses are presented in Sect. 4.4 and a summary is given in Sect. 4.5.

### 4.1 Optimal thrust allocation

As already stated in Ch. 1, thrust allocation in dynamic positioning is an efficient distribution of a control force or, in static analyses, a counteracting

environmental force, among the thrusters, aiming to reject the environmental disturbances.

One or more objectives can be considered at the same time. Usual choices concerning static analyses are power minimization, fuel consumption minimization (which relates to power), minimization of position error, or minimization of tear and wear of the thrusters (Johansen and Fossen, 2013; Gao et al., 2019). Although the last would not be applicable to the static analyses but to the dynamic.

Decision variables are usually thrust forces that are later translated to thruster angles and propeller revolutions. Nevertheless, the choice of those variables will eventually depend on the applied TA method. The same applies to the constraints, although an obvious constraint is the physical capabilities of the thrusters, such as saturation, forbidden zones of the azimuth thrusters, and fixed direction of the force produced by the tunnel thrusters. Proposed decision variables, constraints and corresponding objective function formulations can be found in (Ruth, 2008; Wang et al., 2018; Lu et al., 2021; Tuo et al., 2021; Raghunathan et al., 2023; Wei et al., 2024).

If minimizing power, objective function could be a relation between power and thrust. Then the constraints would be imposed on the decision variables that are thrusts. This is the simplest and most intuitive way, as the static balance, that is an equality constraint in this case, is defined with forces such as thrust and environmental forces. The problem defined that way could be treated with QP, with some necessary simplifications.

However, an alternative approach could be implemented, where the power and thruster angle would be the decision variables. The problem would be then solved without simplifications. That would, however, imply utilization of a different method such as NSGAII where a multi-objective, nonlinear problem could be constructed.

Both algorithms, QP and NSGAII, will be presented in subsequent sections.

## 4.2 An approach based on quadratic programming

In this section, a step-by-step implementation of the quadratic programming algorithm as optimal thrust allocation to the DNV method is given. Decision

variables, constraints, and objective function are provided, concerning three different types of thrusters.

### 4.2.1 Decision variables

Considering the Eq. (2.8) introduced in Section 2.4, a vector of decision variables  $\mathbf{u}$  is given as in Eq. (4.1).

$$\mathbf{u} \stackrel{\text{def}}{=} [T_{x1} \ T_{y1} \ T_{x2} \ T_{y2} \ \dots \ T_{xN} \ T_{yN}]^T. \quad (4.1)$$

where  $T_{xi}$  and  $T_{yi}$  are forces generated by the  $i$ th thruster in [N], considered as control inputs.

The choice of thruster forces is not arbitrary but is subject to constraints resulting from propulsion type and respective mount points (location) in the considered coordinate frame. Hence, the following inequality and equality constraints need to be taken into account.

### 4.2.2 Inequality constraints

Invoking Asm. 4 allows one to preserve the linear nature of the constraints by utilizing linearization mechanisms. This applies to the constraints resulting from the use of azimuth thrusters, propellers with rudders, and tunnel thrusters.

**Azimuth thrusters** There are three types of constraints of the azimuth thruster that arise from their operational restrictions. First is a thrust maximum saturation zone. Second is a lowered thrust efficiency zone resulting from the thruster directing its flux (flushing) towards a skeg or another dead (not working) thruster. This results in the so-called spoiled zone. Third is flushing another working thruster, which introduces the so-called forbidden zone, where the thruster is not allowed to operate in.

An example of handling constraints for azimuth thruster is shown in Fig. 4.1. In general, the approach is to divide the thrust constraint region into convex sets, in this case labeled I, II, III, IV. Sets I and II describe the spoiled zone and III and IV a maximum saturation zone. Then the zones are divided into polygons that can be defined by linear equations, as will be shown.

Quadratic programming can be used as an optimization algorithm for each such defined linear (and convex) sub-problem separately.

In practice, the number of polygons, which the zone is divided into, determines the accuracy of the method and shall be chosen individually; however, an error not exceeding 1% is recommended (de Wit, 2009).

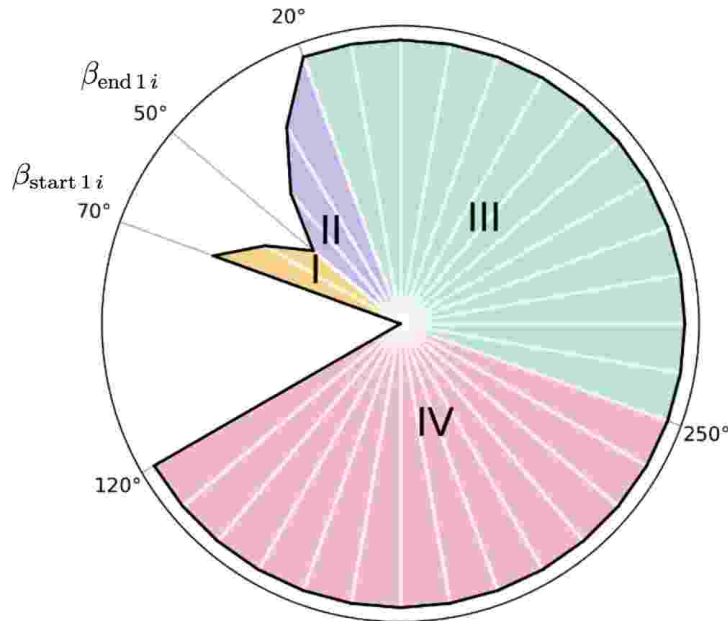


Figure 4.1: Linearization of a typical azimuth thruster saturation region

First one has to define the boundaries of the zone as given in Eq. (4.2). Subsequently, within each zone, the polygons are defined with linear equations as given in Eq. (4.3) for the saturation within zone type III, IV and in Eq. (4.4) for the saturation within spoiled zone type I, II.

$$\begin{aligned} T_{xi} \sin(\beta_{start z i}) - T_{yi} \cos(\beta_{start z i}) &\leq 0, \\ -T_{xi} \sin(\beta_{end z i}) + T_{yi} \cos(\beta_{end z i}) &\leq 0, \end{aligned} \quad (4.2)$$

where  $\beta_{start z i}$  and  $\beta_{end z i}$  denote angles at which the  $z$ th zone starts and ends, respectively.

Total number of zones for the  $i$ th thruster is denoted with  $Z_i$ , where  $i \in \{1 \dots N\}$ . Total number of polygons within each  $z$ th zone is denoted with  $J_{zi}$ , where  $j \in \{1 \dots J_{zi}\}$  is the number of the specific polygon within the  $z$ th zone where  $z \in \{1 \dots Z_i\}$ .

$$T_{xi} \cos(\varphi_{jzi}) + T_{yi} \sin(\varphi_{jzi}) \leq r_i, \quad (4.3)$$

where  $r_i$  is the maximum effective thrust of the  $i$ th thruster and  $\varphi_{jzi}$  refers to  $j$ th polygon of the  $z$ th zone of the  $i$ th thruster.

An illustration of the polygon as described with Eq. (4.3) is provided in Fig. 4.2.

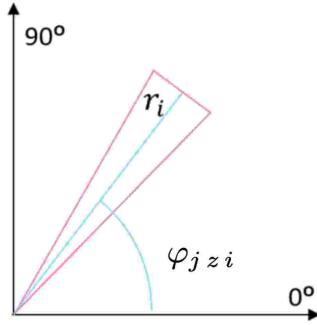


Figure 4.2: Definition of a  $j$ th polygon, Eq. 4.3, within zone III, IV

$$T_{xi} (y_{k+1} - y_k) + T_{yi} (x_{k+1} - x_k) \leq x_k y_{k+1} - x_{k+1} y_k, \quad (4.4)$$

where  $x_k$  and  $y_k$  are the coordinates of the first point, while  $x_{k+1}$  and  $y_{k+1}$  are the coordinates of the subsequent point on the polygon outline;  $k \in \{1 \dots J_{zi} + 1\}$

An illustration of the polygon as described with Eq. (4.4) is provided in Fig. 4.3.

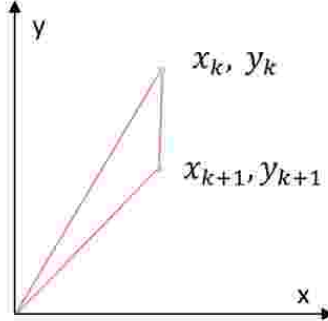


Figure 4.3: Definition of  $j$ th polygon, Eq. (4.4) within zone I, II

In Eq. (4.5) is a representation of Eq. (4.4), where  $a_{yjzi} = y_{k+1} - y_k$ ,  $a_{xjzi} = x_{k+1} - x_k$ , and  $a_{jzi} = x_k y_{k+1} - x_{k+1} y_k$  are introduced to simplify the notation.

$$T_{xi} a_{yjzi} + T_{yi} a_{xjzi} \leq a_{jzi} \quad (4.5)$$

where  $a_{yjzi}$ ,  $a_{xjzi}$ ,  $a_{jzi}$  are coefficients corresponding to coordinates in Eq. (4.4) where  $j$  is a considered polygon.

**Propeller with rudder** In the presented approach, the rudder angle is not a decision variable. However, considering the boundaries of the maximum angle of the rudder on both sides, two convex thrust zones for a typical propeller with rudder can be defined. Zone II can be described with the application of the method presented in Fig. 4.1 and with the utilization of Eq. (4.2) and Eq. (4.4). Another constraint needs to be defined for the reverse mode of the propeller (zone I), as given in Eq. (4.6). These create two separate convex zones of the propeller with the rudder and are to be optimized separately.

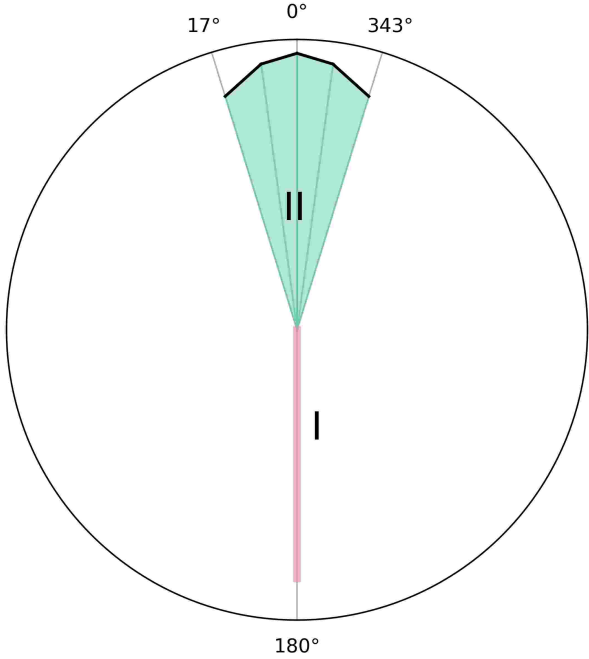


Figure 4.4: Linearization of the propeller with rudder constraints

$$\begin{aligned} T_{xi} &\leq 0 \\ -T_{xi} &\leq T_{\max i} \end{aligned} \tag{4.6}$$

where  $T_{\max i}$  is a maximum thrust of the  $i$ th thruster.

**Tunnel thruster** Constraints of tunnel thrusters can be adopted with an original DNV definition. No additional linearization is needed. Therefore, the constraints can be adopted as in Eq. (4.7).

$$\begin{aligned} T_{yi} &\leq T_{\max i} \\ -T_{yi} &\leq T_{\max i} \end{aligned} \tag{4.7}$$

### 4.2.3 Equality Constraints

One of the equality constraints is static balance Eq. (2.8) introduced in Section 2.4, given here in a form presented in Eq. (4.8).

$$\begin{aligned}
\sum_{i=1}^N T_{xi} &= -F_{x\text{env}} \\
\sum_{i=1}^N T_{yi} &= -F_{y\text{env}} \quad (4.8) \\
\sum_{i=1}^N (-T_{xi} y_{\text{thri}_i} + T_{yi} x_{\text{thri}_i}) &= -M_{z\text{env}}
\end{aligned}$$

Additionally, two other types of equality constraints must be taken into account for propeller reverse mode (zone I), Eq. (4.9) and for tunnel thruster Eq. (4.10).

$$T_{yi} = 0 \quad (4.9)$$

$$T_{xi} = 0 \quad (4.10)$$

#### 4.2.4 Objective function

As the objective function in optimization, the total power consumption minimization was adopted. By the virtue of Asm. 3, the TA is solved by considering an objective function ( $P_{\text{total}}$ ) which yields a quadratic approximation of total power consumption as a function of thrust.

$$P_{\text{total}}(\mathbf{u}) \stackrel{\text{def}}{=} \mathbf{u}^T \mathbf{W} \mathbf{u} \quad (4.11)$$

where  $\mathbf{W} \stackrel{\text{def}}{=} \text{diag}(w_1, w_1, w_2, w_2, \dots, w_N, w_N)$  is a diagonal matrix of weight coefficients  $w_i$ ,  $\forall i$ , corresponding to each thruster.

Weight coefficients are determined according to (DNV, 2021) with the exception that the maximum thrust loss in case of spoiled zones is also taken into account in determining the weights (not the loss at each polygon separately).

#### 4.2.5 Optimization task decomposition

Due to the nature of the constraints, the problem of thrust allocation is decomposed into several sub-problems to be solved independently using a

QP approach. Such problems are denoted with  $l \in \{1 : L\}$  and are given with Eq. (4.12).

$$\begin{aligned} QP_l : \quad & \mathbf{u}_l := \arg \min_{\mathbf{u}} P_{\text{total}}(\mathbf{u}) \\ & \text{s.t. } \mathbf{A}_l \mathbf{u} = \mathbf{b}_l \\ & \quad \mathbf{G}_l \mathbf{u} = \mathbf{h}_l \end{aligned} \quad (4.12)$$

where  $\mathbf{A}_l$  and  $\mathbf{b}_l$  describe equality constraints on all considered thrusters based on equations (4.8), (4.9) and (4.10);  $\mathbf{G}_l$  and  $\mathbf{h}_l$  describe inequality constraints on all thrusters based on equations (4.2), (4.3), (4.5), (4.6), and (4.7).

Considering all possible combinations of the thruster's convex zones, the number of optimization problems is  $L = \prod_{i=1}^N Z_i$ , where  $Z_i$  represents the total number of zones of the  $i$ th thruster. Hence, the optimal thrust allocation task yields Eq. (4.13), where the best thrust allocation ( $\mathbf{u}^*$ ) is found by comparison between  $L$  results.

$$\begin{aligned} \mathbf{u}^* := \arg \min_{\mathbf{u}_l} & \{P_{\text{total}}(\mathbf{u}_l)\} \\ \text{s.t. } & \mathbf{u}_l \leftarrow QP_l \wedge l \in \{1 \dots L\} \end{aligned} \quad (4.13)$$

#### 4.2.6 TA algorithm

DP capability assessment program has been developed using Python 3.8 programming language extended with *qpsolvers* library delivering *quadprog* solver used to handle the optimization problem Eq. (4.12), (Goldfarb and Idnani, 1983). The flowchart illustrating the program data flow is presented in Fig. 4.5. On the left side of the figure, the main part of the program routine has been presented, while the sub-process directly invoking the optimization task has been illustrated on the right side.

The logic of the program is as follows. First, the program reads the user-generated inputs, namely basic hull and thrusters' data including thrusters' layout. Those data are delivered by a regular engineer into the design support system (Fig. 1.4). Subsequently, parameters of the thrusters' zones are calculated, (DNV, 2010), while the loop of environmental angles ( $\alpha$ ) and DP numbers as defined in Tab. 2.1, ( $k_{DP} \in \{1 \dots 11\}$ ) is initiated. Next, the environmental forces are calculated with the utilization of the basic hull data and environmental (wind, current, and wave) conditions, (DNV, 2021). Next, the maximum ventilation losses and maximum effective thrust for each

thruster are calculated, (DNV, 2021). Further, the DP capability assessment sub-process is initiated. Within the sub-process, all combinations of linear matrices  $\mathbf{G}_l$ ,  $\mathbf{h}_l$ ,  $\mathbf{A}_l$ ,  $\mathbf{b}_l$ , and  $\mathbf{W}_l$ , for  $l \in \{1 \dots L\}$  are calculated based on input data and linearization method given with equations (4.2) - (4.10). These matrices are defined for all ( $L$ ) possible combinations of the convex sets comprising the constraints. The process loops through these combinations, solving each time the problem defined by Eq. (4.12). The DP capability assessment sub-process ends by finding vector  $\mathbf{u}^*$ , which corresponds to the minimal power consumption as defined by Eq. (4.13). At this point, the control flow is returned to the main routine, and the program iterates until the environmental angle and DP number conditions are satisfied. Finally, the solution - DP capability plot data - is saved and the plot is generated. The algorithm was implemented in the decision support system as one of the developments of the dissertation, regarding all mentioned calculations being in accordance with the DNV-ST-0111 standard, (DNV, 2021) and as summarized in Ch. 2. The method was implemented in such a way that it is universal to use for all listed propulsion types, their layout, and any mono-hull ship type.

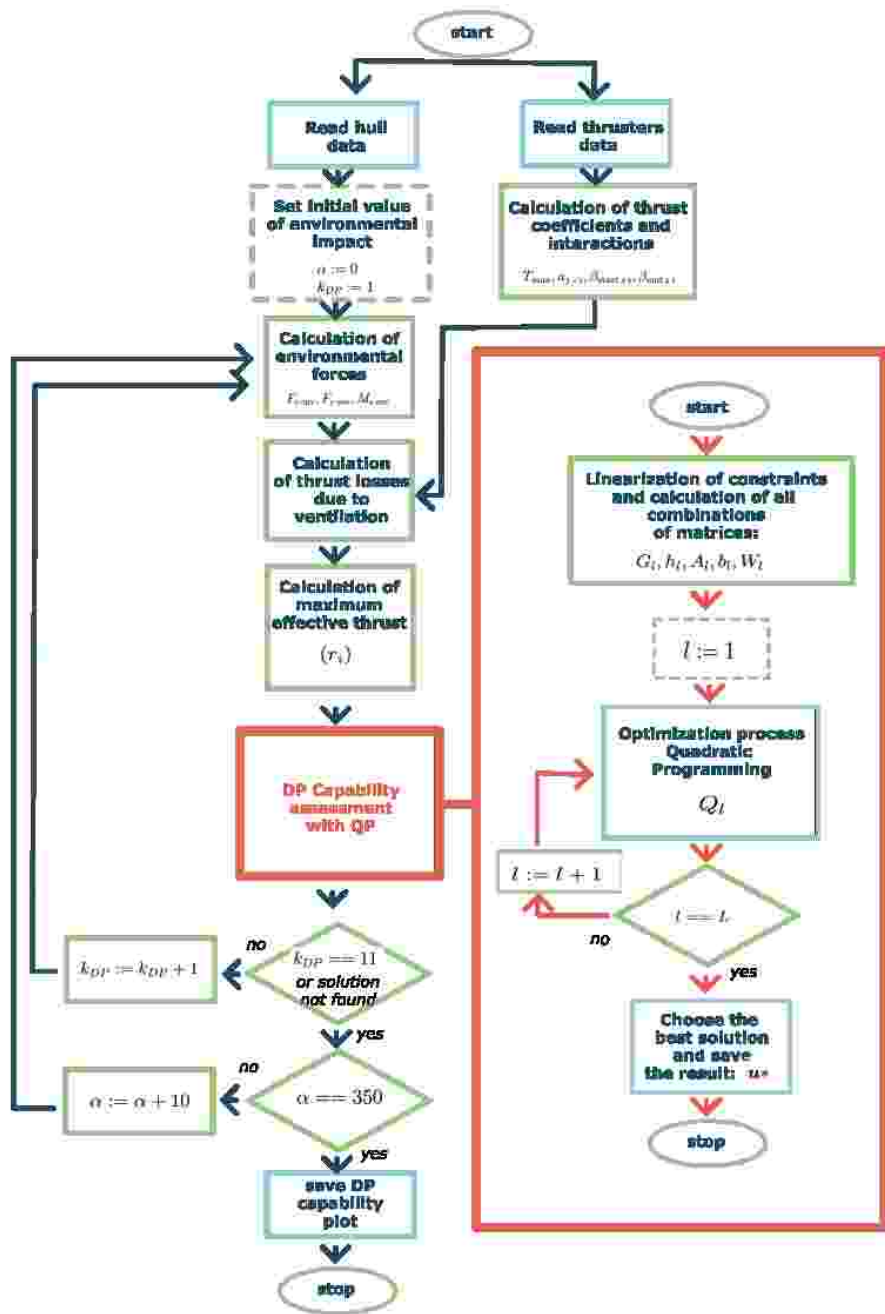


Figure 4.5: Flowchart of DP capability assessment program with QP algorithm utilization

### 4.2.7 Case study

For the sake of the presentation of defined constraint types, a hypothetical four-thruster setup is considered, taking into account all discussed thruster types. The layout of the thrusters is shown in Fig. 4.6. Matrices  $\mathbf{A}_l$ ,  $\mathbf{b}_l$ ,  $\mathbf{G}_l$ ,  $\mathbf{h}_l$ , and  $\mathbf{W}_l$  for a chosen  $l = 1$  convex sub-problem of  $L = 4$  problems will be given. The following zones are considered for each thruster.

- $i = 1$  : Port propeller with rudder in reverse zone type I (Fig. 4.4)  $z = 1$  ( $Z_1 = 2$ ) - zone definition given by Eq. (4.6) and Eq. (4.9).
- $i = 2$  : Starboard propeller with rudder in forward zone type II (Fig. 4.4)  $z = 2$  ( $Z_2 = 2$ ,  $J_{22} = 2$ ) - zone definition as shown in Fig. 4.3 and given by Eq. (4.5) and additionally constrained with Eq. (4.2).
- $i = 3$  : Azimuth thruster at the bow in maximum saturation zone type III (Fig. 4.1)  $z = 1$  ( $Z_3 = 1$ ,  $J_{13} = 35$ ) - zone definition as showed in Fig. 4.2 and given by Eq. (4.3)
- $i = 4$  : Tunnel thruster at the bow  $z = 1$ ,  $Z_i = 1$  - given with Eq. (4.7) and Eq. (4.10).

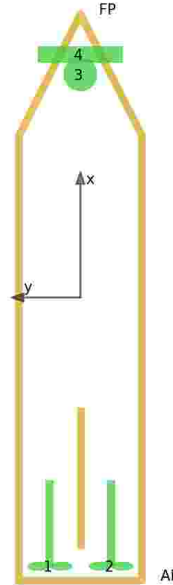


Figure 4.6: Thrusters layout - exemplary case

$$\mathbf{A}_{l=1} = \begin{bmatrix} 1 & 0 & 1 & 0 & 1 & 0 & 1 & 0 \\ 0 & 1 & 0 & 1 & 0 & 1 & 0 & 1 \\ -y_{\text{thr1}} & x_{\text{thr1}} & -y_{\text{thr2}} & x_{\text{thr2}} & -y_{\text{thr3}} & x_{\text{thr3}} & -y_{\text{thr4}} & x_{\text{thr4}} \\ 0 & 0 & 0 & 0 & 0 & 0 & 1 & 0 \\ 0 & 1 & 0 & 0 & 0 & 0 & 0 & 0 \end{bmatrix} \quad (4.14)$$

$$\mathbf{b}_{l=1} = \begin{bmatrix} -F_{x\text{env}} & -F_{y\text{env}} & -M_{z\text{env}} & 0 & 0 \end{bmatrix}^T \quad (4.15)$$

$$\mathbf{G}_{l=1} = \begin{bmatrix} -1 & 0 & 0 & 0 & 0 & 0 & 0 & 0 \\ 1 & 0 & 0 & 0 & 0 & 0 & 0 & 0 \\ 0 & 0 & \sin(\beta_{\text{start } 2_2}) & -\cos(\beta_{\text{start } 2_2}) & 0 & 0 & 0 & 0 \\ 0 & 0 & -\sin(\beta_{\text{end } 2_2}) & \cos(\beta_{\text{end } 2_2}) & 0 & 0 & 0 & 0 \\ 0 & 0 & a_{y1\ 2} & a_{x1\ 2} & 0 & 0 & 0 & 0 \\ 0 & 0 & a_{y2\ 2} & a_{x2\ 2} & 0 & 0 & 0 & 0 \\ 0 & 0 & 0 & 0 & \cos(\varphi_{13}) & \sin(\varphi_{13}) & 0 & 0 \\ 0 & 0 & 0 & 0 & \cos(\varphi_{23}) & \sin(\varphi_{23}) & 0 & 0 \\ \vdots & \vdots \\ 0 & 0 & 0 & 0 & \cos(\varphi_{J_{1\ 3}}) & \sin(\varphi_{J_{1\ 3}}) & 0 & 0 \\ 0 & 0 & 0 & 0 & 0 & 0 & 0 & 1 \\ 0 & 0 & 0 & 0 & 0 & 0 & 0 & -1 \end{bmatrix} \quad (4.16)$$

$$\mathbf{h}_{l=1} = [T_{\max 1} \ 0 \ 0 \ 0 \ a_{1\ 2} \ a_{2\ 2} \ r_3 \ r_3 \ \dots \ r_3 \ T_{\max 4} \ T_{\max 4}]^T \quad (4.17)$$

Above example can be modified to fit any DP vessel with a propeller with a rudder, azimuth thruster, or tunnel thruster propulsion type. The structure of given matrices will be different for each set of thrusters.

### 4.3 An approach based on nonlinear programming

In this section, a step-by-step implementation of the Non-dominated Sorting Genetic Algorithm II as optimal thrust allocation to the DNV method is given in accordance with (Deb et al., 2002; Gao et al., 2019).

### 4.3.1 Decision variables

Decision variables are control inputs on the ship such as the orientation angle of the thruster and the power utilization of the thruster.

$$\mathbf{u} \stackrel{\text{def}}{=} \begin{bmatrix} P_1 & \beta_1 & P_2 & \beta_2 & \dots & P_N & \beta_N \end{bmatrix}^T. \quad (4.18)$$

where  $P_i$  is power at the  $i$ th thruster in [kW] and  $\beta_i$  is the thruster orientation angle in [°].

### 4.3.2 Constraints

Boundary constraints are imposed on the decision variables as given in Tab. 4.1.

Table 4.1: Boundary constraints

Thruster type	Power range $[P_1, P_2, \dots, P_N]$	Angle range $[\beta_1, \beta_2, \dots, \beta_N]$	Application in NSGAII algorithm
Azimuth thruster	$[0 \dots P_{\max i}]$	$[0^\circ \dots 360^\circ]$	Thrust components on x and y axis is calculated based on both decision variables.
Propeller with rudder	$[-P_{\max i} \dots P_{\max i}]$	$[-30^\circ \dots 30^\circ]$	Angle range concern rudder angle. For negative power a reverse thrust at x axis is calculated and the rudder angle is ignored. In forward mode the thrust components on x and y axis are calculated based on power and rudder angle.
Tunnel thruster	$[0 \dots P_{\max i}]$	$[-1 \dots 1]$	Thrust at y axis is calculated from power. Angle range denotes the negative or positive thruster direction on y axis.

Relation between power and thrust is calculated based on original, non-linear formulas given by the DNV standard (DNV, 2021) including losses due to flushing another dead thruster and skeg. Forbidden zones are expressed

by a penalty function - whenever the thruster is within the zone, the power consumption is increased.

### 4.3.3 Objective functions

As one of the objectives, power minimization is selected, given in its original representation as given by (DNV, 2021) and as presented in Eq. (4.19).

$$P_{\text{total}}(\mathbf{u}) \stackrel{\text{def}}{=} \sum_{i=1}^N P_i \quad (4.19)$$

The equality constraints expressed by the static balance in Eq. (4.8) are taken into account in NSGAII in the form of minimization of the error between environmental and thruster forces and moments, constituting the second objective as given in Eq. (4.20), (Gao et al., 2019).

$$J_e = \mathbf{e}^T \mathbf{Q} \mathbf{e} \quad (4.20)$$

where  $\mathbf{e} = \boldsymbol{\tau}_{\text{env}} - \boldsymbol{\tau}_{\text{thr}}$ ;  $\mathbf{Q} = \text{diag}(q_1, q_2, q_3)$  represents the weight of the error;  $\boldsymbol{\tau}_{\text{env}} = [F_{x\text{env}}, F_{y\text{env}}, M_{z\text{env}}]^T$  are environmental forces and moments, and  $\boldsymbol{\tau}_{\text{thr}} = [F_{x\text{thr}}, F_{y\text{thr}}, M_{z\text{thr}}]^T$  are thrusters' total forces and moments.

### 4.3.4 Optimization task decomposition

Optimization of two criteria is applied to the thrust allocation problem. Both power consumption given with Eq. (4.19) and quadratic balance error function given with Eq. (4.20) are minimized. The optimization task can be expressed as in Eq. (4.21).

$$\begin{aligned} \text{NSGA2} := \arg \min_{\mathbf{u}} & [P_{\text{total}}(\mathbf{u}), J_e(\mathbf{u})] \\ \text{s.t. } & \mathbf{u}_{\min} \leq \mathbf{u} \leq \mathbf{u}_{\max} \end{aligned} \quad (4.21)$$

where  $\mathbf{u}_{\min}$  and  $\mathbf{u}_{\max}$  are decision variables boundaries as given in Tab. 4.1.

### 4.3.5 TA algorithm

In Fig. 4.7 a flowchart of the NSGAII algorithm is presented.

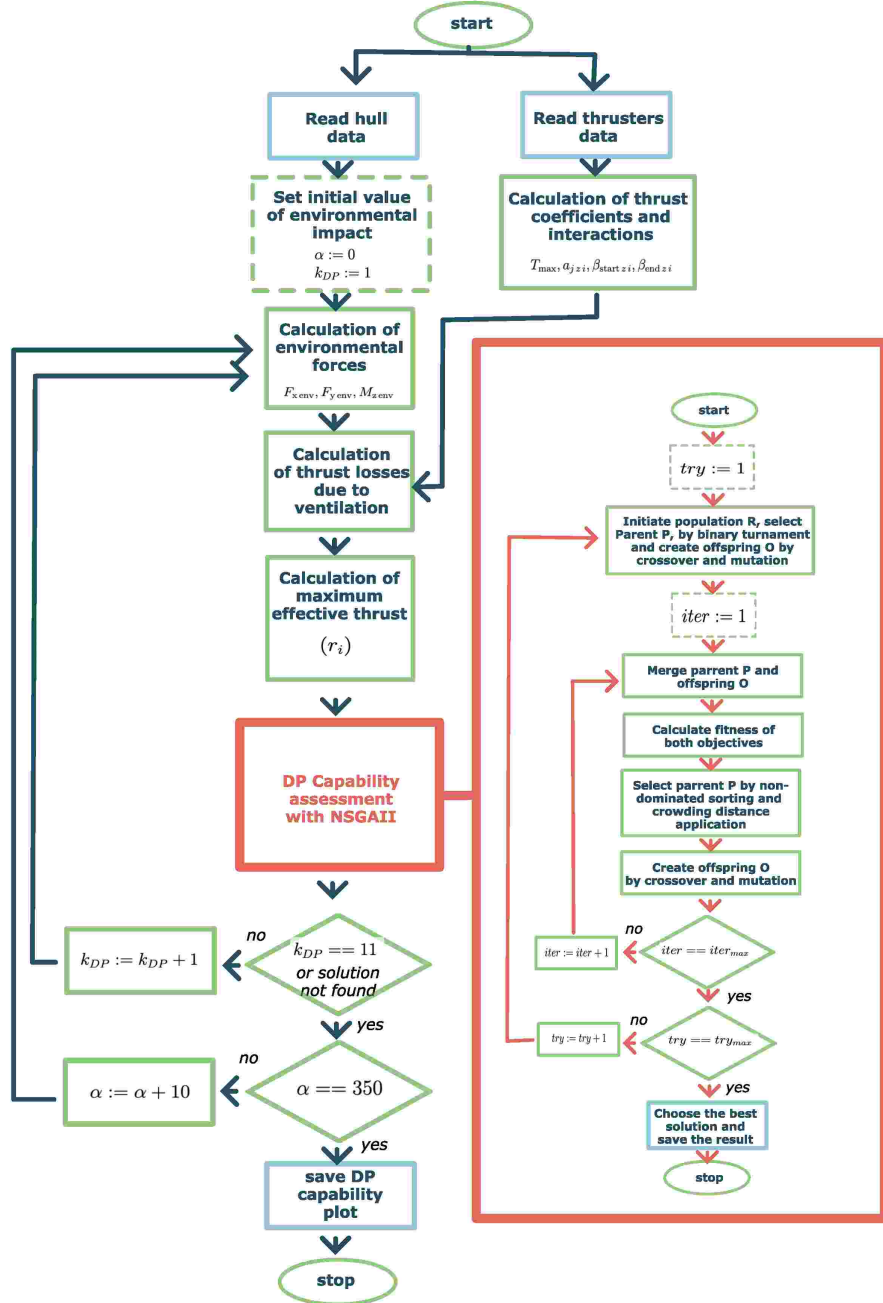


Figure 4.7: Flowchart of DP capability assessment program with NSGAII algorithm utilization

Both QP and NSGAII algorithms are incorporated in the DP capability assessment script as interchangeable components. Hence, in Fig. 4.7, the left side of the chart is identical to that in Fig. 4.5. Therefore, only the NSGAII algorithm will be shortly discussed here.

Following the flowchart, concerning the NSGAII algorithm, first the initial population of  $[P_1, \beta_1, P_2, \beta_2, \dots, P_N, \beta_N]$  is randomly selected. Subsequently, offspring are obtained by binary tournament, crossover, and mutation. Next, parent and offspring are merged to calculate the fitness of both objectives. Further, non-dominated sorting and crowding distance are applied to the results, which output the Pareto front, the parent. The procedure of crossover and mutation is repeated, and the resulting offspring are merged with the parent to undergo the next iteration. The algorithm is initiated a few times with variable *try*. Finally, the best solution is chosen based on the Pareto front for all tries.

## 4.4 Results

For the study of static methods, within the dissertation, a Rescue Vessel (RV) as described in Apx. A was selected. The vessel's main particulars can be found in Tab. A.3 and Tab. A.4, while the thruster layout is given in Fig. A.3. The choice was dictated by the previously conducted multiple analyses on that ship in CTO S.A. Concerning wind tunnel tests, numerical computations of wave forces, and static DP capability analyses attempts.

A comparison of performance and results of both applied TA optimization algorithms was done within the dissertation. In Fig. 4.8 DP capability in a form of polar plot is shown. A total power utilization comparison in a DP number 6 environmental condition is given in Fig. 4.9, also in polar form. Finally, one case of environmental conditions - DP number 7 and 30° is analyzed in terms of thrust allocation in Fig. 4.10 and Fig. 4.11 for the QP and NSGAII methods respectively.

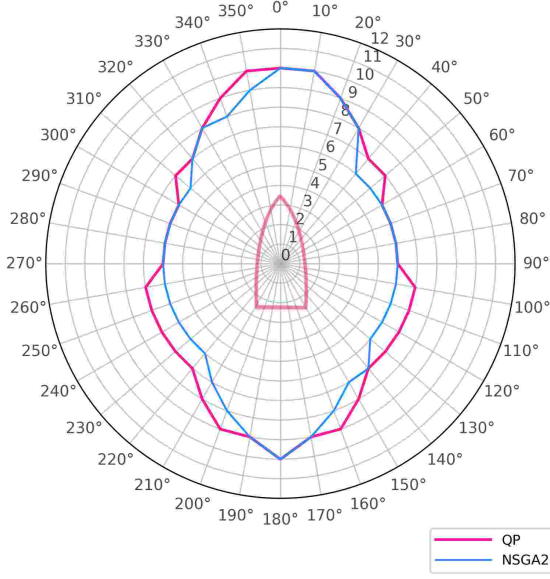


Figure 4.8: DP capability plots of a RV with QP and NSGAII algorithms

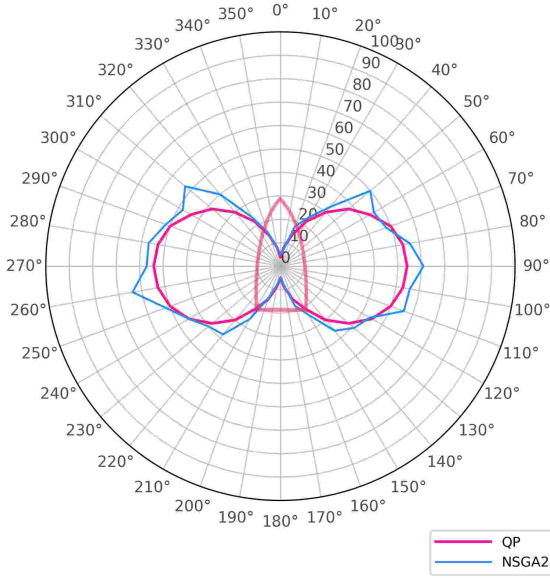


Figure 4.9: Power utilization in DP operations of a RV with QP and NSGAII algorithms

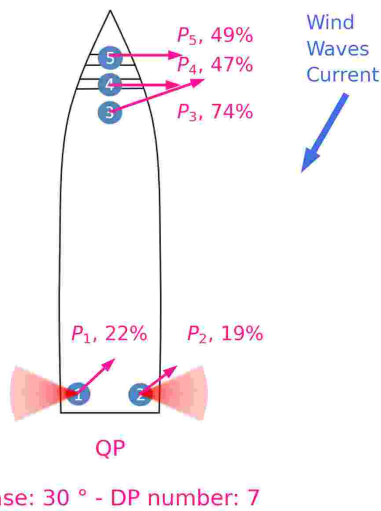


Figure 4.10: Thrust allocation of RV (QP)

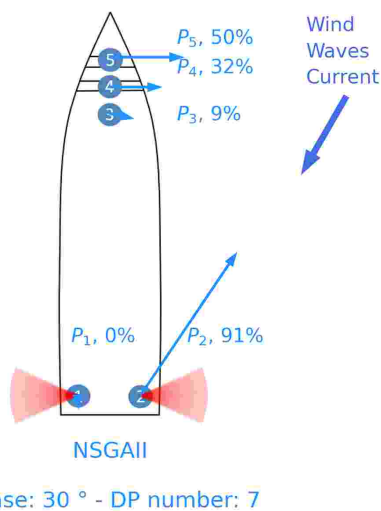


Figure 4.11: Thrust allocation of RV (NSGAII)

As can be concluded from the DP capability plots in Fig. 4.8, application of NSGAII shows a random nature of this algorithm since the corresponding plot is asymmetrical. This effect can also be observed in the plot in Fig. 4.9 where the natural smooth transition of power from one environmental angle to the next is not contained for NSGAII. The random and visibly unoptimal nature of applied NSGAII is also depicted in Fig. 4.11. As opposed to the TA determined with QP (Fig. 4.10) which results in an even contribution of all thrusters, the NSGAII favors the stern starboard thruster over all the rest.

Performance of QP is also shown in the case of analysis of RV capability under failures. A comparison between intact and failure cases is given in Fig. 4.12 and power utilization differences are shown in Fig. 4.13 at DP number 3.

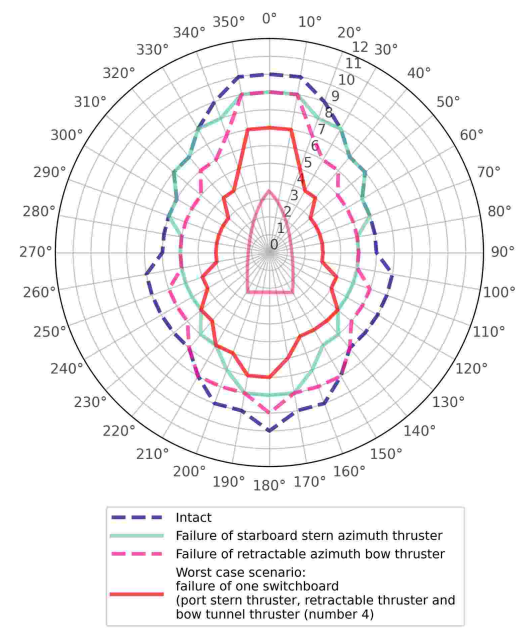


Figure 4.12: DP capability plots of a RV for intact and failure cases

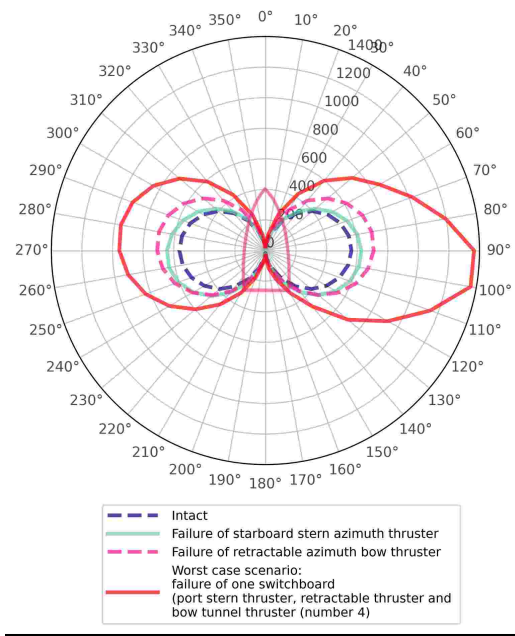


Figure 4.13: Power utilization in DP operations of RV for intact and failure cases for a DP number 3

## 4.5 Summary

Within this chapter, both QP and NSGAII algorithms were applied to the TA problem as optimization solutions. Both are described in detail, which allows a potential engineer to implement them in a design office.

Applied NSGAII shows obvious flaws. Such as very long computation time and random nature of the results, which makes it not applicable to static TA, and even more so to the dynamic analyses. However, the application of this algorithm within the dissertation supported the verification of the QP method. The QP algorithm shows simplicity of application, allows fast computations, and gives higher accuracy of optimization. Hence, the rest of the analyses within the dissertation, both static and dynamic (simulator) concern only the QP.

Above all, presented QP approach allows for universal application, to any ship kind, with any thrusters layout and for a variety of thrusters types.

# Chapter 5

## Dynamic DP capability analysis

Dynamic analyzes of DP ships allow accounting for the dynamic response of the ships' hull to time-varying environmental disturbances and dynamic actuator forces. The aforementioned is covered in Ch. 3, while the main functionalities of the DPS employed to handle those dynamics are described in this chapter.

An illustration of a DPS is shown in Fig. 5.1, where three main components of the system that will be discussed are highlighted: state observer (SO), controller (C), and thrust allocation (TA).

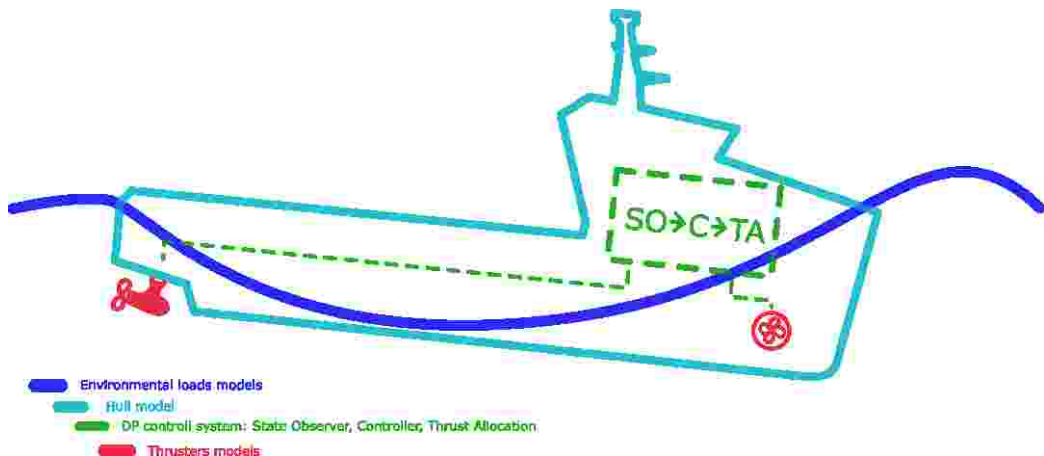


Figure 5.1: DP simulator main components

Dynamic DP capability assessment is carried out either with simulation (level 3 and 3-site according to DNV-ST-0111) or with experiments. The

former is accomplished within the scope of this dissertation (concerning level 3-site), while the latter was performed prior to the studies.

In Sect. 5.1 DPS components (observer, controller and thrust allocation) are specified and subsequently described in Sect. 5.2, 5.3 and 5.4 respectively.

## 5.1 DPS components

A dynamic positioning system concept is depicted in Fig. 5.2. This system was implemented in experiments and in the simulation with the distinction in the following text. The highlighted components are discussed in subsequent sections of this chapter. The elements above the system with assigned arrows denote information that the system uses to perform the DP task. Dashed lined box elements concern only experiments. The variable inputs and outputs of the DPS are explained in the following text.

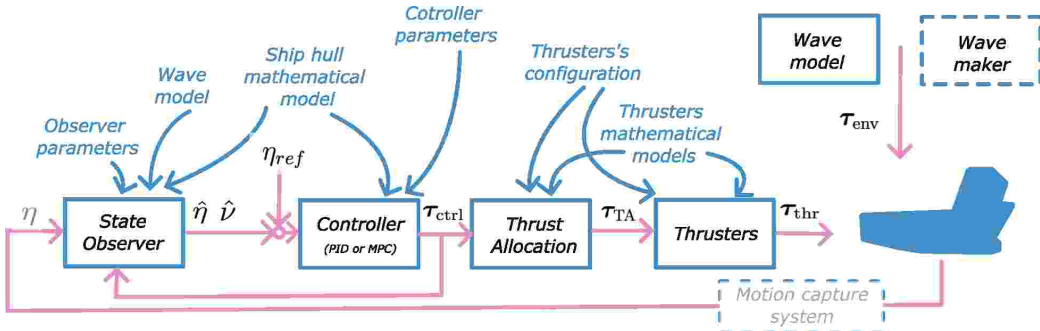


Figure 5.2: DP Control system concept

- $\boldsymbol{\eta} = [x \ y \ \psi]^T$  is a measured position and heading vector in global reference frame. In case of DP operations at sea this vector comes from GPS signal. In the DP simulator developed within the dissertation  $\boldsymbol{\eta}$  results from double integration of acceleration vector  $\hat{\nu}$  that results of Eq. (3.7) given in Sect. 3.2.1. In the experiments carried out, the signal comes from a motion capture system (Qualisys). Vector  $\boldsymbol{\eta}$  is further utilized by SO.
- $\hat{\boldsymbol{\eta}} = [\hat{x} \ \hat{y} \ \hat{\psi}]^T$  and  $\hat{\boldsymbol{\nu}} = [\hat{u} \ \hat{v} \ \hat{r}]^T$  are state observer estimated position and heading vector in global reference frame and velocity vector in body-

fixed frame. Estimated,  $\hat{\boldsymbol{\eta}}$  and reference position,  $\boldsymbol{\eta}_{ref}$  error is further utilized by the controller.

- $\boldsymbol{\tau}_{ctrl} = [F_{x_{ctrl}} F_{y_{ctrl}} M_{z_{ctrl}}]^T$  is control forces vector determined by the controller in body fixed frame, fed to TA module.
- $\boldsymbol{\tau}_{TA} = [T_{x_1} T_{y_1} T_{x_2} T_{y_2} \dots T_{x_N} T_{y_N}]^T$  is a command thrust vector determined by optimal mapping of the  $\boldsymbol{\tau}_{ctrl}$  over all available thrusters where  $N$  is total number of thrusters. This is achieved in the TA module. Vector  $\boldsymbol{\tau}_{TA}$  is further fed to the thrusters module (or thruster control system in experiments).
- $\boldsymbol{\tau}_{thr} = [F_{x_{thr}} F_{y_{thr}} M_{z_{thr}}]^T$  is the resultant force and moment acting on the hull, due to actual propeller revolutions,  $n_{actual}$  and azimuth thruster angle,  $\beta_{actual}$ . Those are calculated based on  $\boldsymbol{\tau}_{TA}$  translated to the thruster settings  $n_{set}$ ,  $\beta_{set}$  while accounting for the thrusters inertia as given in Sect. 3.2.2.
- $\boldsymbol{\tau}_{env} = [F_{x_{env}} F_{y_{env}} M_{z_{env}}]^T$  is environmental force vector concerning wave loads.

## 5.2 State observer

Ship in a DP operation is considered observable as the internal state (position and speed) can be inferred from the measured outputs of the system (position and control inputs), (Fossen, 2021).

In case of DP control, the task of the observer is twofold. First, the observer filters wave frequency, 1st order motions from the measured position; thus, it is also sometimes called a wave filter. Second, it estimates the ship's state, position, and velocity based on the filtered signal. Attempting control of the 1st order wave motions is not feasible, since it could cause aggressive control tearing and wearing of the thrusters, resulting in poor overall control performance.

For many years, Kalman filter and its extended version were employed for that task (Fossen and Perez, 2009). The drawbacks of the Kalman filter solution were that it required a significant amount of parameters to tune it. To identify those parameters, multiple experiments are usually required. A review of Kalman filters is given in (Selimović et al., 2020; Værnø et al., 2019).

A mile stone in state estimation in DP was a nonlinear passive observer proposed by (Fossen, 2021). Since the passivity allows the estimation error and bias convergence to zero, only one set of observer gains is required. This decreases the number of experiments needed for gains determination.

A nonlinear passive observer introduced by (Fossen, 2021) was utilized within the dissertation, both in experiments and simulations.

The state observer is to filter 1st order wave induced motion based on the mathematical model of the ship, current control forces vector, measured position vector and 1st order wave model. By this operation, a 2nd order ship motion and velocity are estimated, which allows further control of a ship. The observer equations, in a form implemented in the DP simulation, are presented in discrete form to simplify the implementation in the decision support system for an engineer.

First an estimation error  $\tilde{\mathbf{y}}$  is calculated as given in Eq. (5.1).

$$\tilde{\mathbf{y}}_i = \boldsymbol{\eta}_{i-1} - (\hat{\boldsymbol{\eta}}_{i-1} + \hat{\boldsymbol{\eta}}_{w_{i-1}}) \quad (5.1)$$

where  $\boldsymbol{\eta}_{i-1} \in R^3$  is the previous iteration (sample) position and heading vector (from integration in the simulator);  $\hat{\boldsymbol{\eta}}_{i-1}$  is the 2nd order (low frequency) estimated position and heading vector determined by the observer in a previous iteration,  $\hat{\boldsymbol{\eta}}_{w_{i-1}}$  is the 1st order estimated position and heading vector from the previous iteration. Further  $i$  denotes the current iteration of simulation and  $i - 1$  the previous iteration.

In simulation, no noise on  $\boldsymbol{\eta}_i$  was overlayed, and no filters were applied. Hence,  $\boldsymbol{\eta}_i$  signal that enters the observer includes 1st order wave-induced motion and 2nd order wave-induced motions.

The following equations sequence was implemented in the simulator.

$$\dot{\hat{\boldsymbol{\eta}}}_{w_i} = \mathbf{K}_{12}\tilde{\mathbf{y}}_i - \hat{\boldsymbol{\xi}}_{w_{i-1}}\omega_0^2 - 2\lambda\omega_0\hat{\boldsymbol{\eta}}_{w_{i-1}} \quad (5.2)$$

$$\hat{\boldsymbol{\eta}}_{w_i} = \hat{\boldsymbol{\eta}}_{w_{i-1}} + \frac{1}{2}\Delta t(\dot{\hat{\boldsymbol{\eta}}}_{w_{i-1}} + \dot{\hat{\boldsymbol{\eta}}}_{w_i}) \quad (5.3)$$

$$\dot{\hat{\boldsymbol{\xi}}}_{w_i} = \mathbf{K}_{11}\tilde{\mathbf{y}}_i + \hat{\boldsymbol{\eta}}_{w_i} \quad (5.4)$$

$$\hat{\boldsymbol{\xi}}_{w_i} = \hat{\boldsymbol{\xi}}_{w_{i-1}} + \frac{1}{2}\Delta t(\dot{\hat{\boldsymbol{\xi}}}_{w_{i-1}} + \dot{\hat{\boldsymbol{\xi}}}_{w_i}) \quad (5.5)$$

where  $\hat{\boldsymbol{\xi}} \in R^3$  is the so-called seakeeping domain state vector, (Fossen, 2021);

$\omega_0$  is the wave peak frequency,  $\lambda$  is the damping ratio, typically of value 0.1;

$$\mathbf{K}_{11} = \begin{bmatrix} -\lambda \frac{\omega_c}{\omega_0} & 0 & 0 \\ 0 & -\lambda \frac{\omega_c}{\omega_0} & 0 \\ 0 & 0 & -\lambda \frac{\omega_c}{\omega_0} \end{bmatrix}, \quad (5.6)$$

$$\mathbf{K}_{12} = \begin{bmatrix} 2\omega_0(1-\lambda) & 0 & 0 \\ 0 & 2\omega_0(1-\lambda) & 0 \\ 0 & 0 & 2\omega_0(1-\lambda) \end{bmatrix} \quad (5.7)$$

where typically,  $\omega_c = 1.23\omega_0$  is the cutoff frequency, (Fossen, 2021). Subsequently, the following equations are executed in the state observer.

$$\dot{\hat{\boldsymbol{\nu}}}_i = \mathbf{M}^{-1} \left( \mathbf{D} + \mathbf{R}^T (\hat{\psi}'_{i-1}) \hat{\mathbf{b}}_{i-1} + \boldsymbol{\tau}_{\text{ctrl}i-1} + \mathbf{R}^T (\hat{\psi}'_{i-1}) \mathbf{K}_4 \tilde{\mathbf{y}}_i \right) \quad (5.8)$$

$$\mathbf{D} = \mathbf{D}_L \hat{\boldsymbol{\nu}}_{i-1} + \mathbf{D}_{NL} \hat{\boldsymbol{\nu}}_{i-1} |\hat{\boldsymbol{\nu}}_{i-1}| \quad (5.9)$$

$$\hat{\boldsymbol{\nu}}_i = \hat{\boldsymbol{\nu}}_{i-1} + \frac{1}{2} \Delta t (\dot{\hat{\boldsymbol{\nu}}}_{i-1} + \dot{\hat{\boldsymbol{\nu}}}_i) \quad (5.10)$$

$$\dot{\hat{\mathbf{b}}}_i = -\mathbf{T}^{-1} \hat{\mathbf{b}}_{i-1} + \mathbf{K}_3 \tilde{\mathbf{y}}_i \quad (5.11)$$

$$\hat{\mathbf{b}}_i = \hat{\mathbf{b}}_{i-1} + \Delta t \dot{\hat{\mathbf{b}}}_i \quad (5.12)$$

$$\dot{\hat{\boldsymbol{\eta}}}_i = \mathbf{R} (\hat{\psi}'_{i-1}) \hat{\boldsymbol{\nu}}_{i-1} + \mathbf{K}_2 \tilde{\mathbf{y}}_i \quad (5.13)$$

where  $\hat{\boldsymbol{\nu}}$  is the estimated velocity vector;  $\mathbf{M} = \mathbf{M}_{RB} + \mathbf{M}_A$ ;  $\mathbf{D}$  are the mathematical model of the ship matrices, mass (with added mass) and damping that consist of linear and nonlinear components  $\mathbf{D}_L$  and  $\mathbf{D}_{NL}$  respectively as defined in Sect. 3.2;  $\mathbf{R}^T$  is the rotation matrix from global to body-fixed frame;  $\hat{\mathbf{b}}$  is the estimated bias;  $\hat{\psi}' = \hat{\psi} + \hat{\psi}_w$  is the heading resultant from both 1st and 2nd wave induced estimated motions;  $\boldsymbol{\tau}_{\text{ctrl}}$  is the controller output;  $\mathbf{T} = \text{diag}([1000 \ 1000 \ 1000])$  is the bias time constants;  $\Delta t$  is the simulation time step;

$$\mathbf{K}_2 = \begin{bmatrix} \omega_c & 0 & 0 \\ 0 & \omega_c & 0 \\ 0 & 0 & \omega_c \end{bmatrix}; \quad (5.14)$$

$$\mathbf{K}_4 = \begin{bmatrix} 0.1 & 0 & 0 \\ 0 & 0.1 & 0 \\ 0 & 0 & 0.01 \end{bmatrix}; \quad (5.15)$$

$$\mathbf{K}_3 = 0.1\mathbf{K}_4. \quad (5.16)$$

Eq. (5.2) - (5.5) gives a procedure for the separation/isolation of the 1st and 2nd order motions to determine the estimation error, Eq. (5.1) while Eq. (5.8) - (5.13) are to estimate the ship's position and velocity. Parameters of matrices  $\mathbf{T}$ ,  $\mathbf{K}_{11}$ ,  $\mathbf{K}_{12}$ ,  $\mathbf{K}_2$ ,  $\mathbf{K}_3$ ,  $\mathbf{K}_4$  are initially determined based on (Fossen, 2021) aiming for further tuning.

### 5.3 DP controller

As given in Sect. 1.1 there are many possible control laws that can be applied in DP systems that were utilized over the years. In (Mehrjadi et al., 2020) an overview of different control applications to DP of a ship is given. PID controller is a precursor of DP control; however, it requires gain scheduling depending on environmental conditions. Fuzzy logic controllers, on the other hand, require a set of rules and a learning algorithm, which is not always simple and is time-consuming. However, when set, those controllers show high quality. A procedure for the application of fuzzy controllers is given in (Wang et al., 2021; Dang et al., 2020). Adaptive neural network control is worth mentioning as, once trained, it shows highly satisfactory results. Its benefit is that in operation it is fast and does not require a ship model; however, it requires training based on that model. Model Predictive Control (MPC) was presented as most beneficial in terms of smooth, highly precise control; however, it was found not to be resistant to rapid environmental load changes such as wind gusts.

Implementation of MPC was proposed in (Veksler et al., 2016), where it was found to be advantageous compared to other control methods. However,

it presents certain challenges such as demanding software for implementation in real-time operations. The main advantage of MPC is the possibility to impose constraints on the vessel states, control outputs, and also control the dynamics of the output signal, as shown in (Xia et al., 2015).

In (Alagili et al., 2020), authors prove that among tested controllers only PID and MPC were able to control the ship in extreme weather conditions.

For experimental purposes within the dissertation, a simple PID controller was applied. Therefore, this type of control was also utilized in the simulator, following the theory that for validation purposes both systems' design should be as close as possible. In addition, an alternative control with MPC was studied in the simulator to capture the controller type's influence on the DP performance as opposed to the environment's influence.

### 5.3.1 PID

Application of PID control in a DP system is relatively simple and with sufficient information from the state observer ( $\hat{\eta}, \hat{v}$ ), one can write it down with a single equation, Eq. (5.17).

$$\tau_{ctrl} = \mathbf{R}^T(\hat{\psi}) \mathbf{K}_P \Delta \hat{\eta} + \mathbf{R}^T(\hat{\psi}) \mathbf{K}_I \int_0^t \Delta \hat{\eta} dt + \mathbf{K}_D \hat{v}_i \quad (5.17)$$

where  $\Delta \hat{\eta} = \eta_{ref} - \hat{\eta}$ ;  $\eta_{ref}$  is the reference position and heading vector which, in the case of simulation analyses, was set to zero;  $\hat{\eta}$  is the estimated position vector;  $\hat{v}$  is the estimated velocity vector;  $\mathbf{R}^T(\hat{\psi})$  is the rotation matrix from global to body-fixed frame and  $\mathbf{K}_P, \mathbf{K}_I, \mathbf{K}_D \in R^{3 \times 3}$  are the proportional, integral, and derivative controller gain matrices, respectively.

### 5.3.2 Model Predictive Control

As opposed to PID control which mainly accounts for the current moment in time and also the past moments, MPC control is based on the current and future behavior of the system. In other words, MPC controller has features and structure that allow for the prediction of object behavior in a finite time horizon. That further supports the decision on the current control action and allows for sophisticated control.

MPC control is achieved with the utilization of a mathematical model of the controlled object (in DP it is the ship's hull) and a chosen optimization

algorithm that would determine a control action in the current time (at the current simulation iteration).

First, one has to determine a state space model of a ship in DP operations, in body fixed frame, Eq. (5.18).

$$\dot{\mathbf{x}} = \begin{bmatrix} \dot{\boldsymbol{\eta}} \\ \dot{\boldsymbol{\nu}} \end{bmatrix} = \begin{bmatrix} \boldsymbol{\nu} \\ \mathbf{M}^{-1} \mathbf{D}_L \boldsymbol{\nu} + \mathbf{M}^{-1} \mathbf{D}_{NL} \boldsymbol{\nu} |\boldsymbol{\nu}| + \mathbf{M}^{-1} \mathbf{u} \end{bmatrix} \quad (5.18)$$

where  $\mathbf{x} = [x, y, \psi, u, v, r]^T$  is a state vector in the body-fixed frame,  $\mathbf{u} = \boldsymbol{\tau}_{ctrl} = [F_{x,ctrl}, F_{y,ctrl}, M_{z,ctrl}]^T$  is a control forces vector, and  $\mathbf{M} = \mathbf{M}_{RB} + \mathbf{M}_A$ ,  $\mathbf{D}_L$ ,  $\mathbf{D}_{NL}$  are parameters of mathematical models of the hull: mass, linear, and nonlinear damping, respectively, as defined in Sect. 3.2.

By solving Eq. (5.18) for a given  $\mathbf{u}$  and utilizing the current state  $\boldsymbol{\nu}$ , one can determine the future state  $\mathbf{x}$  on the left side of the equation. Analogically, by setting the desired state (in DP  $\mathbf{x} = [0, 0, 0, 0, 0, 0]^T$ ), one can find the  $\mathbf{u}$  that would allow achieving that state in a finite time horizon of  $N$  steps and  $\Delta t_{MPC}$  time step. This is achieved through optimization of the control quality with the QP approach. It is applied in the simulation within the dissertation as defined in Eq. (5.19) - (5.21).

$$\min_{u(i)} \left\{ \sum_{j=0}^N \left( \mathbf{x}_j^{ref} - \mathbf{x}_j^{pred} \right)^2 + \boldsymbol{\lambda}_{MPC} \sum_{j=0}^N (\Delta \mathbf{u}_j)^2 \right\} \quad (5.19)$$

$$\mathbf{u}_{min} \leq \mathbf{u} \leq \mathbf{u}_{max} \quad (5.20)$$

$$\mathbf{x}_{min} \leq \mathbf{x} \leq \mathbf{x}_{max} \quad (5.21)$$

where  $i$  is the current simulation iteration;  $j$  is the step notation over the  $N$  prediction horizon length;  $\mathbf{x} = [\boldsymbol{\eta}, \boldsymbol{\nu}]^T$  is the ship response, position, and speed;  $\mathbf{x}_j^{ref}$  is a reference trajectory response (in the studied DP case it is  $\mathbf{x}_j^{ref} = \mathbf{x}^{ref} = const. = [0, 0, 0, 0, 0, 0]$ );  $\mathbf{x}_j^{pred}$  is the predicted response due to  $\Delta \mathbf{u}_j$ ;  $\Delta \mathbf{u}_j = \mathbf{u}_j - \mathbf{u}_{j-1}$  is the control forces vector change over one step along the prediction horizon, and  $\boldsymbol{\lambda}_{MPC}$  is a weight coefficient to account for the control signal change.

MPC optimization steps are listed below.

1. Optimization constraints for  $\mathbf{x}$  and  $\mathbf{u}$  are set prior simulation. They are relatively easy to determine as ship in DP is assumed to move within few meter radius circle and within few degrees deviation of heading, the maximum allowed speed is usually below 2 m/s. Constraints on  $\mathbf{u}$  will result from the propulsion system capabilities and can also be easily calculated.
2. Prediction horizon  $N$  and time step  $\Delta t_{\text{MPC}}$  are set prior simulation. Prediction horizon is usually 5 - 20 steps, with a selected time step usually higher than the simulation time step.
3. Weight coefficient of the control signal change,  $\lambda_{\text{MPC}}$  is set. By adjusting  $\lambda_{\text{MPC}}$ , one can impose more aggressive or more smooth control. This parameter needs to account for thrusters inertia, tear and wear of the thrusters.
4. At any simulation iteration  $i$ , actual state  $\mathbf{x}(i)$  of the ship is determined by the state observer and passed to the MPC.
5. As an initial state in the prediction horizon,  $\mathbf{x}_{j=0} = \mathbf{x}(i)$  is adopted.
6. MPC utilizes the state  $\mathbf{x}_{j=0}$  and discretized state space model given in Eq. (5.18) to find optimal  $\mathbf{u}(i+1)$  by defining optimal sequence of controls regarding Eq. (5.19) - (5.21).
7. The first control over the optimal sequence is passed to the thrust allocation module,  $\boldsymbol{\tau}_{\text{ctrl}(i+1)} = \mathbf{u}_{(i+1)} = \mathbf{u}_{j=0}$ .

Presented concept is repeated for each next iteration of the simulation, up to  $N$ . Even though the whole control sequence is determined in MPC, this only serves to find the first step of control action. The whole trajectory needs to be determined to be able to judge if this first step is the best possible considering the objective function and constraints.

## 5.4 Thrust allocation

Within the dissertation, quadratic programming was deployed in simulation. However, the objective function given in Eq. (4.12) in Sect. 4.2.4 is extended by the dynamic term as follows.

$$\min_{\mathbf{u}_T} \left\{ \mathbf{u}_T^T \mathbf{W}_l \mathbf{u}_T \right\} \quad (5.22)$$

$$\mathbf{A}_l \mathbf{u}_{TA} = \mathbf{b}_l \quad (5.23)$$

$$\mathbf{G}_l \mathbf{u}_T \leq \mathbf{h}_l; \quad (5.24)$$

where  $\mathbf{u}_{TA} = \boldsymbol{\tau}_{TA} = [T_{x1}, T_{y1}, T_{x2}, T_{y2}, \dots, T_{xN}, T_{yN}]^T$  is thrust components on x and y axes;  $N$  is the total number of thrusters;  $\mathbf{u}_T = [\mathbf{u}_{TA}, \mathbf{u}_{\Delta T}]^T$ , where  $\mathbf{u}_{\Delta T} = [\Delta T_{x1}, \Delta T_{y1}, \Delta T_{x2}, \Delta T_{y2}, \dots, \Delta T_{xN}, \Delta T_{yN}]^T$ ;

Part of weight coefficients in matrix  $\mathbf{W}$  corresponding to thrust forces,  $\mathbf{u}_T$  are dictated by the dependencies between thrust and power. The part of  $\mathbf{W}_l$  corresponding to  $\mathbf{u}_{\Delta T}$  weighs the thrust component change between the previous iteration and the current iteration. Part of the matrix  $\mathbf{G}_l, \mathbf{h}_l$  that defines constraints on  $\mathbf{u}_{TA}$  consists of saturation constraints and accounts for thruster losses and forbidden zones of azimuth thrusters as defined in Sect. 4.2. The other half of  $\mathbf{G}_l, \mathbf{h}_l$  that concerns  $\mathbf{u}_{\Delta T}$  defines a maximum allowed thrust vector change from the previous iteration to the current iteration. This constraint is based on the thrusters' inertia. Equality constraint  $\mathbf{A}_l, \mathbf{b}_l$  and inequality constraints  $\mathbf{G}_l, \mathbf{h}_l$  concerning  $\mathbf{u}_{TA}$  are defined as given in Sect. 4.2.

# Chapter 6

## Numerical experiments

With utilization of methods given in Ch. 3 and Ch. ?? the simulations were conducted within the dissertation and based on DNV level 3-site. For simulator validation purposes, the MSV ship model in scale 1:36 was used as it was also tested in DP experiments prior to the study. The main particulars of the model are given in Ch. 3 and the basic data of the MSV in full scale are presented in Apx. A.

The utilized simulation tools are listed in Sect. 6.1. Subsequently, results and summary are presented in Sect. 6.2 and 6.3 respectively.

### 6.1 Methods and tools

For the purpose of dynamic analyses, a DP capability assessment tool was developed. The tool allows for dynamic analyses with DNV level 3 and 3 - site. Users have control over the DP control system setup (observer, PID, MPC parameters), hull model, thruster models and their dynamics (by setting azimuth thruster rotation and propeller revolution rate). The wind, waves, and current increase over the first few seconds of the simulation is applied.

The tool is a powerful engine for potential future validation with more examples, and DP capability assessment. The tool also allows for static analyses (DNV level - 1, level - 2, and level 2-site). A screenshot of the web application user interface is shown in Fig. 6.1.

Other tools that served to determine input data, hull and thruster models were:

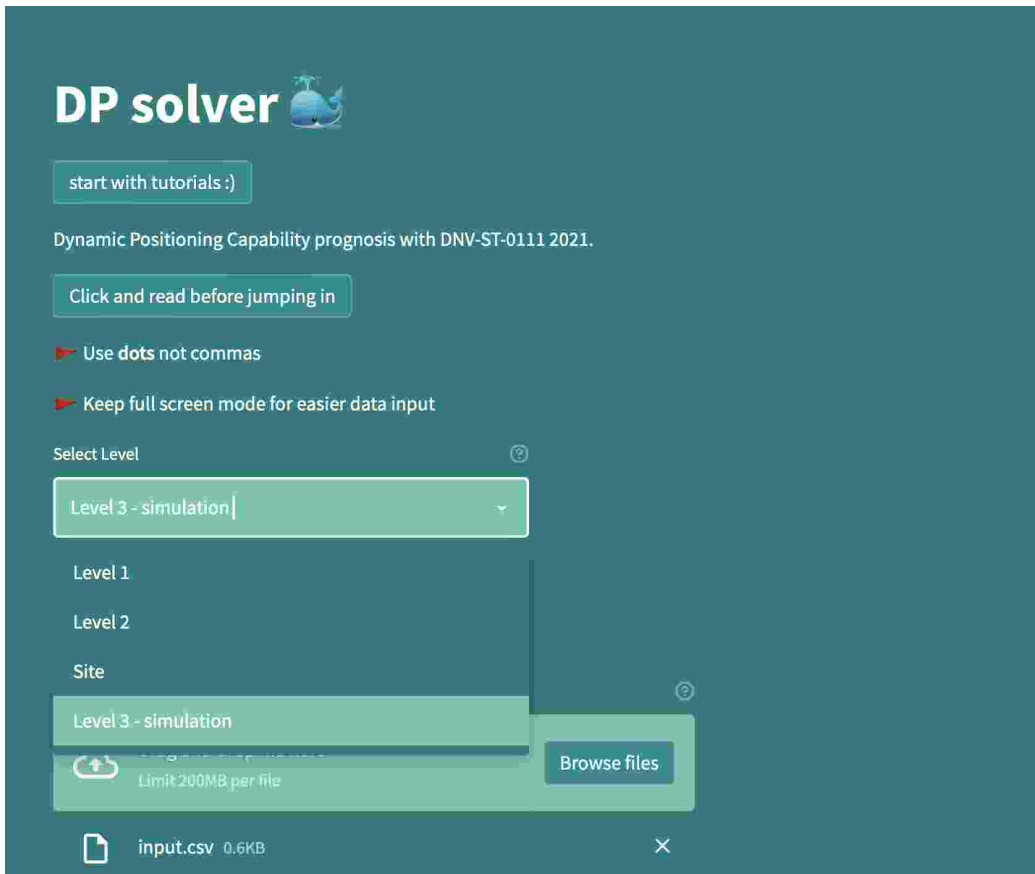


Figure 6.1: Introduction of the tool

1. *Ansys Aqwa* - hull mathematical model (added masses), Wave loads (QTF, 2nd order wave drift forces and RAO, 1st order wave frequency forces).
2. *Stac CCM+* - hull mathematical model (damping) and azimuth thrusters models. This tool could also be used for wind coefficients determination.

The above was implemented as described in Ch. 3. The simulator structure is shown in Fig. 5.1 in Ch. 5.

## 6.2 Results and discussion

Following the experiments, three cases of environmental disturbances were simulated: current, short, and long wave, corresponding to test cases 21, 29, and 30 given in Ch. 7. In this section, only simulation results will be discussed, while the comparison to the experiment is presented in Ch. 8.

Figures 6.2 - 6.7 present results of simulations and a comparison between PID and MPC controllers. In all cases, revolutions and azimuth thruster angles stabilize over time.

DP simulation with current conditions shows excellent results. The position variations are negligible and the heading remains constant over the whole simulation. Both controllers result in similar footprints (Fig. 6.2). Also in the case of thrusters control settings (revolutions,  $n$  and thruster angle,  $\beta$ ) both controllers show stability and result in similar control (Fig. 6.3). Both converge to a constant value within the realization time of the simulation.

In case of simulation with short wave, both controllers fail to keep position (Fig. 6.4). While the PID controller results in position oscillation, in the case of the MPC, the control is lost and the hull model drifts fast away from the reference position. Heading is kept stable and within the station-keeping requirements in the case of the PID controller. The faulty behavior of the MPC is directly caused by a relatively rapid increase of the environmental disturbances from zero to a final value of wave force. While the PID handles this change in wave forces, the MPC fails. The conclusion is that the MPC operates better in stationary conditions that are also quite typical for real-world operations. The not stationary character of initial conditions of the wave or current is a more general issue with experiments, and for future research, an adequate method to account for that should be developed if possible. For the sake of simulation validation, the same physical conditions at the experiments were mirrored in simulation.

Since the control inputs to TA are not fulfilling the QP constraints, the algorithm stops at a constant value that does not change until the QP finds the solution, which in this case does not happen. Hence, the thrusters' control inputs in Fig. 6.5 are constant after about 20 seconds of the simulation. In the case of PID and starboard azimuth thruster, at about 180 seconds of the simulation, TA outputs an opposite direction of the thruster (from 180° to 0°). At the same time, this thruster has a minor effect on ship motion as, at that moment of the simulation, Revolutions  $n$  are low compared to other thrusters, generating respectively low thrust. At low thrust values resulting

in TA, the change from positive to negative value can occur randomly. That has, however, a negligible effect on DP control as the forces are very low.

DP capability assessment for a long wave showed excellent performance of both controllers in terms of station keeping and the thrusters set controls. However, as will also be shown in experiments, the faulty performance of the observer is visible in thrusters set controls. This does not affect the DP capability prognosis, and for that purpose, is considered sufficient. However, in real operations, it is necessary to improve it.

Current direction 90 deg,  $v_c = 0.03$  m/s  
case: 21

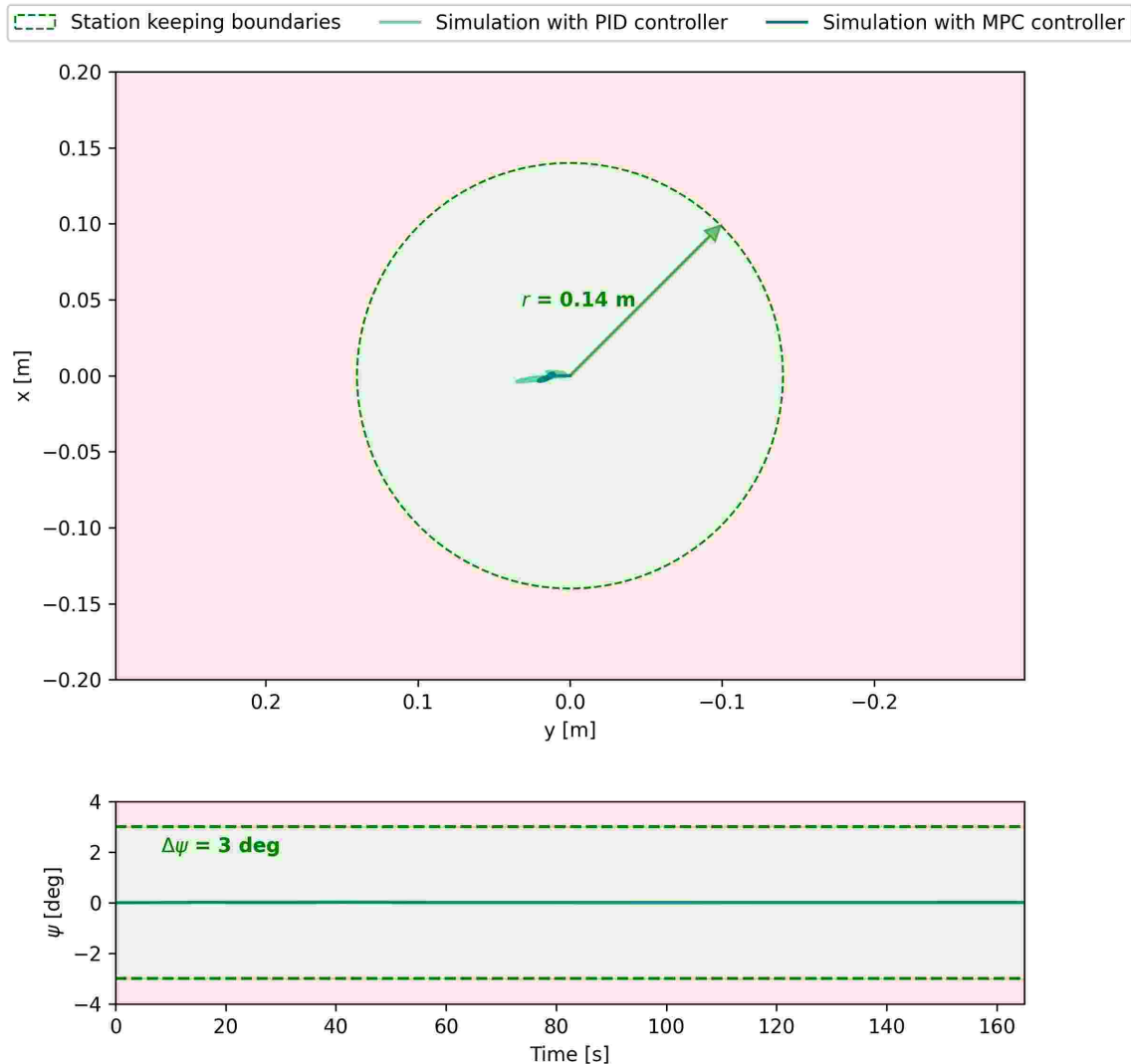


Figure 6.2: Ship model footprint: current

Current direction 90 deg,  $v_c = 0.03$  m/s  
case: 21

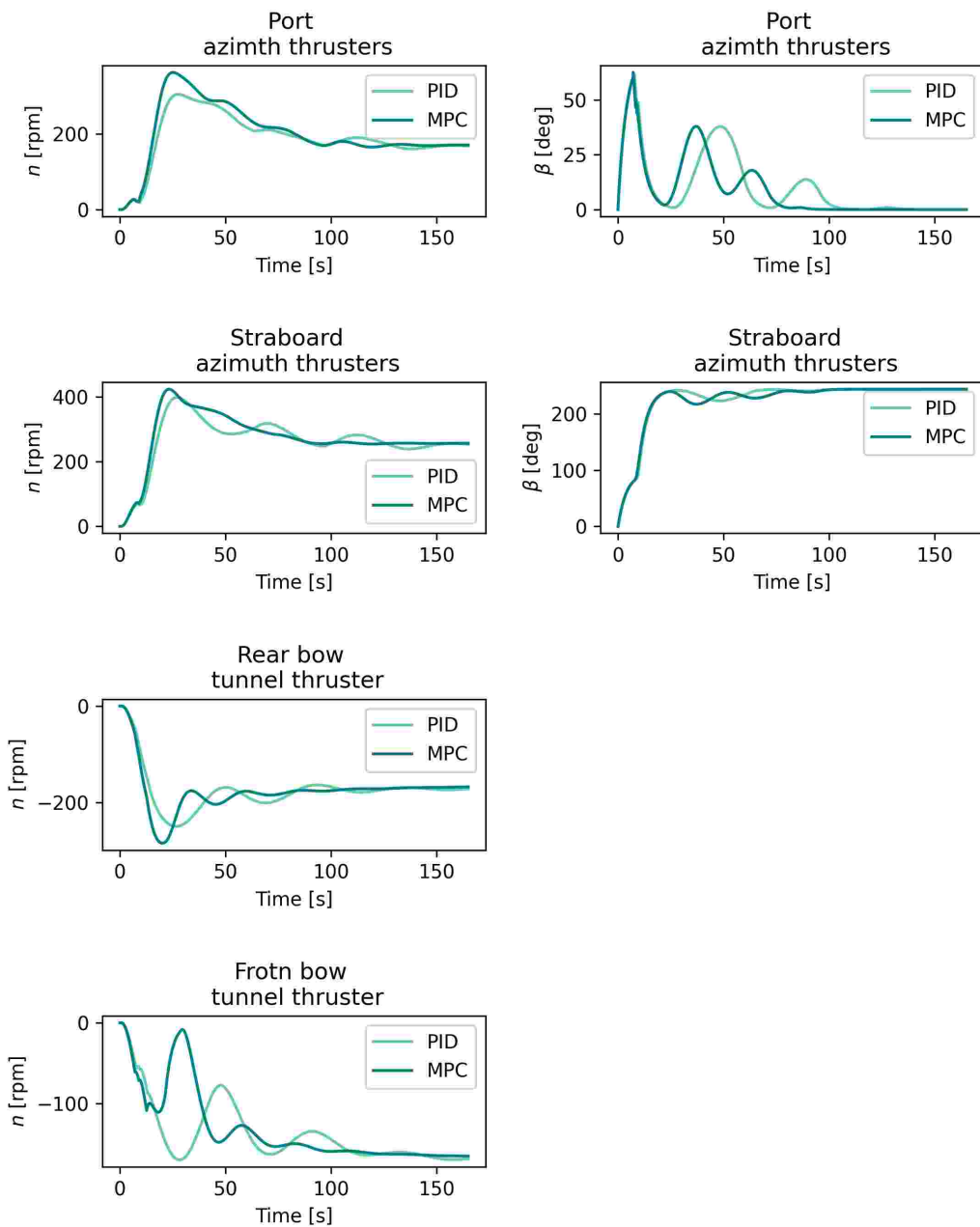


Figure 6.3: Thrusters settings: current

Wave direction 90 deg,  $H_s = 0.04$  m,  $T_p = 0.92$  s  
case: 29

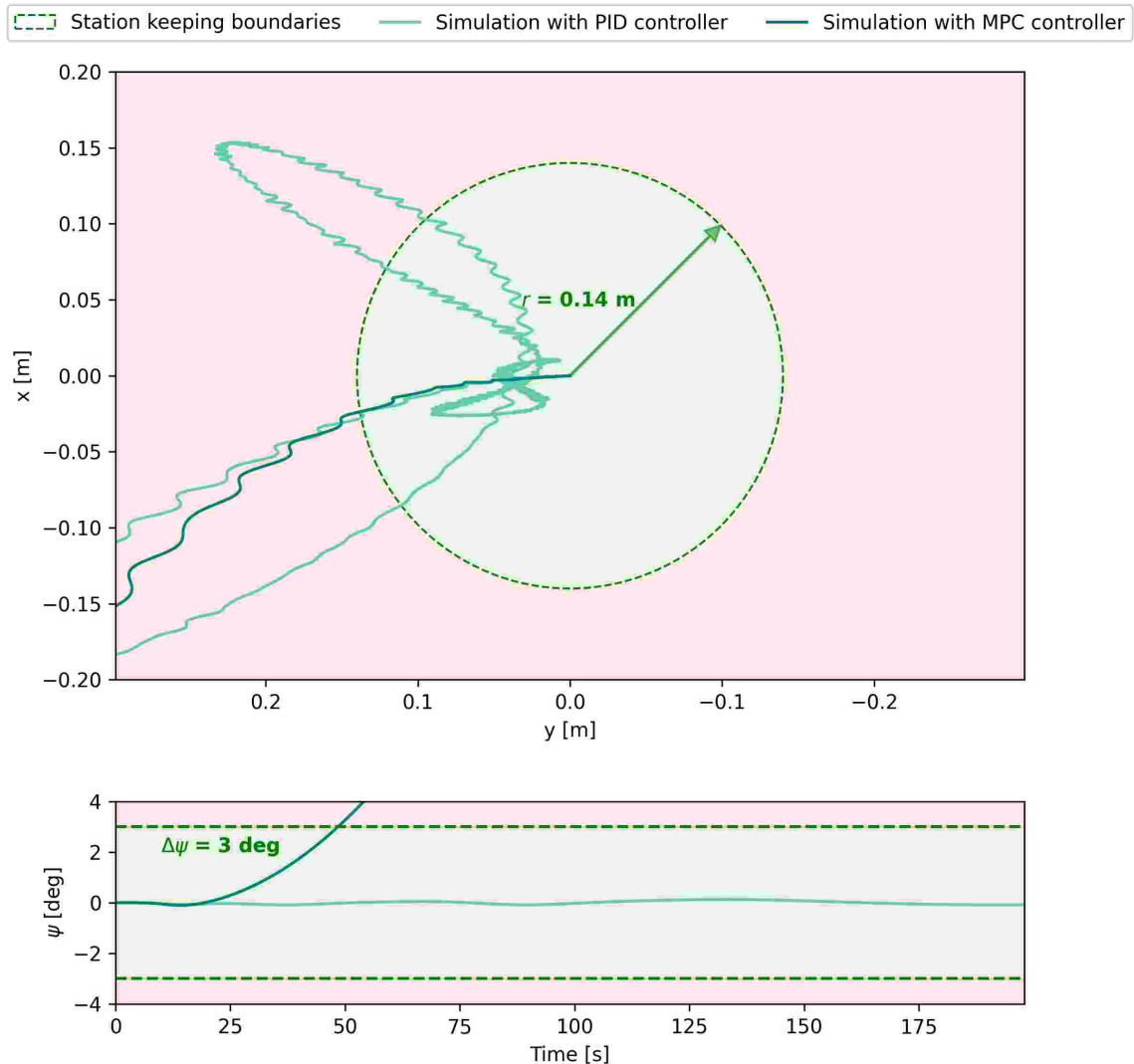


Figure 6.4: Ship model footprint: short waves

Wave direction 90 deg,  $H_S = 0.04$  m,  $T_P = 0.92$  s  
case: 29

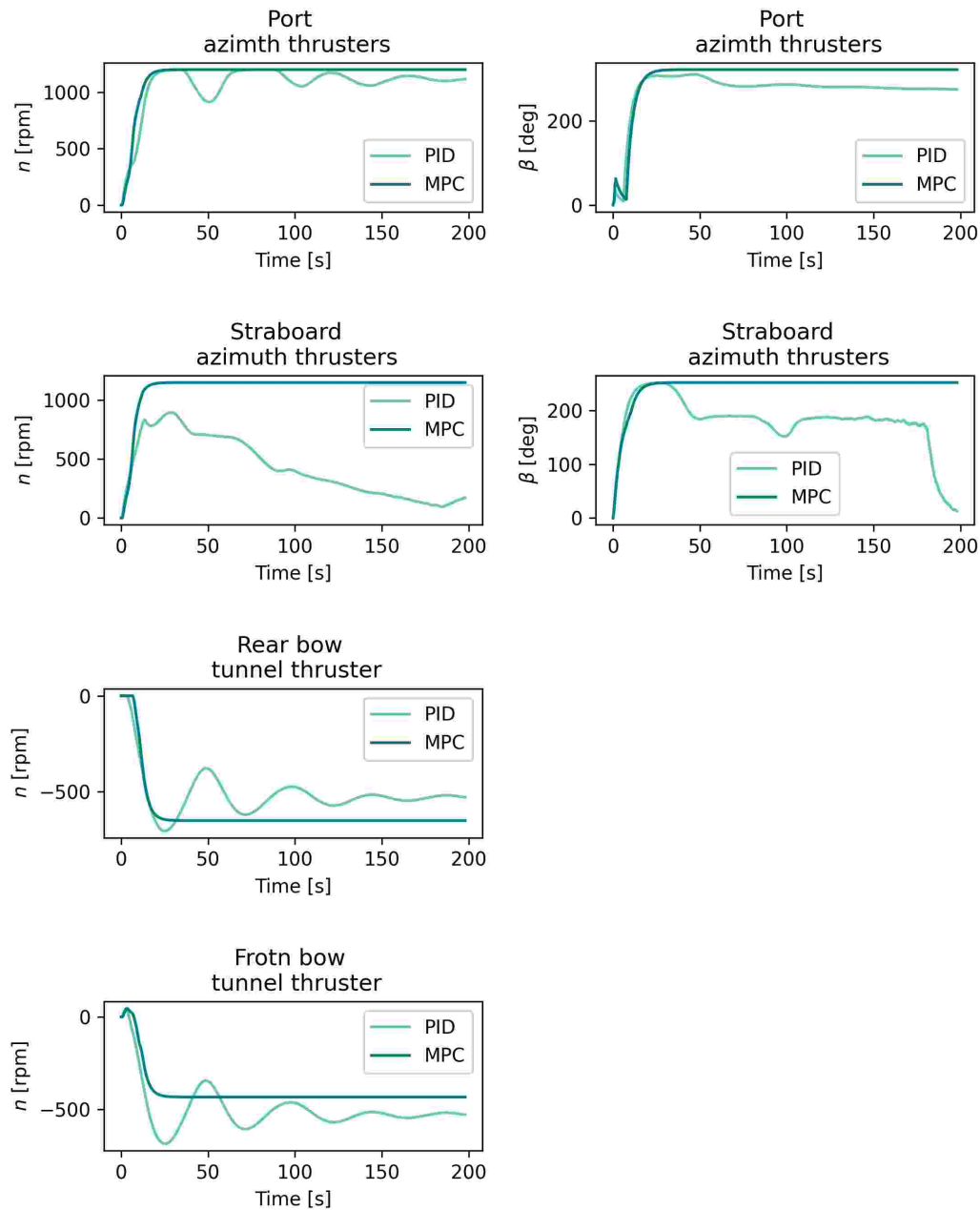


Figure 6.5: Thrusters settings: short waves

Wave direction 90 deg,  $H_S = 0.04$  m,  $T_P = 1.60$  s  
case: 30

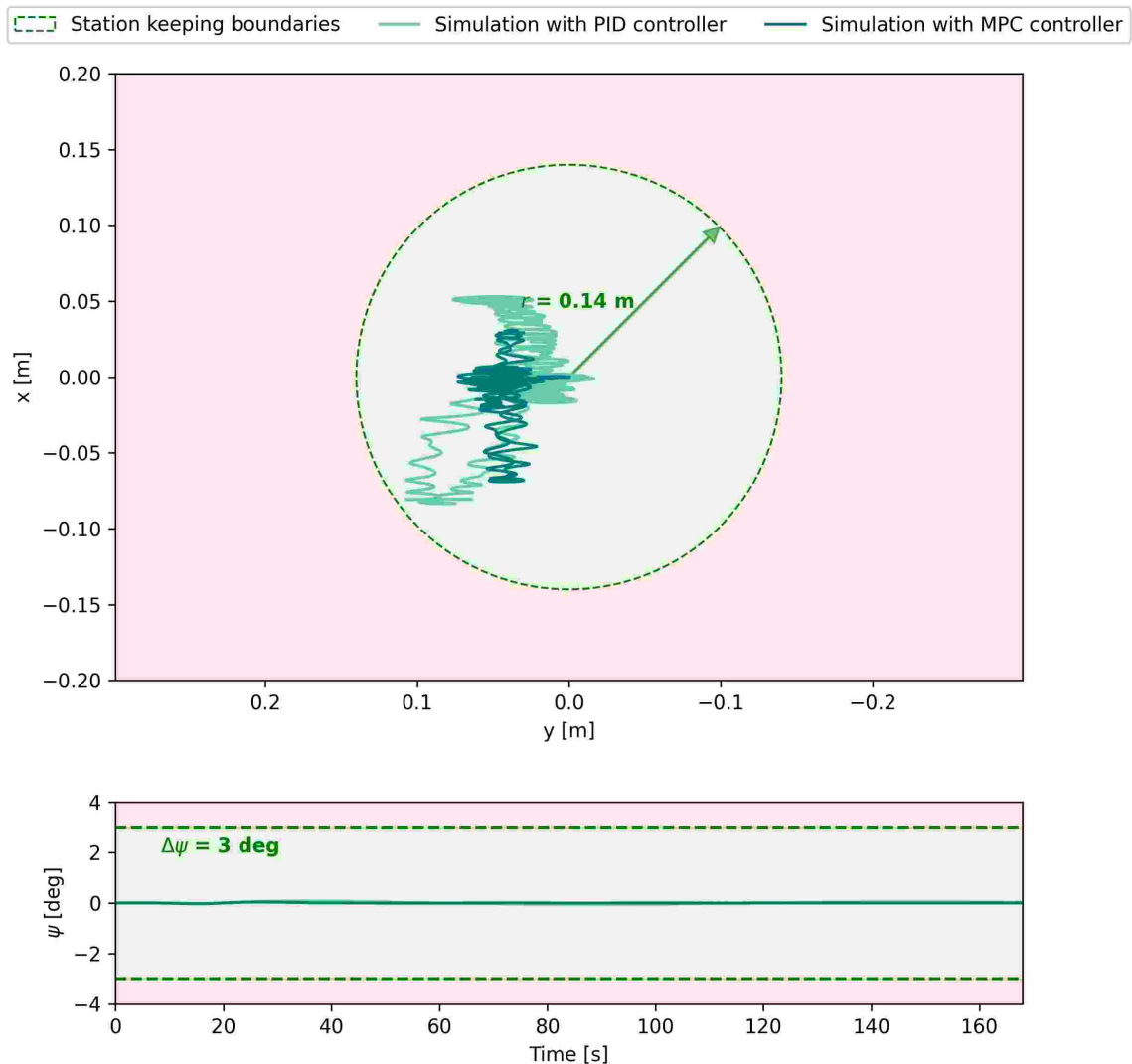


Figure 6.6: Ship model footprint: long waves

Wave direction 90 deg,  $H_S = 0.04$  m,  $T_P = 1.60$  s  
case: 30

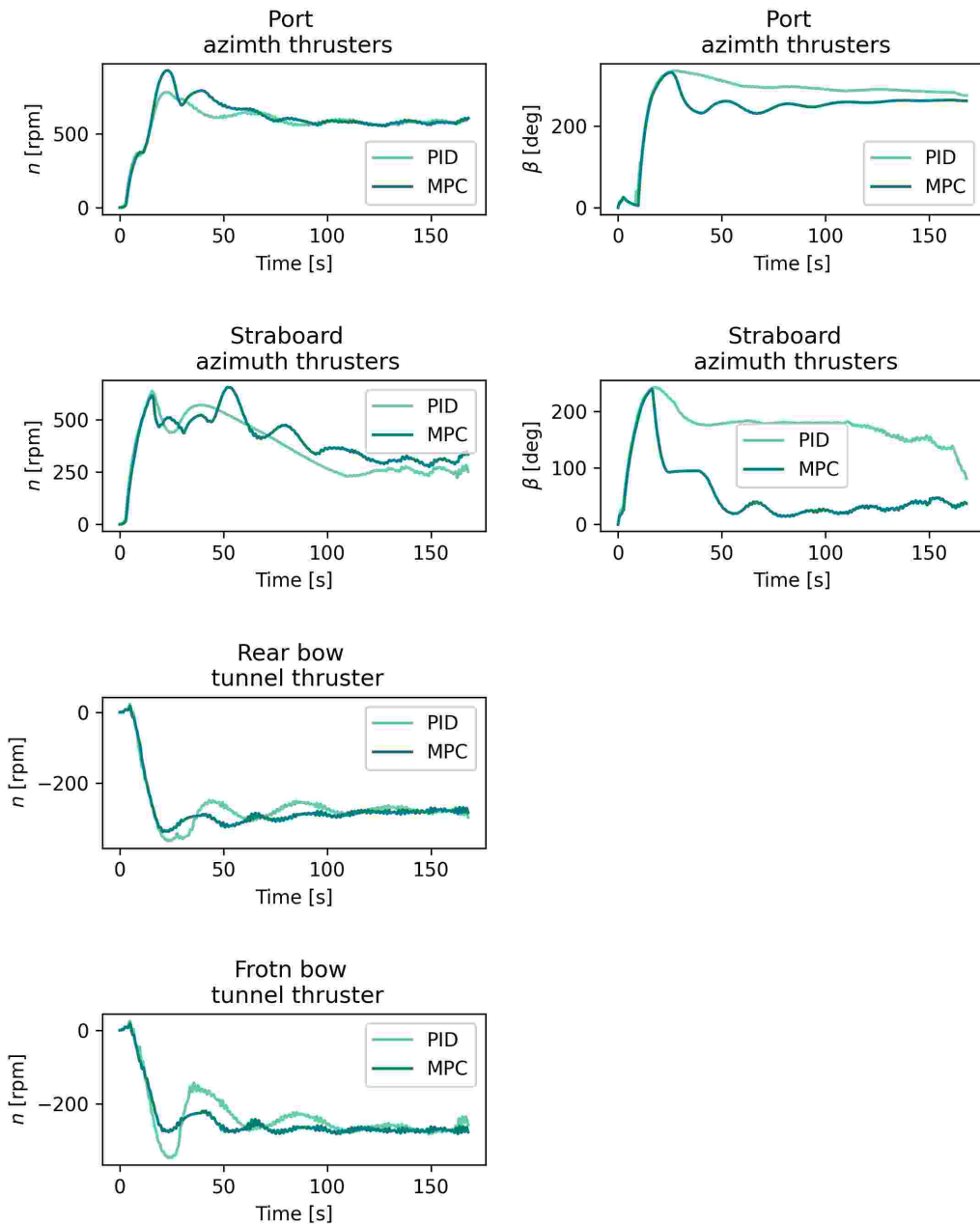


Figure 6.7: Thrusters settings: long waves

## 6.3 Summary

In all cases (except for short wave) the thrusters follow the control command very closely, testifying to the correct thrust allocation algorithm and fast enough thruster rates.

As the MPC controller optimizes for an objective function as given in Eq. (5.19), the value of that function over time was also compared to a value of the same function calculated while using the PID controller. This value over time was very similar for both controllers. Which in turn leads to the conclusion that the PID controller results in a similar effect of control. Moreover, PID controller showed better performance for a short wave, even though it also lost position.

DP simulator tool deployed for DP capability assessment is relatively fast (PID control - 2 min simulation time, MPC control - 7 min simulation time). Gathering input data is, however, time-consuming. As an alternative, one can utilize a similar vessel to model hull, thrusters, waves, and wind.

# Chapter 7

## Physical model experiments

For the purpose of the dynamic and static DP capability analyses validation, the data from several physical experiments were utilized. The experiments were carried out in the research facility of Maritime Advanced Research Centre (CTO S.A.) prior to the study done within the dissertation. A Multi-Service Vessel (MSV) model in scale of 1:36 was used as introduced in Sect. 3.1. MSV data in full scale are given in Tab. A.3 and Tab. A.5 (in Apx. A).

The environmental setup of the tests is given in Sect. 7.1. Subsequently, in Sect. 7.2 DPS discrepancies between the simulation and experiments are presented. The test results are shown and discussed in Sect. 7.3. Sect. 7.4 summarizes the experiments which complete the Chapter.

The details concerning the in-house developed DPS for the purpose of those tests are given in Apx. C together with the results that are not directly utilized within the dissertation.

### 7.1 Setup

The tests were conducted at the offshore towing tank of dimensions 50 m × 7 m × 3 m denoting length, breadth, and depth respectively. The towing tank is equipped with the test stand carriage that can move along the tank (Fig. 7.1).

The DPS test stand is designed to carry out DP capability tests on the ship model in scale equipped with a propulsion system consisting of two azimuth thrusters and two tunnel thrusters. The system was designed mainly

based on (Fossen, 2002; IMCA, 2007). The test stand includes both the physical model propulsion control system and the measuring equipment, which comprise the DPS.



Figure 7.1: The test stand carriage at the offshore towing tank in CTO S.A.

To simulate irregular waves representing a desired sea state, the flap type wave maker located at the end of the tank is utilized (Fig. 7.2).

Two wave spectra were modeled in the towing tank to assess the DP capability performance in long and short waves, associated with longer and shorter  $T_p$  respectively as given in Tab. 7.1. The same height of the waves was preserved.

Current conditions were simulated by imposing a motion of the model along the tank. This was achieved by setting the fixed reference position of the model relative to the carriage and moving the carriage with a constant speed along the tank.

No wind conditions were modeled due to similarity law constraints, as explained in Sect. 3.4.

Quantities that describe the environmental conditions tested are given in Tab. 7.1 both in model scale and full scale.

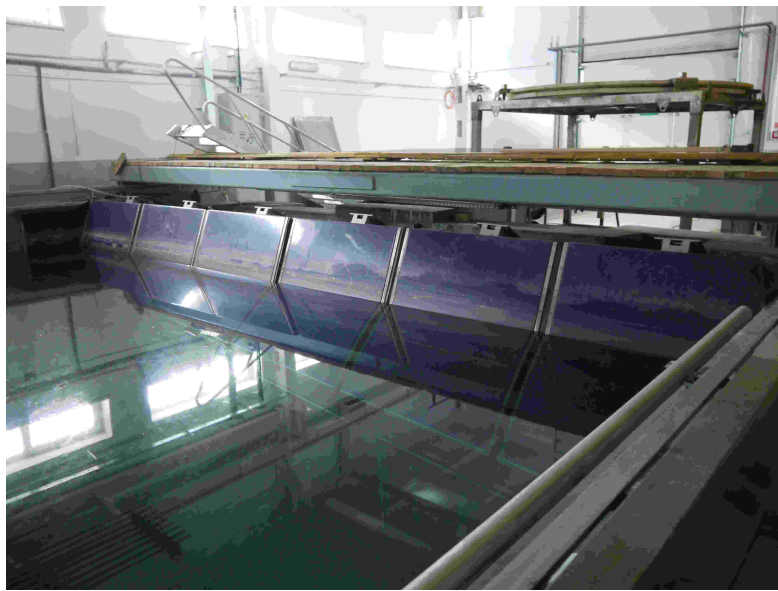


Figure 7.2: The flap type wave maker at the offshore towing tank in CTO S.A.

Table 7.1: DP model tests conditions

Quantity	Symbol	Units	Model scale 1:36	Full scale
Current speed	$v_c$	m/s	0.030	0.180
Wave height	$H_S$	m	0.04	1.44
Wave period - short waves	$T_p$	s	0.92	5.52
Wave period - long waves	$T_p$	s	1.60	9.20
Wave spectrum type	$\gamma$	-	3.3	3.3

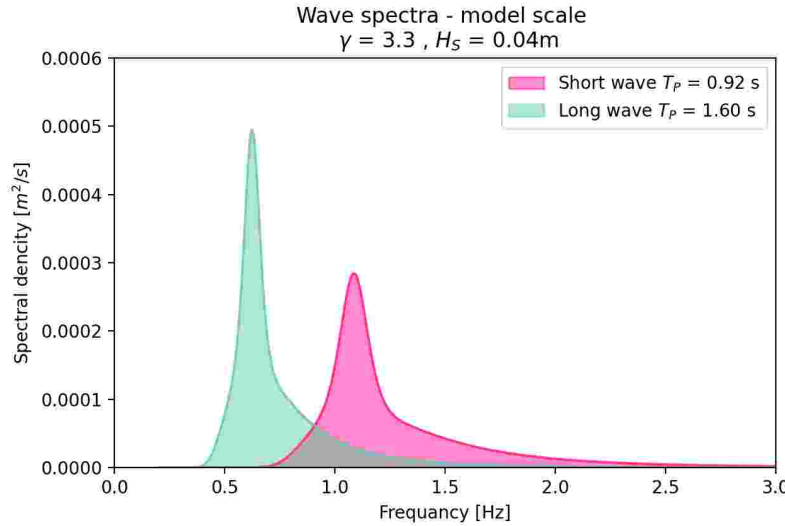


Figure 7.3: Theoretical wave spectra for short and long wave - model scale

## 7.2 DPS incorporation

DP system structure as implemented during the experiments was presented in Fig. 5.1 in Ch. 5. Experimental DPS is mirrored to some extent in the simulation as given in Ch. 5, except for TA handling.

In the DP simulation carried out within the dissertation, the QP method was implemented to TA, while in experiments, the TA was tailored for the physical model MSV. Prior to the experiments, the azimuth thruster angles were constrained to fixed settings based on the static analysis with the utilization of suboptimal thrust allocation for environmental conditions corresponding to the tested ones. During the experiment, only revolutions of the thrusters were controlled and based on mapped thrust and thruster models. To simplify the problem, an overactuated system was reduced, which allowed finding thrust forces (which translate to revolutions) by simply solving 3 DOF equations with three thrust force unknowns. Two azimuth thrusters were kept (at angle  $\beta$ ) while two bow tunnel thrusters were treated as one. The thrust on the latter was divided into two physical thrusters with the

application of weights on those actuators.

The virtual control forces  $\boldsymbol{\tau}_{\text{ctrl}}$  are distributed among a reduced amount of three thrusters in the relation given in Eq. (7.1).

$$\boldsymbol{\tau}_{\text{ctrl}} = \mathbf{L}(\beta)[T_1 T_2 T_3 T_4]^T = \mathbf{L}(\beta)\boldsymbol{\tau}_{\text{TA}} \quad (7.1)$$

where  $T_1, T_2, T_3, T_4$  are values of the allocated thrust on each thruster (1,2 - azimuth thrusters, 3,4 - tunnel thrusters) and  $\mathbf{L}(\beta)$  is a location matrix given by Eq. (7.2), depending on the azimuth thrusters' angles  $\beta \in \{\beta_1, \beta_2\}$ .

$$\mathbf{L}(\beta) = \begin{bmatrix} \cos \beta_1 & \cos \beta_2 & 0 & 0 \\ \sin \beta_1 & \cos \sin \beta_2 & 0 & 0 \\ x_{\text{thr}1} \sin \beta_1 - y_{\text{thr}1} \cos \beta_1 & x_{\text{thr}2} \sin \beta_2 - y_{\text{thr}2} \cos \beta_2 & x_{\text{thr}3} & x_{\text{thr}4} \end{bmatrix} \quad (7.2)$$

where  $\beta_1$  and  $\beta_2$  are orientation angles of azimuth thrusters and  $x_{\text{thr}1}, y_{\text{thr}1}, x_{\text{thr}2}, y_{\text{thr}2}, x_{\text{thr}3}, x_{\text{thr}4}$  are thruster location coordinates.

Subsequently, a pseudo-inverse matrix is applied as in Eq. (7.3) to solve the allocation problem, which is equivalent to determining the thrust vector,  $\boldsymbol{\tau}_{\text{TA}}$ .

$$\boldsymbol{\tau}_{\text{TA}} = L^{pinv} \boldsymbol{\tau}_{\text{ctrl}} \quad (7.3)$$

where  $\mathbf{L}^{pinv} = \mathbf{L}^T (\mathbf{L} \mathbf{L}^T)^{-1}$ .

Subsequently, through thruster models and weights on bow thruster revolutions, the settings on all thrusters are established.

### 7.3 Results and discussion

Several test runs on a dynamically positioning controlled physical model, under current and wave conditions, were performed. Tab. 7.2 gathers all cases postprocessed within the dissertation. The angles of the azimuth thrusters, predefined prior to the analyses, are specified in the table.

Table 7.2: Model tests runs

No.	Test reference No.	Condition in model scale		Reference model heading	Main thrusters fixed orientation angle	
		current	wave		port thruster	starboard thruster
1	21	0.030 m/s	×	90°	315°	252°
2	22	0.030 m/s	×	90°	315°	252°
3	23	0.030 m/s	×	270°	315°	252°
4	24	0.030 m/s	×	270°	315°	252°
5	25	×	$H_S = 0.04 \text{ m}$ $T_p = 0.92 \text{ s}$ $\gamma = 3.3$	90°	315°	252°
6	27*	×	$H_S = 0.04 \text{ m}$ , $T_p = 0.92 \text{ s}$ $\gamma = 3.3$	90°	40°	320°
7	28	×	$H_S = 0.04 \text{ m}$ $T_p = 0.92 \text{ s}$ $\gamma = 3.3$	90°	40°	320°
8	29	×	$H_S = 0.04 \text{ m}$ $T_p = 0.92 \text{ s}$ $\gamma = 3.3$	90°	40°	320°
9	30	×	$H_S = 0.04 \text{ m}$ $T_p = 1.60 \text{ s}$ $\gamma = 3.3$	90°	40°	320°

\* without state observer

For each case, position and heading are measured. To assess DP capability based on those experimental results, DNV guidelines on the station keeping are adopted, based on DNV Level-3. Accuracy and minimum exposure are given in Tab. 7.3. Subsequently, Tab. 7.4 presents a summary of the results in relation to those guidelines.

Table 7.3: Dynamic positioning limits and realization according to DNV standard (DNV, 2021)

Scale	Minimum realization time	Maximum position offset radius	Maximum heading offset
Full scale	180 min	5.00 m	3 deg
Model scale 1:36	30 min	0.14 m	3 deg

Table 7.4: Summary of the DP experiments results

Test reference No.	Realization [min:sec]	Position accuracy - offset radius [m]	Heading accuracy - offset [deg]	Keep position
21	2:45	0.03	0.3	yes
22	2:00	0.02	0.3	yes
23	1:50	0.03	0.2	yes
24	2:25	0.05	0.6	yes
25	3:20	0.71	16.3	no
27*	3:20	0.58	21.0	no
28	3:20	0.64	24.7	no
29	3:20	0.56	21.3	no
30	3:20	0.11	5.8	no

\* without state observer

Concerning three different disturbances - current, short wave, and long wave - all available results were analyzed in terms of quality of control, DP accuracy, and exposure time. For each disturbance, one representative result was selected for further validation of the simulator. The rest of experimental results are presented in Apx. C.2.

Figures 7.4 - 7.8 show DP capability results in current and waves, while figures 7.5 - 7.9 present measured revolution signals corresponding to those test results.

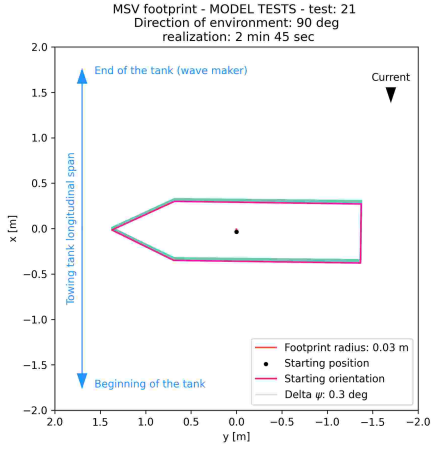


Figure 7.4: Footprint of the physical ship model in dynamic positioning under current conditions - test 21

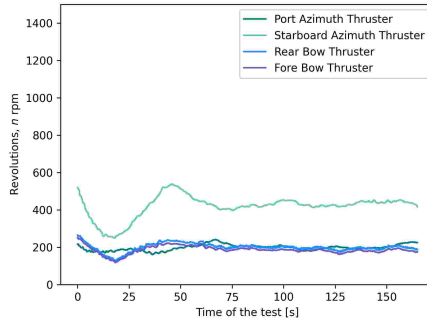


Figure 7.5: Revolutions of the propellers recorded during test 21

In current condition, the DPS results in good stability of the thruster control signals (revolutions  $n$ ). Moreover, a relatively small fraction of the thrusters' capacity is utilized. The position and heading of the physical model are not affected.

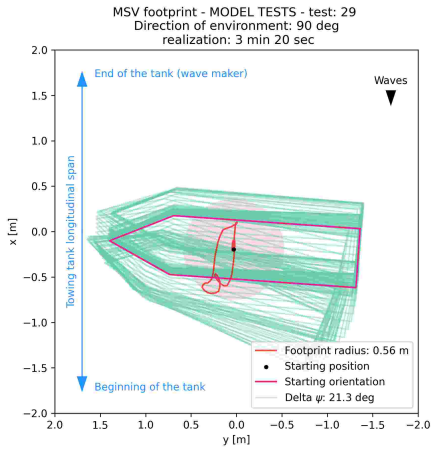


Figure 7.6: Footprint of the physical ship model in dynamic positioning under short wave conditions - test 29

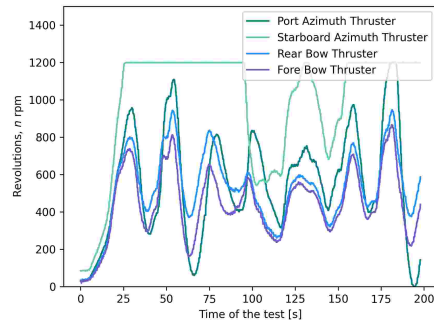


Figure 7.7: Revolutions of the propellers recorded during test 29

In the case of a short wave, the DPS could not handle the wave disturbances. The system resulted in highly variable thruster control signals, destabilizing the physical model. The position and heading were not maintained in terms of DNV defined limits (Tab. 7.3).

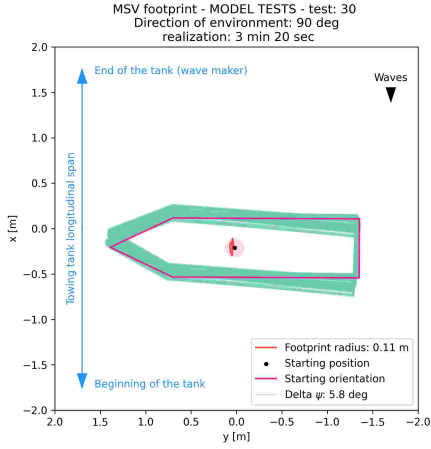


Figure 7.8: Footprint of the physical ship model in dynamic positioning under long wave condition - test 30

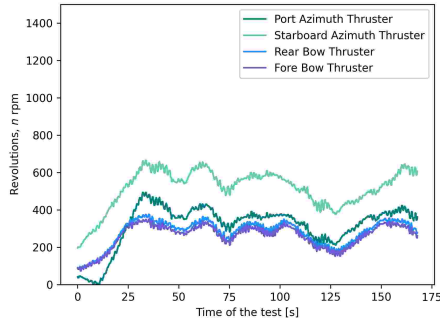


Figure 7.9: Revolutions of the propellers recorded during test 30

In the case of a long wave of the same height as the previously discussed short wave, a significant improvement in control is observed. The physical model keeps position in terms of DNV defined limits (Tab. 7.3) while heading variations are exceeded. Thruster control inputs are relatively stable; however, filtering of wave frequency induced motion could be further improved.

## 7.4 Summary

In all tested cases, the exposure was under 5 minutes, which is shorter than what the DNV guidelines state (Tab. 7.3). However, based on the stability of the control signals over the tested period of time (in all cases except for short wave) it is considered that the test realization time is sufficient for the validation purposes.

Revolutions signal for case 29 (short wave) shows very aggressive control that in terms of DP is undesired since it causes tear and wear of the thrusters and overall low efficiency (expensive in terms of fuel consumption). This noisy response of the control system (observer, controller and thrust allocation together) could be improved with further research on controller and observer gains as well as thrust allocation algorithm.

DP performance is drastically deteriorated for the shorter wave compared to the wave of the same height but longer period. This is justified with the utilization of numerical tools for wave forces estimation in full scale. Drift forces at 90° for the MSV ship are significantly higher than those for the longer wave.

The tests were conducted prior to this study and were the first tests of such kind carried out in CTO S.A. towing tank facility. Concerning the prototype DPS on a physical model, the acquired data was a significant number for such a case. Taking into account the laborious character of all conducted research, three cases were selected to proceed with comparison to other DP assessment methods.

Based on the results, the DPS mounted on the ship model in scale could be improved. Possibly, this study could result in the implementation of a more sophisticated TA algorithm and introduce MPC control in physical experiments.

Nevertheless, the experiments are a valuable reference to the simulation results. Major deviations of results would indicate the low quality of the DP simulator design. Hence, the tests are a valid contribution to the study.

# Chapter 8

## Comparative analysis of numerical and physical experiments

The research presented in this dissertation leads to the development of a design support system for assessing DP capability based on both static and dynamic methods. The prototype DSS is tested using a single case study involving an MSV ship and three distinct weather conditions. However, developed tools are the basis for future extensive validation involving many ship cases. By utilizing the developed tool (DP solver program) for performing prognosis (with the support of other numerical tools) and model test results, a valuable insight into the accuracy of DP capability predictions can be obtained, with a particular emphasis on the reliability of static methods.

Ship fulfills station keeping criteria when footprint radius remains within 5 m and heading variation does not exceed 3 deg (DNV, 2021). These criteria are specifically applicable to dynamic analyses and tests. Three suggested methods (static, dynamic simulation, and experimental) differ in terms of input parameters, the approach to parameter determination, and the techniques used for data processing and application. A detailed comparison of these methods is provided in Tab. 8.1.

Methods cross-referenced with environmental conditions are gathered in the Tab. 8.2 together with the results in respect to the station keeping criteria.

Static DP capability prognosis is compared to DP simulation and to model tests. To ensure a more accurate comparison, simulation is carried out for the ship in model scale; however, the results are presented in full scale (rescaled

according to scaling laws).

The conditions at the towing tank are not normalized with the DNV environmental table (Tab. 2.1). Tested conditions are waves of 1.44 m and peak periods of 5.52 s and 9.20 s comprising short and long waves; current speed is 0.18 m/s. Those conditions are not specified in the referred table. According to DNV-ST-0111, the minimum defined current speed is 0.25 m/s and the closest wave height to the one tested is 1.3 m with the corresponding peak period of 6.5 s. Moreover, DNV level 1, 2, 3 assumes wave, current, and wind acting simultaneously and of values strictly given by the table (Tab. 2.1). Hence, DNV level 1, 2, and 3 are not analyzed for the purpose of comparison. Only level 2-site and level 3-site are taken into the analyses. Since level 2-site is solved in a static approach and level 3-site in dynamic (simulation), the static and dynamic methods are compared within the dissertation. In the static method level 2-site, current forces are determined with wind tunnel model tests on a similar vessel (RV - also used within the study in Ch. 4) and wave coefficients are defined with *Ansys Aqwa* software, the same as for dynamic methods but only drift static forces are taken into account based on quadratic transfer functions. In simulation, on the other hand, also 1st order wave forces are accounted. Thruster models in level 2-site are calculated based on level 1 formulas provided by DNV-ST-0111 while simulation uses numerically identified models. In experiment, naturally physical models of thrusters and environment are utilized.

Table 8.1: Static and dynamic methods distinction

Parameter/variable	Level 2 - site	Level 3 - site	Experiment
Virtual nominal thrust vector*	QP Optimal thrust allocation with power minimization	PID or MPC controller together with QP Optimal thrust allocation with power and thrust vector variation in time minimization	PID controller with Pseudo inverse matrix method with predefined thrust direction
Propeller revolutions	N/A	Determined from nominal thrust using thrusters models identified numerically (mean value after stabilization is taken to the comparative studies)	Determined from nominal thrust using thrusters models identified experimentally (mean value after stabilization is taken to the comparative studies)
Thruster angle	Determined from thrust allocation results (thrust vector)	Determined from thrust allocation results - thrust vector (mean value after stabilizing is taken to the comparative studies)	Fixed value is set prior the tests based on static optimal thrust allocation calculations
Nominal thrust acting on a hull	Determined from thrust allocation results (thrust vector)	From propeller revolutions using thrusters models identified numerically	From propeller revolutions using thrusters models identified experimentally
Brake power	DNV formula using nominal thrust, thruster characteristics and propeller diameter		
Wave forces	Slow varying drift forces from numerical seakeeping analyses	Slow varying drift forces and wave frequency forces from numerical seakeeping analyses	Towing tank wave-maker induced physical waves
Current forces	Wind tunnel tests coefficients for a similar ship	Based on ship hull mathematical model identified numerically	Induced side motion of the model relative to the towing tank

\* A result from thrust allocation module serving as command signal for the thrusters controller directly or indirectly. It is a result of control force mapping onto thrusters

## 8.1 Quality indicators

Three methods; static (level 2-site), dynamic (level 3-site) and experiments, utilize different environmental conditions definition and different thruster models. This is dictated by the data availability at each stage of ship design

and represents a real situation at a typical design office. For better comparison of DP capability performance in each method, selected indicators are analyzed.

1. Absolute value of footprint radius and maximum heading variation in time (applicable to simulation and experiments):

$$r = \max(r_0, r_1, \dots, r_n), \quad (8.1)$$

$$\Delta_\psi = \max(\Delta_{\psi,0}, \Delta_{\psi,1}, \dots, \Delta_{\psi,n}), \quad (8.2)$$

where  $n$  is the sample number;  $r_n = \sqrt{(x_n - x_{ref})^2 + (y_n - y_{ref})^2}$ ;  $\Delta_{\psi,n} = \psi_n - \psi_{ref}$ ;  $x_{ref}$  and  $y_{ref}$  are set fixed reference position coordinates;  $\psi_{ref}$  is set fixed reference heading.

Those values are a good measure of the ship performance in a dynamic environment. They account for the environment dynamics and DP system response in time with emphasis on the control system performance. In DP simulation, MPC controller is compared to the PID controller assuming their parameters/gains are optimally selected. Other than that, the ship absolute response in experimental and simulation conditions can be assessed this way.

2. RMS (Root Mean Square) value of position and heading variations from reference position in time (refers to simulation and experiments).

$$RMS_r = \sqrt{\frac{1}{n} \sum_{i=0}^n r_i^2} \quad (8.3)$$

$$RMS_{\Delta\psi} = \sqrt{\frac{1}{n} \sum_{i=0}^n \Delta\psi_i^2} \quad (8.4)$$

where  $n$  is the total number iterations of the simulation or samples of the measurement in the experiments;  $i$  is number of the sample in experiment or iteration in simulation.

RMS value is a measure of degree of position/heading relative variance in time which can show the stability of the system.

3. Total utilized thrust:

$$T_{\text{total}} = T_1 + T_2 + \cdots + T_N \quad (8.5)$$

$$T_i = \frac{1}{n} \sum_{j=0}^n T_j \quad (8.6)$$

where  $N$  is the total number of thrusters;  $T_i$  is the thrust of the  $i$ th thruster;  $n$  denotes the maximum number of iterations in simulation or samples in the experimentation measurements, and  $j$  is an iteration in simulation or a sample

In cases where the ship maintains position it can be assumed that mean forces (produced by thrusters and caused by the environment) are balanced. The mean thrust forces resulting from simulation and experiments at stabilized conditions are taken to the analyses.

4. Total available power ratio:

$$P_{\text{total}} = \sum_{i=1}^N P_i / P_{\text{max total}} \cdot 100\% \quad (8.7)$$

where  $P_i$  is total power utilized by the  $i$  thrusters.

5. Dynamic factor:

$$f_{\text{dyn}} = \frac{T_{\text{dyn}}}{T_{\text{stat}}}, \quad (8.8)$$

where  $T_{\text{stat}}$  is total thrust utilization resulting from static method and  $T_{\text{dyn}}$  is total thrust utilization resulting from dynamic methods.

This factor enables to correct a static methods in respect to dynamic methods. The dynamic factor of 1.25, specified by DNV (DNV, 2021) multiplied by determined dynamic factor ( $f_{\text{dyn}}$ ) can be applied to the static analysis to account for the environment, vessel and control system dynamics.

Those listed indicators of dynamic positioning quality/performance can be compared across all methods (static and dynamic), except for footprint which cannot be obtained in static methods. The comparison of quality

indicators is presented in subsequent tables (Tab. 8.2 - 8.4) with respect to the assumptions and methods description in Tab. 8.1.

Tab. 8.2 shows the footprint indicator results and corresponding DNV levels. It also gathers the environmental condition parameters such as significant wave height ( $H_S$ ), wave peak period ( $T_P$ ) and current speed ( $v_c$ ) as well as exposure time, which is dictated by the duration of the experiment. Each cell in the table indicates whether the ship was able to maintain station keeping and provides footprint data where applicable.

Table 8.2: Dynamic positioning capability results with all tested methods

Type of analyses	Approach	Considered conditions		
		Current 90 deg $v_c = 0.180 \text{ m/s}$ exposure*: 16 min 30 sec	Short wave 90 deg $H_S = 1.44 \text{ m}$ $T_P = 5.52 \text{ s}$ exposure*: 19 min 48 sec	Long wave 90 deg $H_S = 1.44 \text{ m}$ $T_P = 9.20 \text{ s}$ exposure*: 16 min 48 min
Level 2 - site	static	keeps position	keeps position	keeps position
Level 3 - site with PID	dynamic	keeps position $r = 1.44 \text{ m}$ $\Delta\psi = 0.0 \text{ deg}$	failed $r = 17.64 \text{ m}$ $\Delta\psi = 0.1 \text{ deg}$	keeps positions $r = 4.68 \text{ m}$ $\Delta\psi = 0.1 \text{ deg}$
Level 3 - site with MPC	dynamic	keeps position $r = 0.72 \text{ m}$ $\Delta\psi = 0.0 \text{ deg}$	failed $r = 898.2 \text{ m}$ $\Delta\psi = 4.5 \text{ deg}$	keeps position $r = 3.24 \text{ m}$ $\Delta\psi = 0.0 \text{ deg}$
Experiment	dynamic	keeps position $r = 4.32 \text{ m}$ $\Delta\psi = 3.0 \text{ deg}$	failed $r = 20.52 \text{ m}$ $\Delta\psi = 25.6 \text{ deg}$	failed $r = 4.32 \text{ m}$ $\Delta\psi = 6.1 \text{ deg}$

\* Only applicable to dynamic analyses/tests

Tab. 8.3 presents dynamic factor calculations and Tab. 8.4 shows the RMS values of footprint radius and heading based on time history. In both tables, the cases where the ship did not maintain position and/or heading were marked in red.

All results summarizing the dissertation are shown in Fig. 8.1 - 8.3. The plots present power utilization for each thruster and in total, as well as the absolute value of nominal thrust. Finally, each figure includes thrust allocation graphs for each method.

Table 8.3: Dynamic factor based on thrust utilization

Condition	Level 2 - site	Leve 3 -site with PID		Level 3- site with MPC		Experiment	
	$T_{\text{total}}$ [kN]	$T_{\text{total}}$ [kN]	$f_{\text{dyn}}$ [-]	Total thrust [kN]	$f_{\text{dyn}}$ [-]	$T_{\text{total}}$ [kN]	$f_{\text{dyn}}$ [-]
Current	10.1	9.6	0.94	9.5	0.93	16.4	1.61
Short wave	161.6	110.2	0.68	173.2	1.07	114.7	0.71
Long wave	45.9	30.7	0.67	32.9	0.72	32.1	0.70

Items marked with red color indicate that the ships' position was not maintained

Table 8.4: RMS of radius and heading relative values variations

Type of analyses	Current		Short wave		Long wave	
	$RMS_r$ [m]	$RMS_{\Delta\psi}$ [deg]	$RMS_r$ [m]	$RMS_{\Delta\psi}$ [deg]	$RMS_r$ [m]	$RMS_{\Delta\psi}$ [deg]
Level 2 - site	N/A	N/A	N/A	N/A	N/A	N/A
Level 3 - site with PID	0.468	0.017	6.480	0.06	1.836	0.041
Level 3 - site with MPC	0.468	0.009	288.80	32.24	1.692	0.010
Experiment	2.376	1.196	9.756	11.06	2.340	4.165

Items marked with red color indicate that the ship position was not maintained

N/A - not applicable

The DP capability prognosis accuracy study should take into account both the quality indicators presented in the previous section (footprint radius, heading variation, RMS values of radius and heading, thrust utilization and dynamic factor) but also the specifics of the tests, simulations, and static calculations. The problem is complex and in this case it is not possible to determine the accuracy in the form of a specific, absolute, and unambiguous value. Each case should be examined and compared individually, taking into account the specification of simulation and model tests.

Thus, based on the study presented in this dissertation, no unique mea-

sure of accuracy of static methods can be derived. Instead, a deep insight into all methods can be presented, and as a result, specific guidance is developed and shared.

Current direction 90 deg,  $v_c = 0.18$  m/s  
case: 21

■ Static calculation Level 2 - site ■ Simulation with PID Level 3 ■ Simulation with MPC Level 3 ■ Experiment

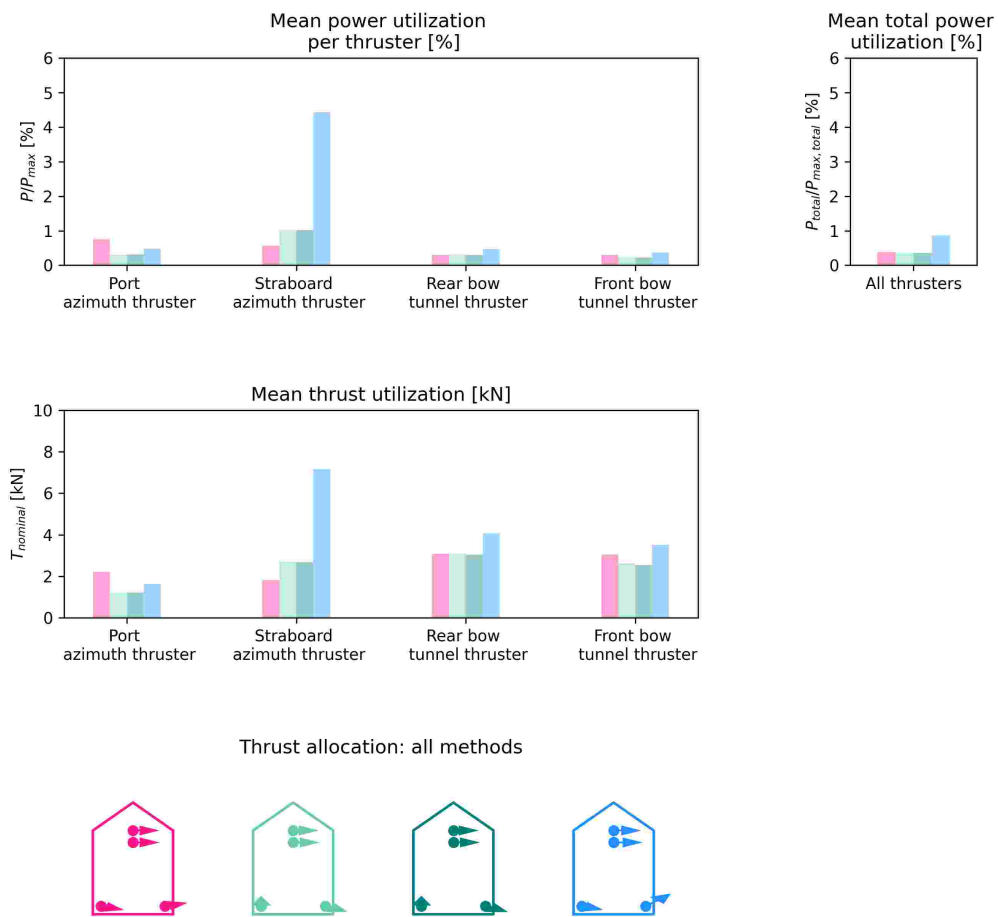
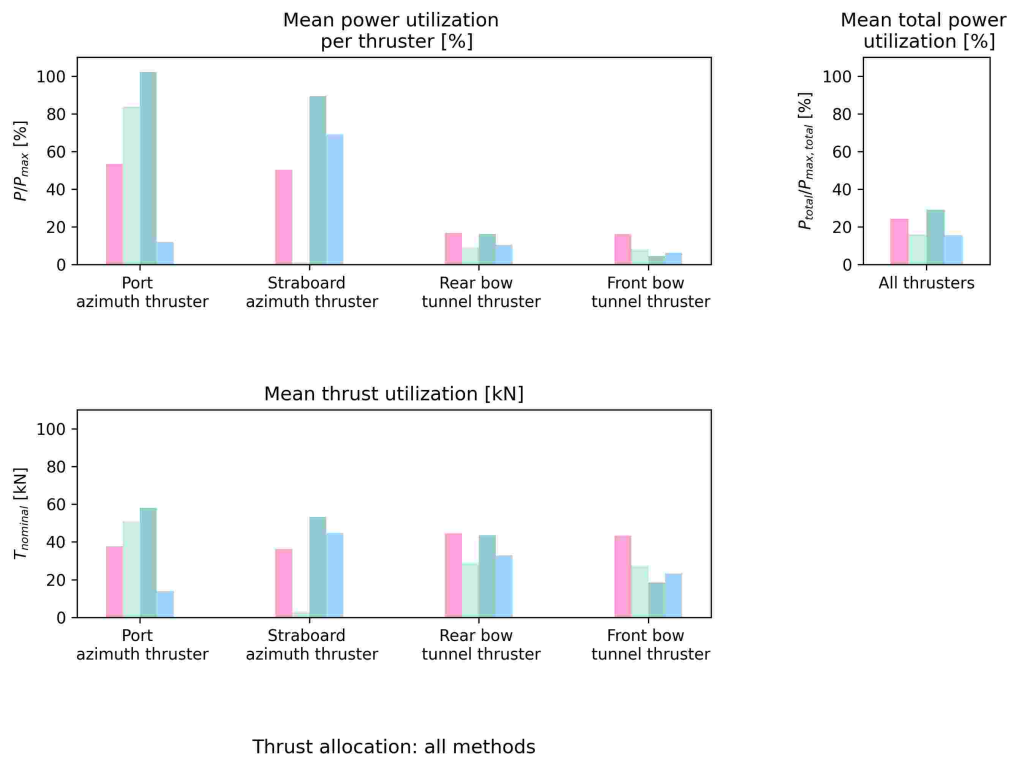


Figure 8.1: All methods: Current

Wave direction 90 deg,  $H_s = 1.44$  m,  $T_P = 5.56$  s  
case: 29

■ Static calculation Level 2 - site ■ Simulation with PID Level 3 ■ Simulation with MPC Level 3 ■ Experiment



Thrust allocation: all methods

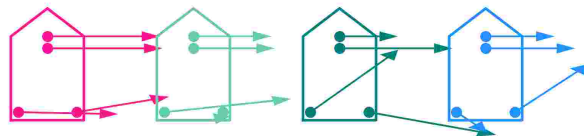


Figure 8.2: All methods: Short wave

Wave direction 90 deg,  $H_s = 1.44$  m,  $T_p = 9.20$  s  
case: 30

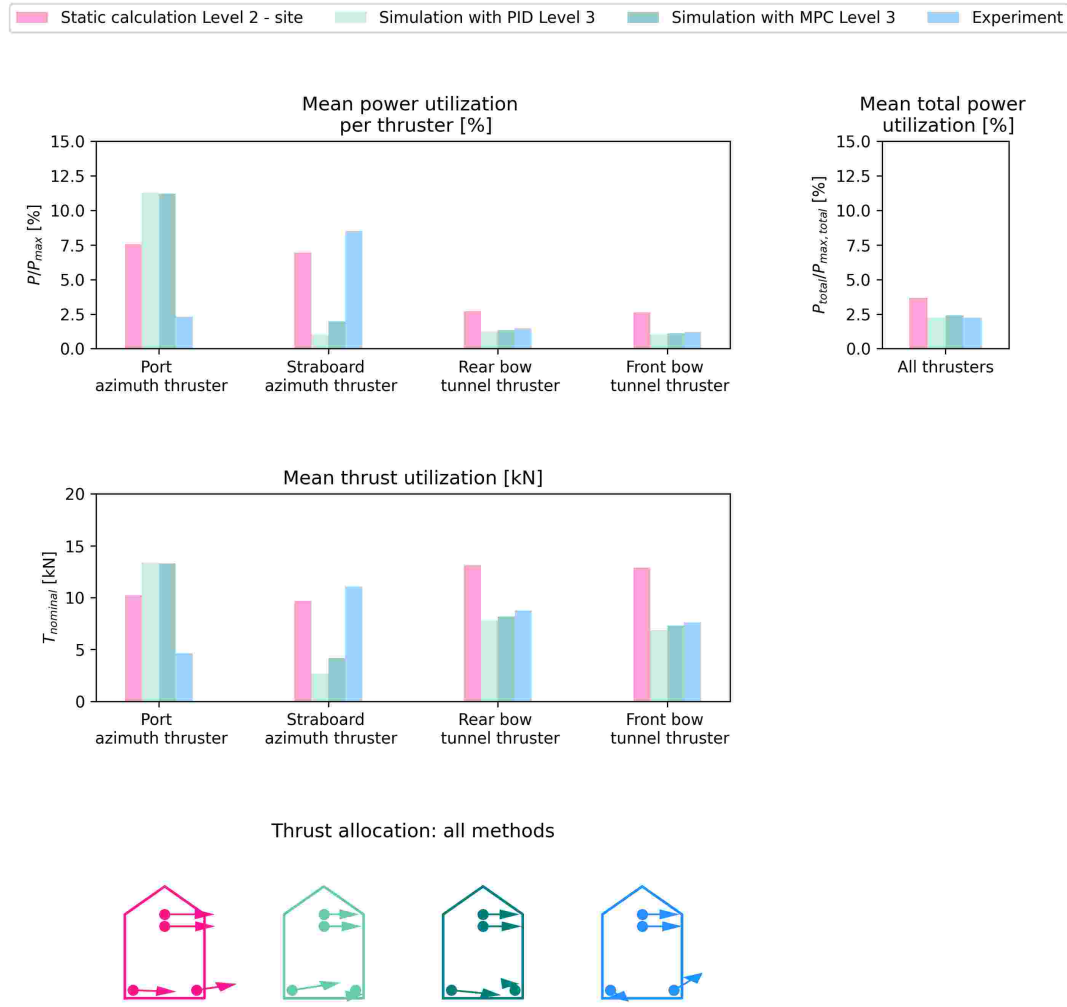


Figure 8.3: All methods: Long wave

## 8.2 Summary and discussion

Based on results given in Sec. 8.1 a thorough analysis of the acquired data can be done. As each method is compared across all conditions, the following

text will focus separately on current, short waves, and long waves.

In case of current disturbances, it is clear that simulation with PID and MPC controller gives similar results (Tab. 8.3, Tab. 8.4). Thrust distribution and power consumption are almost identical, as shown in Fig. 8.1. However, MPC controller performs better in terms of maximum footprint radius (Tab. 8.2) which is twice smaller than in the case of the PID controller. Variation of footprint is the same for both controllers (Tab. 8.4) which is indicated by identical RMS values for footprint radius. The MPC controller demonstrates more aggressive control but reaches stability faster than the PID controller, which in this case is more beneficial in terms of station keeping and still beneficial in terms of power utilization, as shown in Sect. 6.2.

At current conditions, static methods overestimate the power consumption by up to 9% compared to simulation but underestimate significantly compared to experiments. However, in the experiment, the current was modeled based on the Frude similarity law, neglecting the viscosity scale effects which add up to the total hydrodynamic force. Therefore, in this case, the control system performance (and thrust allocation) can be somewhat compared, but the absolute values should be treated carefully in the indicators study.

Thrust allocation in current conditions (Fig. 8.1) in terms of azimuth thrusters angles is slightly different for static and dynamic numerical methods, which is dictated by a slightly different approach described in Sect. 4.1 and Sec. 5.4.

Short waves occurred to be the most severe condition regarding dynamic methods, where position and heading were not maintained (Tab. 8.2). This situation was significantly underestimated by static methods, which resulted in station keeping. However, static methods resulted in more fore thruster utilization than other methods. While, for instance, PID controller in simulation did not utilize the starboard azimuth thruster at all (Fig. 8.2). At the same time, MPC controller in simulation was utilizing all thrusters but lost control at the point where saturation occurred for the port azimuth thruster.

In simulation and experiment in the case of a short wave, the DP system fails to use the full resources of available power to balance the forces and instead overloads one of the azimuth thrusters. Except for the MPC controller, which uses both azimuth thrusters evenly; however, it reacts very aggressively already at the beginning of the simulation and destabilizes the system and causes station keeping failure.

At short wave, the experimental maximum footprint radius and dynamic factor is similar to the one resulted from simulation with PID controller, while MPC controller allowed the ship to drift almost 900 m (for a 100 m ship), as given in Tab. 8.2 and accelerate up to 0.8 m/s. This result is unacceptable and indicates issues with MPC controller performance as mentioned previously. However, increasing the time of environmental force build up at the beginning of the simulation improved the MPC performance. Which means that MPC only reacts positively to small variations (gradual variations) of the loads in time. Which in the case of a full scale ship in operation is valid. For the purpose of prognosis, this additional ramp time should be added to the loads to allow the ship to calibrate to primary settings before DP capability can be properly assessed.

In the case of long waves, the static method significantly overestimates the total power consumption by up to 67%. Both regulators in the simulation perform comparably, and the situation is similar to the one with current. In the experiment, the model fails to keep heading but keeps position within the margins.

The fact that the static calculation does not include the variation of forces effect, is clearly recognizable comparing results from the short and long waves and having available results from different methods. The dynamic factor for a short wave should be at least 60% higher, but for a long wave, respectively lower. The exact correction value could be based on multiple simulations with different wave periods (wave slopes) and a reasonable amount of ships. Based on one example tested within the dissertation, a conclusion is to increase the dynamic factor for steeper waves. Generally, shorter waves cause higher slowly varying (drift) forces. This also depends on the ship response. One ship may cope better with certain waves than another ship.

In the experiment, the azimuth thruster angles were fixed in time (set prior to the tests). In case of slightly less optimal orientation of the thruster, the optimal thrust allocation may be achieved slower, which could explain the loss of heading in case of long waves.

Assuming neglecting results of simulation with MPC at the short wave conditions and experiment with current (for explained reasons), the static method dynamic factors could be estimated for all tested conditions. Separate factors depending on the condition. In case of current, a dynamic factor of 0.94 could be accounted to static results, while for long waves a factor of 0.72 could be used. Since the model was not capable of DP in short waves, this factor cannot be estimated based on numbers; however, in terms of los-

ing the position, the factor should not be less than 1.60 (as determined by forcing higher forces in static analysis to finally cause DP failure).

As mentioned before, the numerical study for a variety of conditions and ships should be performed to truly estimate the static calculations' dynamic factors. Based on this case study, the static calculations are generally more pessimistic, more conservative.

Presented indicators for experimental results allow validation of the DP simulator concerning given environmental conditions. The discrepancies for all tested cases are within +/-60% in terms of dynamic factor. Additionally, taking into account overall performance in each case ( $RMS$ ,  $r$  and  $\Delta_\psi$ ) the DP simulation tool is verified based on this study. Meaning that it can be directly implemented to DSS.

Further, a regular engineer in a typical design office should consider dynamic factors based on the comparison between simulation and static methods results. Concerning those, this study showed that the utilized thrust in static analyses level 2-site for current and long wave should be reduced by 6% and 28% respectively. In case of a short wave instead of a dynamic factor of a certain value, the designer should receive information that the ship will not be capable of DP. In practical sense, this allows for better design decisions such as the selection of smaller propulsion and engines of lower power in case of operation in either current or long wave conditions. This directly reduces costs significantly, both purchasing and exploitation costs. If the ship were designed to operate in a specific environment of short waves, static methods would give misleading information to the designer. Having the database of dynamic factors and also in case of loss of position the positive (keep position) or negative (failed to keep position) indicator would prevent poor and costly design decisions.

# Chapter 9

## Conclusions and future research

Within the dissertation, static and dynamic methods were compared. Specifically, experiments on the physical ship model in scale 1:36 were used for the validation of a DP simulator. As previously mentioned, the number of tests carried out is insufficient for full validation of the developed tool; however, it is enough for simulator verification. Developed methods and tools for optimal thrust allocation and mathematical model numerical identification present a significant milestone in future research and further validation of the decision support system. Moreover, a prototype of the system based on the selected DP ship and three environmental conditions was successfully launched. With the acquired knowledge, the developed tool, and the facilities of CTO S.A. it is possible now to perform multiple tests with the same approach. The MSV ship that was utilized in research can serve as a benchmark for other researchers, as the main particulars and results were made available.

### 9.1 Comparative analyses

As shown in detail in Ch. 8, all methods (static, simulation, and model tests) showed compliance in terms of the magnitude of power consumption and thrust allocation. This ultimately shows the correctness of all applied analyses, both in their execution and in terms of the physical relationships (in simulation and static computations) and physical phenomena (in model tests).

Due to site-specific environmental conditions, DNV Level 1 was not applicable in this case. Instead, DNV Level 2-site was compared to the simulation

and physical experiment. In simulation, wind tunnel experimental results of current forces for a similar ship (Rescue Vessel) were utilized as well as numerical tools, *Ansys Aqwa* (wave forces). As for the experiment, the current and waves were physically induced in model scale. It was not possible to measure those forces directly, however, the DP capability was assessed based on thrust utilization.

Dynamic factors  $f_{dyn}$  between static method (DNV level 2-site) and simulation (DNV level 3-site) that were the main focus of comparison were varying between 0.67 and 0.94 (for current and long wave). Static analyses DNV level 2-site already account for dynamic factor of 1.25 as required by DNV. Hence, the new dynamic factor  $f_{dyn}$  determined within the study is a correction to the DNV static prognosis.

In case of the short wave, a dynamic factor was determined within the study; however, just for information's sake to show the magnitude of utilized thrust. The station keeping in this case failed based on simulation analyses (level 3-site) and experiment results as opposed to the results of static methods (level 2-site).

## 9.2 Summary and conclusions

All objectives assumed at the beginning of the dissertation (Ch. 1) were achieved.

1. Development and implementation of the static method of DP capability assessment based on selected nonlinear thrust allocation algorithms and according to the standard DNV-ST-0111, (DNV, 2021)

Thrust allocation problem was solved mainly with quadratic programming application to DNV method in all DNV levels (Ch. 2) showing efficient performance compared to also considered alternative algorithm, NSGAII . Both in sense of time of calculations and optimal thrust allocation. Quadratic programming TA was extended for DNV level 3 and 3-site to account for the thrusters dynamics and thus form an integral part of the DPS. Optimal TA implementation was described in Ch. 4.

2. Parametric identification of hull and thruster mathematical models using numerical techniques.

First mathematical models of the ship's hull and thrusters with propellers were identified based on literature and subsequently a method of parametric identification of models parameters were performed and described in details. Based on given information an engineer can apply the method in a design office with utilization of CFD numerical tools. Mathematical models identification (both ship and disturbances) was described in Ch. 3

3. Development and implementation of the dynamic method (simulation) of DP capability assessment according to the standard DNV-ST-0111, (DNV, 2021).

A complete DP simulator was developed comprising observer, controller, thrust allocation, thrusters models, hull model and disturbances models. Two alternatives controllers were utilized (PID and MPC). All component were designed and tuned by the author with support of respective literature and own studies. The simulator structure was strictly based on (DNV, 2021). DPS is described in Ch. 5. Results of analysis with the simulator are given in Ch. 6.

4. Case study validation of the simulator with DP model tests results and subsequently validation of the static tool with the simulator to define a dynamic factor.

Finally utilizing results of model tests in a MSV ship model in scale 1:36 for current, short and long wave a validation of the simulation tool of those cases was done. Results of model tests are given in Ch. 7. Subsequently, after validation of the simulator it was possible to determine dynamic factor to account for additional dynamics in the static methods, based on simulations. Comparison of static and dynamic methods highlighting the dynamic factor results was described in Ch. 8.

By achieving all the aforementioned objectives, the theses of the dissertation are confirmed as follows.

Fig. 9.1 presents the research conducted in this dissertation in reference to the DSS introduced in Sect. 1.2 and shown in Fig. 1.4. For launching the prototype DSS, an expert utilizes one selected ship (MSV) for identification, simulation, and static analyses according to (DNV, 2021) considering three

disturbance scenarios: current, short wave, and long wave. Based on simulation (DNV level 3-site) and static methods (DNV level 2-site), a dynamic factor  $f_{dyn}$  for those conditions is determined, and information on whether the ship kept position or not is saved to the database. By inputting basic ship and environmental data to the database, the expert cross-references the dynamic factor for that vessel and for chosen environmental conditions. The dynamic factor is applied to the static methods and outputs the corrected prognosis.

The final conclusion is that developing a decision support system in a design office is certainly possible, as demonstrated. Furthermore, it is feasible to define a dynamic factor based on dynamic methods to improve the static prognosis. However, this should be vessel-type and condition-specific. The dynamic factor application enables more accurate prognosis and results in altering decisions. Subsequently, it contributes to cost efficiency.

Concerning that up until now only a few DP ships model tests were performed on a few vessels, the results within the dissertation are a significant contribution to the field.

A practical outcome of the dissertation is a powerful tool for DP capability analyzes, assessment, and prognosis comprising a decision support system. The tool allows for full DP analyses (Level 1, 2, 3, 2-site, 3-site) according to DNV standards and, with the potential for commercialization, as a complete software package. The tool can be utilized and further developed by CTO S.A.

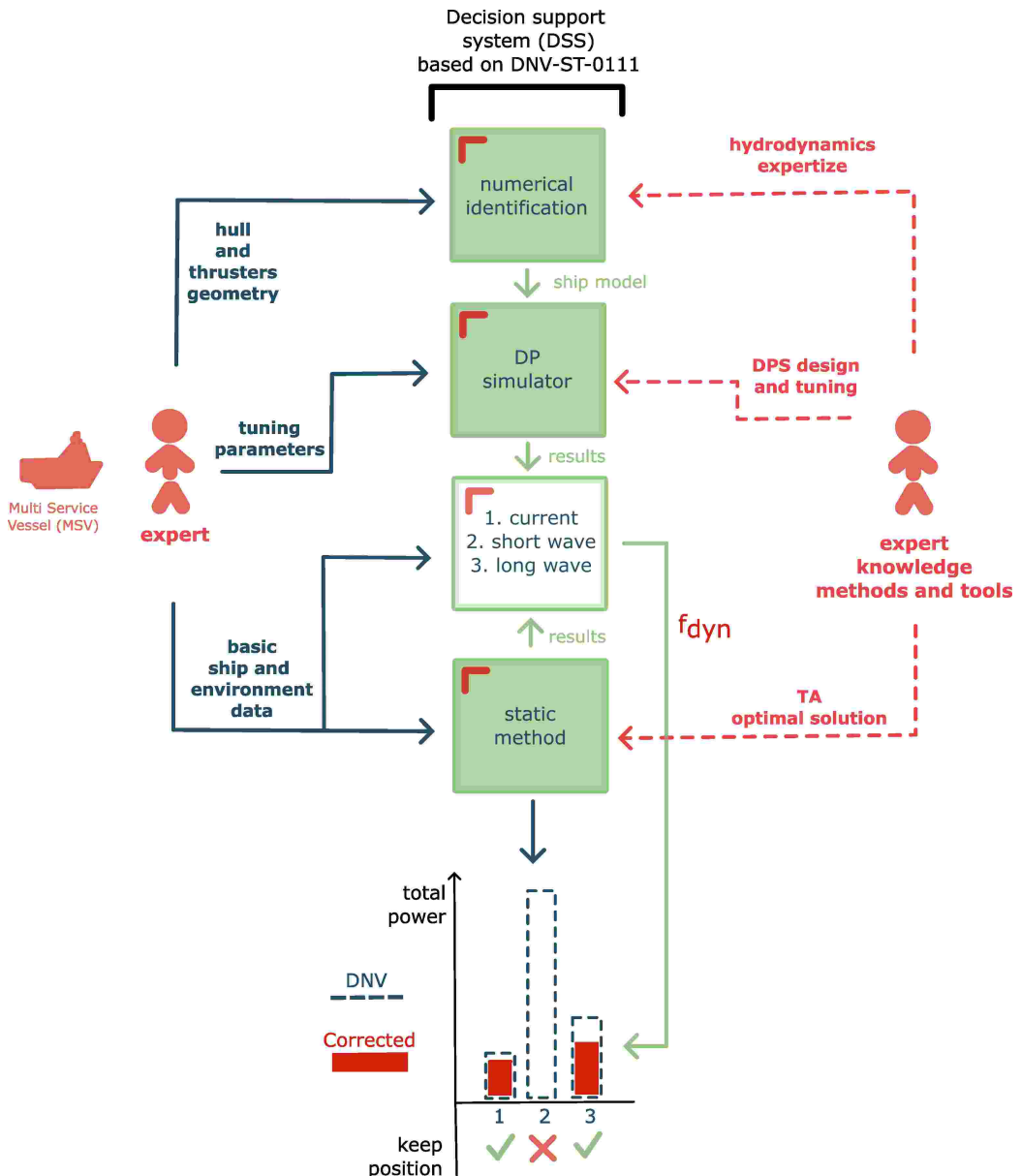


Figure 9.1: Decision support system prototype

### **9.3 Recommendation for future research**

Possible upgrade of developed DP tool would be to add an option allowing to account for azimuth thruster losses models (based on numerical studies) and applied also to the thrust allocation module in the simulator. Since a potential user is rather expert in the field of hydrodynamics and hull design, not control engineering, a module for the determination of optimal gains of the PID, MPC controller, and observer could greatly simplify the work of such a person.

A database of dynamic factors could be created, where the input - output relation could be obtained by simple regression or with machine learning or deep learning techniques. The input to the database would be basic ship data such as main dimensions, type of thrusters, its location, and environmental conditions, while the output would be the dynamic factor. As mentioned before, for full validation, it is recommended to collect designs over the years and utilize that database for validation and better static analysis results assessment.

Already, having the ship model in scale that is equipped with the propulsion system, it would be valuable to perform more tests on it. With appropriate funding, it is possible to create a full DP Capability plot, 36 angles at 11 DP numbers. Keeping the same wave, current, and wind (if possible) parameters defined by DNV (Tab. 2.1) would allow for a full validation and serve as a valuable benchmark for future research all over the world.

# Appendix A

## Data of analyzed ships

Within the dissertation two ships were analyzed: RV - Rescue Vessel and MSV - Multi-Service Vessel. Both ships are similar in terms of thrusters types, hull shape and dimensions. For instance, current and wind coefficients determined in wind tunnel tests for one of the ships can be safely applied to the analyses of the other ship. For the purpose of prognosis, this simplification is sufficient.

RV ship was only tested in the wind tunnel (for current and wind coefficients). Next, those coefficients were used to static prognosis (DNV - Level 2) for both RV and MSV. MSV on the other hand was not tested in the tunnel but mathematical models of the hull and thrusters were identified experimentally and numerically. This allowed dynamic DP prognosis with DNV - Level 3, for that ship.

DNV defines the main particulars of the ship that are then used in proposed formulas (DNV, 2021), for solving the Dynamic Positioning problem (with self-selected Thrust Allocation algorithm). Definition of those parameters, concerning the hull and the thrusters, are given below (based on (DNV, 2021)).

Below are listed main particulars of those two ships. All data required for static analyzes, DNV - Level 1, are listed and can be directly used for validation purposes.

Thrusters layout of the thrusters is presented in Fig. A.4 and Fig. A.3.

Table A.1: Wind, wave, current forces calculation ship input data.

Input value	Unit	Description
$L_{pp}$	m	Length between perpendiculars
$B$	m	Maximum breadth at waterline
$T$	m	Summer load line draft
$L_{os}$	m	Longitudinal distance between the fore most and aft most point under water
$X_{Los}$	m	Longitudinal position of $L_{os}/2$
$Bow_{angle}$	°	Angle between the vessel x-axis and a line drawn from the foremost point in the water line to the point at $y = B/4$ (ahead of $L_{pp}/2$ ) on the water line (Figure A.2)
$C_{WL, aft}$	—	Water plane area coefficient behind mid-ship
$A_{F,wind}$	$m^2$	Frontal projected wind area
$A_{L,wind}$	$m^2$	Longitudinal projected wind area
$X_{L,air}$	m	Longitudinal position of the area center of $A_{L,wind}$
$A_{L,current}$	$m^2$	Longitudinal projected submerged current area
$X_{L,current}$	m	Longitudinal position of the area center of $A_{L,current}$
$x_{skeg}$	m	x position of the skeg aft edge
$y_{skeg}$	m	y position of the skeg aft edge

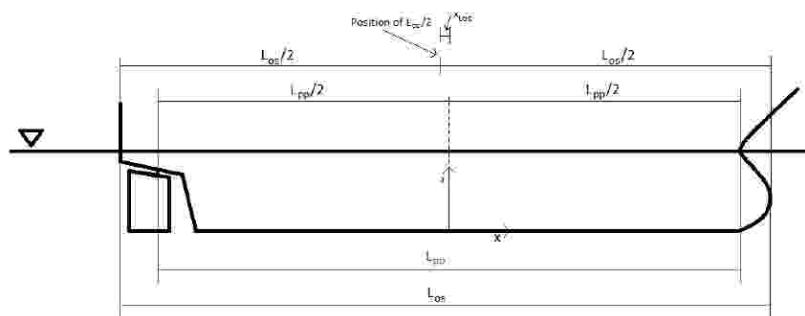


Figure A.1: Vessel geometrical parameters for wave drift.  $X_{Los}$  has a negative value in this case

Table A.2: Thruster data

Input value	Unit	Description
Thruster name	—	The name used for identification purposes only
Thruster type	—	According to (DNV, 2021)
Characteristics of the thruster	—	Reverse mode options and tunnel thruster inlet type according to (DNV, 2021)
Rudder type	—	no rudder, naca, flap, etc. according to (DNV, 2021)
$x$	$m$	Longitudinal position of the thruster from mid-ship A.1
$y$	$m$	Transverse position of the thruster from central line
$z$	$m$	Vertical position of the thruster from central line
$D$	$m$	Propeller diameter
$P_{brake}$	$kW$	Brake power of the thruster motor/engine shaft line, etc. according to (DNV, 2021)
Thruster type - for mechanical efficiency	—	
$A_r$	$m^2$	Area of the movable part of the rudder directly behind the propeller

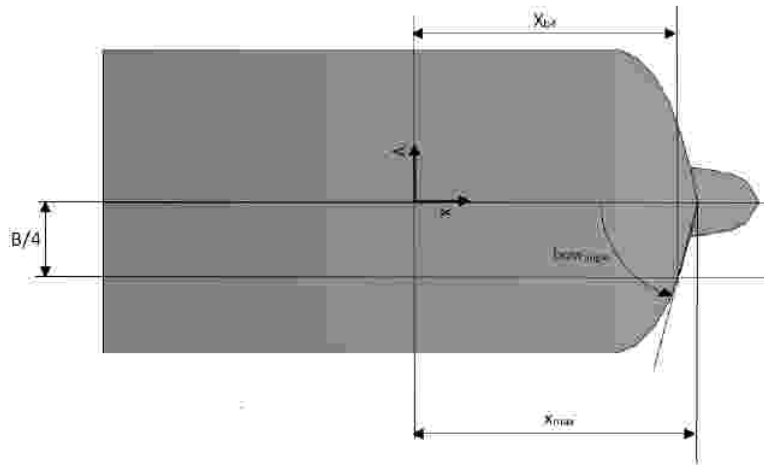


Figure A.2: Bow<sub>angle</sub> definition

Table A.3: Hull data of the Rescue Vessel and Multi-Service Vessel (MSV)

Input value	Unit	Rescue Vessel	MSV
$L_{pp}$	$m$	86.56	98.70
$B$	$m$	18.80	23.40
$T$	$m$	5.00	6.50
$L_{os}$	$m$	95.85	108.34
$X_{Los}$	$m$	-0.13	-0.13
$Bow_{angle}$	$^\circ$	27.4	26.4
$C_{WLaff}$	—	1.034	1.081
$A_{F,wind}$	$m^2$	391.7	611.0
$A_{L,wind}$	$m^2$	1203.3	1769.0
$X_{L,air}$	$m$	6.014	6.035
$A_{L,current}$	$m^2$	440.9	667.4
$X_{L,current}$	$m$	4.717	1.107
$x_{skeg}$	$m$	-37.8	-47.85
$y_{skeg}$	$m$	0	0
$I_z$	$kg\ m^2$	$2.95\ 10^9$	$8.20\ 10^9$
$L_{CB}$	$m$	42.9	51.39
$z_G$	$m$	7.24	8.75
$k_{xx}$	$m$	0.350 $B$	0.350 $B$
$k_{yy}$	$m$	0.250 $L_{PP}$	0.271 $L_{PP}$
$k_{zz}$	$m$	0.250 $L_{PP}$	0.271 $L_{PP}$

Table A.4: Thrusters data - Rescue Vessel

Thruster data	<i>x</i>	<i>y</i>	<i>z</i>	<i>D</i>	<i>P<sub>brake</sub></i>	<i>A<sub>r</sub></i>
Unit	<i>m</i>	<i>m</i>	<i>m</i>	<i>m</i>	<i>kW</i>	<i>m</i> <sup>2</sup>
<b>Rescue Vessel</b>						
Identification				Main azimuth thruster - port side - Thr 1		
Type				Azimuth thruster without nozzle		
Characteristics				Only forward mode		
Rudder type				No rudder		
Data	-41.076	4.690	1.540	3.100	1325	0.000
Identification				Main azimuth thruster - starboard side - Thr 2		
Type				Azimuth thruster without nozzle		
Characteristics				Only forward mode		
Rudder type				No rudder		
Data	-41.076	-4.690	1.540	3.100	1325	0.000
Identification				Bow azimuth thruster - Thr 3		
Type				Azimuth thruster with nozzle		
Characteristics				Only forward mode		
Rudder type				No rudder		
Data	34.120	0.000	-1.100	1.650	880	0.000
Identification				Bow tunnel thruster I - Thr 4		
Type				Tunnel thruster		
Characteristics				Broken inlet		
Rudder type				No rudder		
Data	37.120	0.000	2.000	1.740	900	0.000
Identification				Bow tunnel thruster II - Thr 5		
Type				Tunnel thruster		
Characteristics				Broken inlet		
Rudder type				No rudder		
Data	40.720	0.000	2.000	1.740	900	0.000

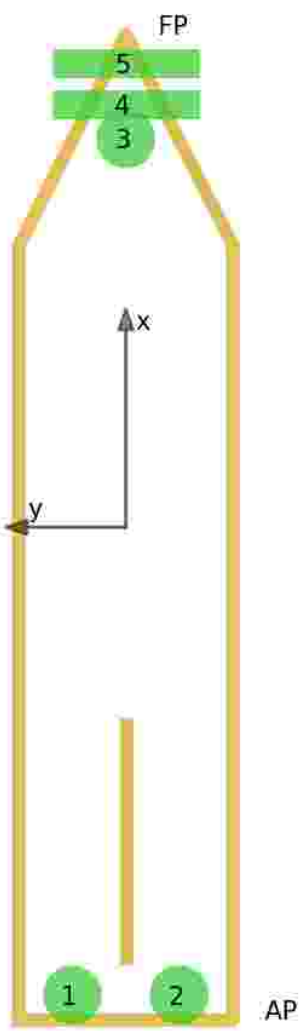


Figure A.3: Rescue Vessel thruster layout

Table A.5: Thrusters data - Multi-Service Vessel

Thruster data	<i>x</i>	<i>y</i>	<i>z</i>	<i>D</i>	<i>P<sub>brake</sub></i>	<i>A<sub>r</sub></i>
Unit	<i>m</i>	<i>m</i>	<i>m</i>	<i>m</i>	<i>kW</i>	<i>m</i> <sup>2</sup>
<b>MSV</b>						
Identification	Azimuth thruster - port side - Thr 1					
Type	Azimuth thruster without nozzle					
Characteristics	Only forward mode					
Rudder type	No rudder					
Data	-49.35	7.000	2.050	2.880	2250	0.000
Identification	Azimuth thruster - starboard side - Thr 2					
Type	Azimuth thruster without nozzle					
Characteristics	Only forward mode					
Rudder type	No rudder					
Data	-49.35	-7.000	2.050	2.880	2250	0.000
Identification	Bow tunnel thruster I - Thr 3					
Type	Tunnel thruster					
Characteristics	Broken inlet					
Rudder type	No rudder					
Data	38.640	0.000	2.000	2.750	1620	0.000
Identification	Bow tunnel thruster II - Thr 4					
Type	Tunnel thruster					
Characteristics	Broken inlet					
Rudder type	No rudder					
Data	42.490	0.000	2.300	2.750	1620	0.000

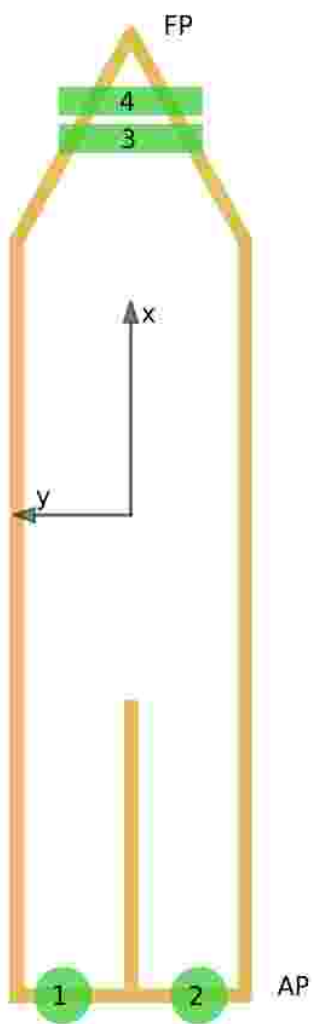


Figure A.4: MSV ship thrusters layout

## Appendix B

### Numerical identification of thrusters losses

A single thruster interaction with the hull was analyzed within the dissertation under bollard pull conditions. Few thruster angles were selected based on earlier analyses of thrust allocation by the authors (Piekło et al., 2023b). The thrust allocation showed that thrusters rarely set their position at 90° or 270° but at the intermediate angles. Therefore, for the analyses, angles of 0 °, 45°, 135°, 180°, 225°, and 315° were selected. Higher revolutions of 2500 rpm were adopted, resulting in a higher force to allow for a higher Reynolds number of  $2 \cdot 10^5$  for more stable results.

Fig. B.1 shows the percentage relation to the thrust at a given thruster angle. A significant drop in effective thrust can be observed at both 225° and 180°. In the former case, the thruster is flushing the skeg, which explains such a significant thrust loss. The visualization of this case is shown in Fig. B.2, where significant pressure can be observed at the skeg. The maximum and minimum pressures in the picture are -5 kPa and -8 kPa, respectively. In the latter (180°) case, the thruster is flushing the part of the hull where it is lowered forward. The noticeable increase in effective thrust occurs at the thruster angle 315°, where the thruster has the clearest inlet wake and outlet.

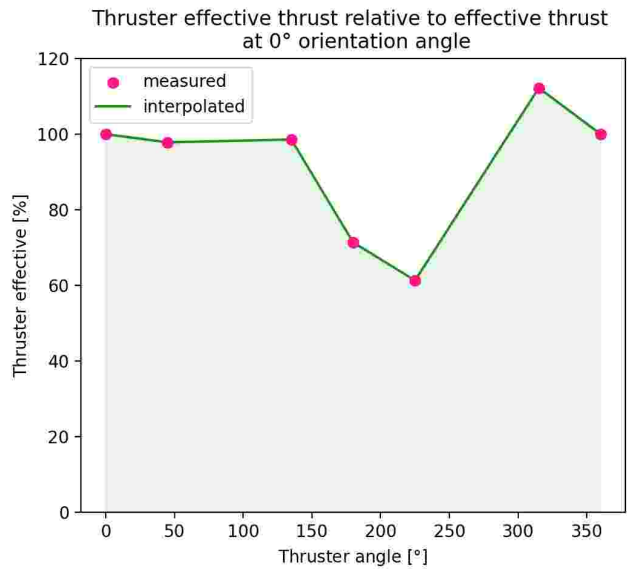


Figure B.1: Thruster efficiency depending on thruster direction

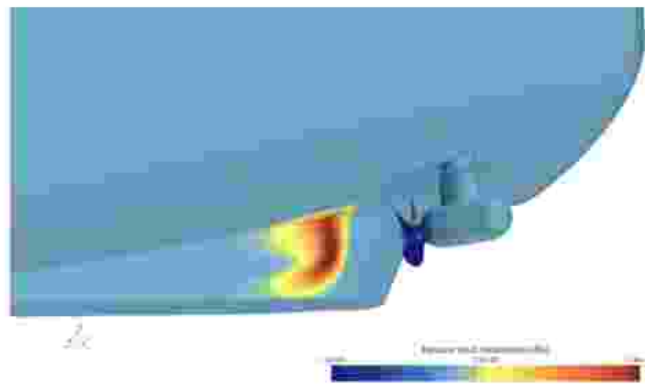


Figure B.2: Thruster interaction with the hull with numerical simulation as pressure distribution

Fig. B.3 shows the deviation of the thrust direction from its original set angle due to interaction with the hull. For angle 225° it is different by -39°, which is caused by the flux directed towards the skeg and causing a

significant side force on the skeg. This phenomenon is rather complicated to model; hence, one should avoid operation of the thruster in such a region.

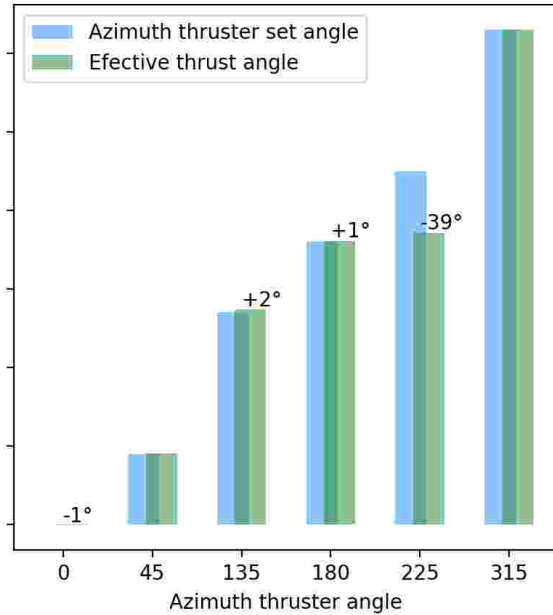


Figure B.3: Thrust divination from its original set direction with numerical simulation

Finally, two cases of typical thruster set angles (Piekło et al., 2024) were analyzed with numerical methods as shown in Fig. B.4. The figure presents the setup and the resulting net force vector. It can be seen that two thrusters pointing in the same direction (left side of the figure) increase the total pull force of the bollard by 5%. That means that two thrusters support each other's performance. In the case presented on the right side of the figure, the thruster setup allows for the generation of almost pure side force (very useful in DP operations under side environmental conditions). However, this also corresponds to the reduced total bollard pull force by 21% as in  $x$  direction the thrusters work against each other; hence, they cancel each other in this direction.

Visualization of the second case - where the thrusters point in different

directions - is presented in Fig. B.5, where the maximum speed on the scale is 5 m/s and the minimum is 0 m/s. The view is from the bottom of the hull. It can be observed that the inflow to the starboard propeller is disturbed by the port thruster. At the same time, the speed values of the inflow to the propellers are close to zero. Therefore, thruster-thruster interactions have a negligible effect on propeller thrust in the two studied cases and for the particular case of the ship.

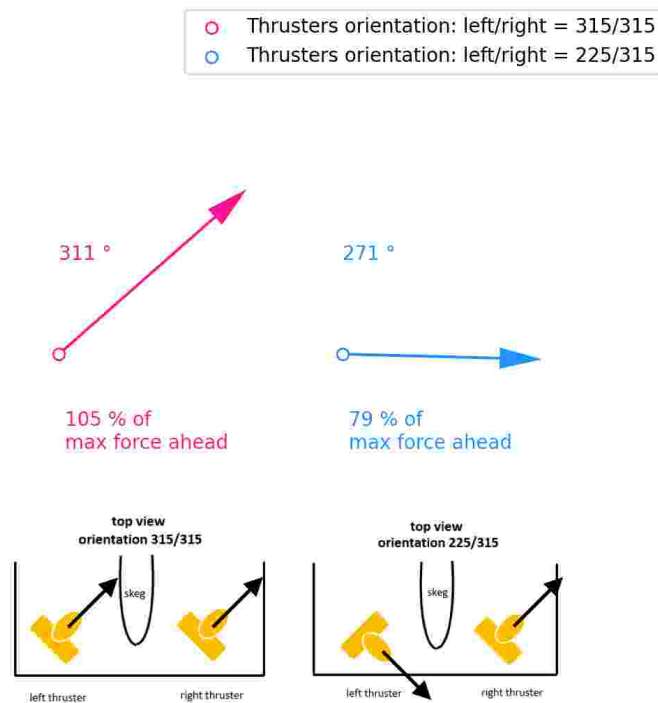


Figure B.4: Thruster interaction with another working thruster in numerical simulation as speed field

Numerical analyses showed a significant effective thrust reduction when the thruster is flushing the skeg; therefore, this region should be avoided while in DP or stand-by. The angles in the vicinity of 0°, 45°, 135° and 315° (for starboard thruster) are the most efficient. The correct implementation of the losses to the thrust allocation algorithm will result in the thrusters being directed within the more efficient regions mentioned above.

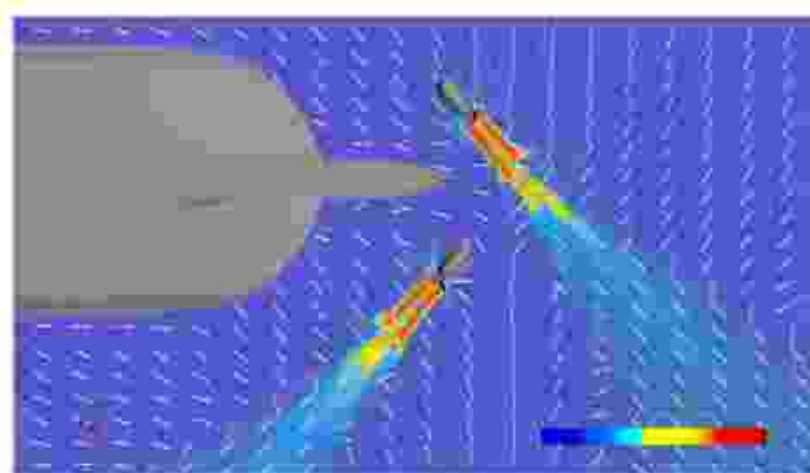


Figure B.5: Thrusters interaction with each other

# Appendix C

## Experimental setup specification and results

### C.1 Specification of MSV physical model DPS

Components of the DPS as implemented in experiments on MSV are presented in Tab. C.1 according to Fig. C.1. In the following pages, each element is discussed.

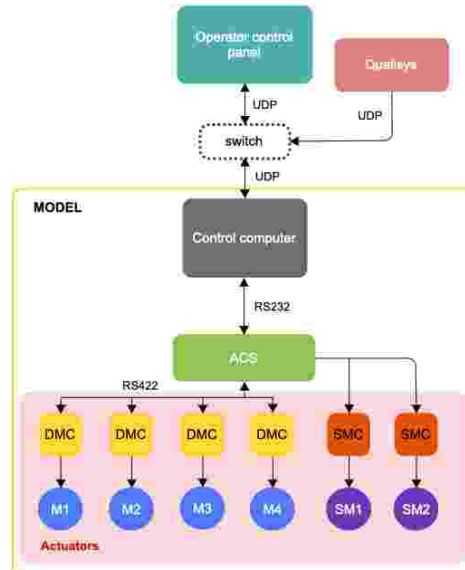


Figure C.1: DP tests stand structure

Table C.1: DP system components

Tool	Task	Details
Operator control panel	DP control system manipulation, observation and recording of measurement signals	A laptop computer with joystick
Control computer	Dynamic positioning	Multidimensional nonlinear modal control based on the estimated value using a nonlinear state observer and nonlinear MIMO PID controller.
	Integration of the ACS	Modbus protocol with RS232 converter
	Communication with the motion capture system Qualisys	Wifi - Ethernet connection with protocol UDP with frequency 10Hz
	Communication with the operator control panel	RB951Ui-2nD from Mikrotik - configured as a wireless bridge operating in the 5 GHz band
Actuators Control System (ACS)	Transmission of the actuators settings from the control computer to the actuators	Connected with RS422 serial interface, two-way transmission with 10Hz frequency
Actuators	Main thrusters orientation angle setting	Stepper Motor (SM) Controller (SMC) from Wobit
	Propeller revolutions setting	Mitsubishi MR3j series Digital Motor Controller (DMC) with HF-MP series Motor (M)

A laptop computer, Dell Vostro 3750 with LabView 2001 SP1 software running on Windows 7 Professional 64-bit, was used as the operator control panel (OCP) station. The computer is equipped with a quad-core Intel i7 processor with 4 Gb of RAM and a 17" monitor. To make it easier to control the movement of the model, as in a typical DP station, the computer comes with a three-axis joystick (Thrustmaster TS1600).

The OCP was developed using the LabView 2011 software. The main reason for choosing Labview is the simplicity of creating an interactive interface for experimental needs and its tuning according to arising needs during the experiment. The user can modify the OCP interface and integrate it with other laboratory measurement systems.

The developed console program allows the following functions:

1. Control of DP functions:

- Switch off and on the DPS

- Modifying the reference position
  - Emergency stopping
2. Manual setting of speed values and orientation angles of azimuth thrusters
  3. Manual control with a joystick, with arbitrarily set values of azimuth thrusters' angles.
  4. Display of measurement data:
    - position and heading vectors from the Qualisys system,
    - vector of current revolutions and orientation angles of azimuth thrusters,
    - current physical model velocities values provided by the observer
  5. Statistical evaluation of signal quality from the Qualisys system
  6. Information on errors and failures
  7. Manual tuning of controller and observer gains
  8. Option to save to a text file all displayed data
  9. Option for analysis of signals from sensors (using FFT) and tuning of the state observer

The control computer consists of Intel Celeron N2930 1.83 GHz, 2GB RAM, SSD mSATA 60 GB, network card Ethernet 10/100/100, built-in bus PCI/104-Plus, full-size miniPCIe, 8-bit GPIO, I2C; 6xUSB2.0, 1xRS-232/422/485 and 2xRS-232. Linux from the Debian 8.1 distribution was installed on the computer. Programming of the computer and access to its resources is done remotely via the Ethernet network using the SSH protocol supported by free software Putty.

The task of the control computer software is the integration of measuring devices and actuators, the implementation of DP algorithm calculations and communication with the Operator Control Panel (OCP). The computer is connected to the Actuators Control System (ACS) (via RS232), the Qualisys position and heading motion capture system (via Ethernet UDP) and the OCP (via Ethernet UDP). A dedicated software has been developed and tested to enable communication with all the above-mentioned devices and enabling the implementation of the DP algorithm. Signal processing and DP algorithms are implemented inside a specially dedicated thread operating in real-time mode.

For the purpose of conducting the tests, measuring devices listed in Tab. C.2 were utilized.

Table C.2: Measured values and measuring devices

Measured value	Measuring device	Details
Model position and heading (velocity and accelerations) relative to the carriage	Qualisys	A 6 high-end and high-precision motion capture cameras system
Propellers revolutions	SERVO/2	in-house developed inverter
Azimuth thrusters orientation angle	ACS	
Carriage speed	measuring wheel	type H-31 No. 4 with a pulse converter type ROD-2 No.S1507 and counter "Racal" type 835 No. 2308
Wave elevation	resistance probe	in-house developed probe based on the electrical resistance measurement in the vertical wire

Grey colored items are not part of a DP system, but were used for environmental condition set-up.

The Actuators Control System (ACS) is a device that integrates all the DP system's actuators, such as thruster controllers and azimuth thruster orientation angle controllers, and transfers data between the control computer and the actuators. Control computer with the ACS is shown in the Fig. C.2.

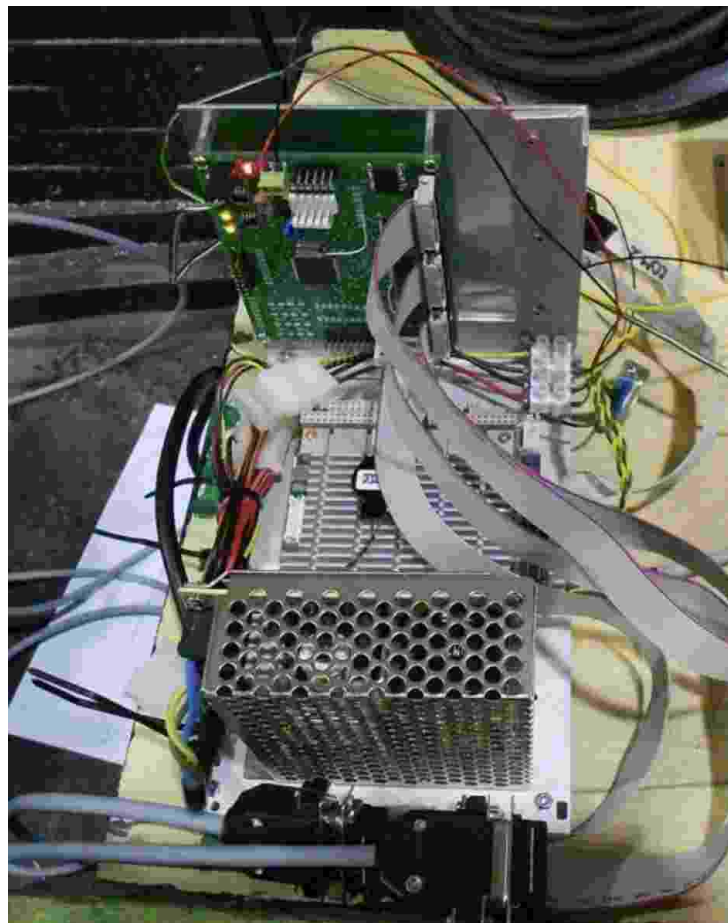


Figure C.2: Control computer with ACS

All actuators are equipped with the same motor units consisting of a Mitsubishi MR-3j series Digital Motor Controller (DMC) and an HF-MP series Motors (M). The thrusters' motors and their controller setup is shown in the Fig. C.3. The Mitsubishi controller allows a fully digital control of the motor revolutions and simultaneous recordings of the actual revolutions and reading their status, i.e. information about a possible fault in the propulsion unit. The revolutions are controlled with binary signals and communicate through RS422 serial interface. The orientation angle of the azimuth thrusters is controlled by a Stepper Motor Controller (SMC) 116-GP type.

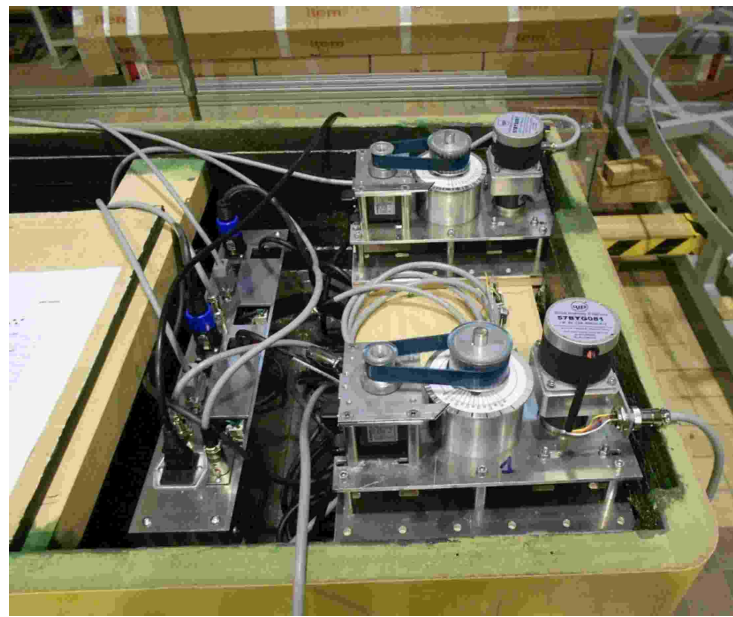


Figure C.3: Ship physical model stern view - stern azimuth thrusters  
motors and controllers

## C.2 Remaining results

In this section, footprints resulting from the model tests for all cases given in Tab. 7.1 are presented, except for three cases (21, 29, and 30) that were already given.

Coordinate system and model orientation shown on the plots correspond to the one adopted at the towing tank and to a test setup.

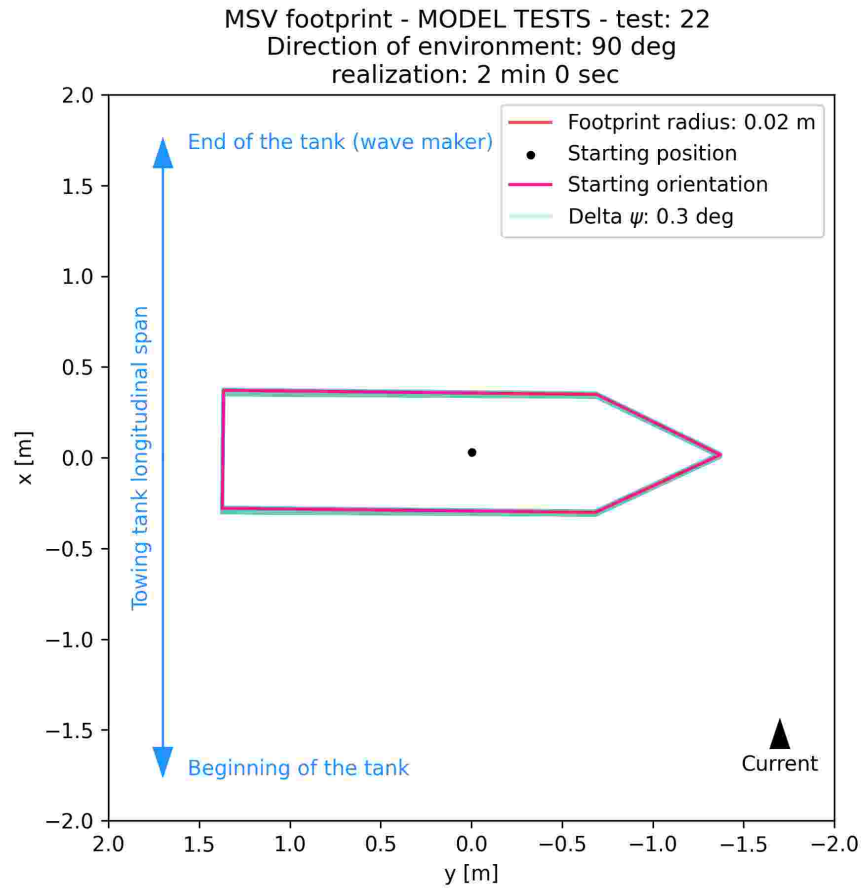


Figure C.4: Footprint of the physical ship model in dynamic positioning under environmental disturbances - test 22

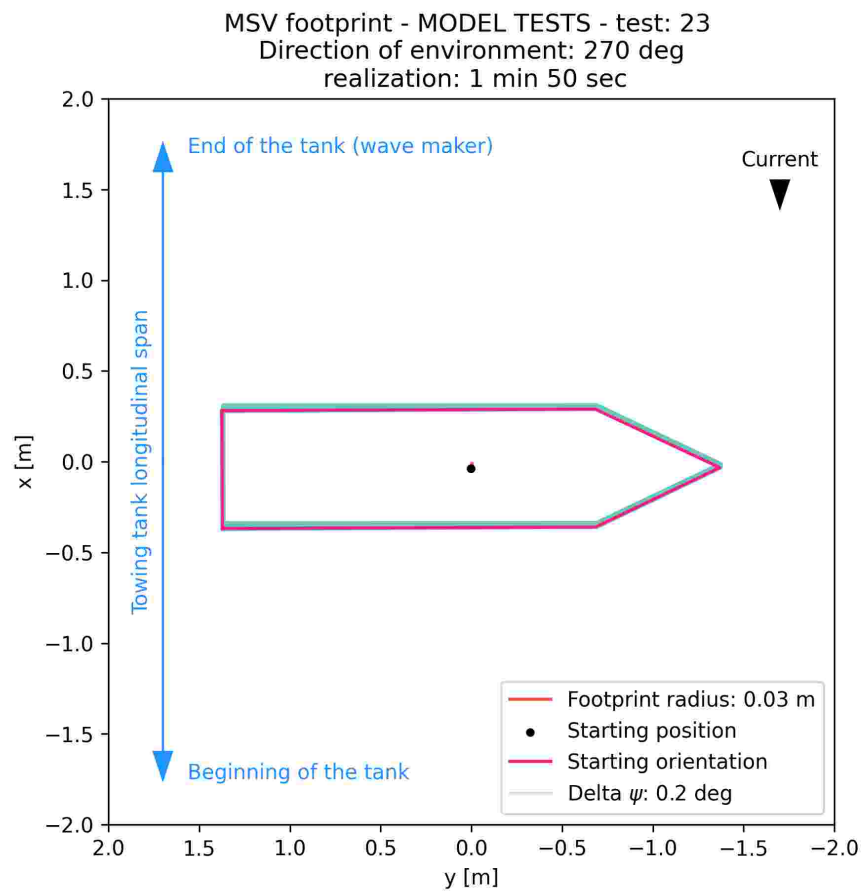


Figure C.5: Footprint of the physical ship model in dynamic positioning under environmental disturbances - test 23

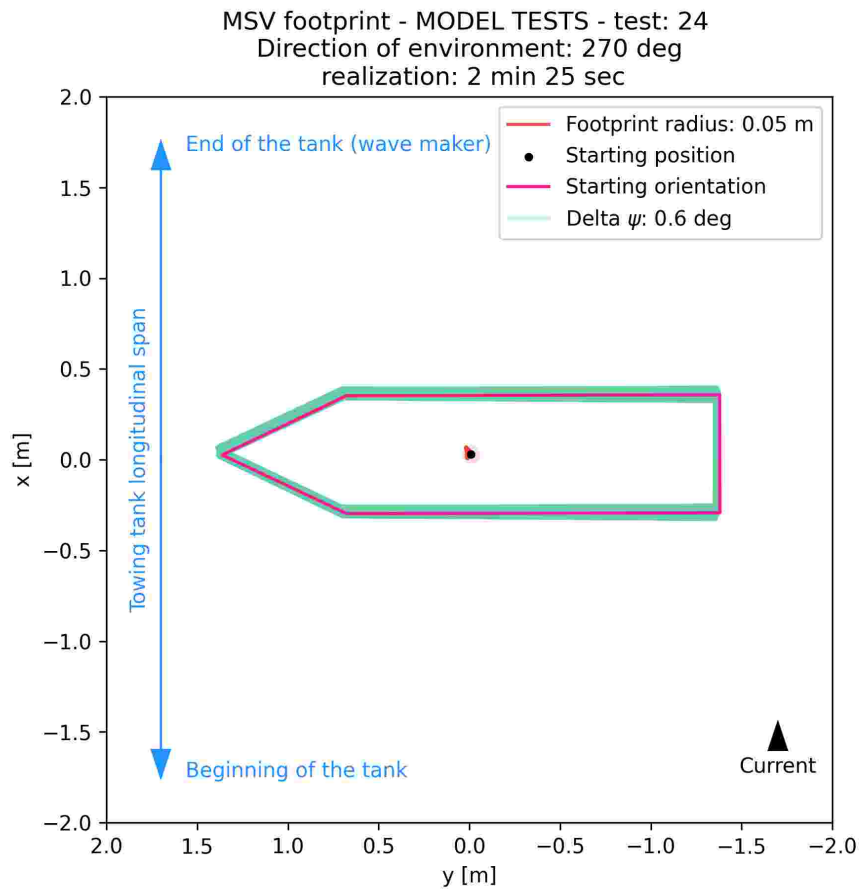


Figure C.6: Footprint of the physical ship model in dynamic positioning under environmental disturbances - test 24

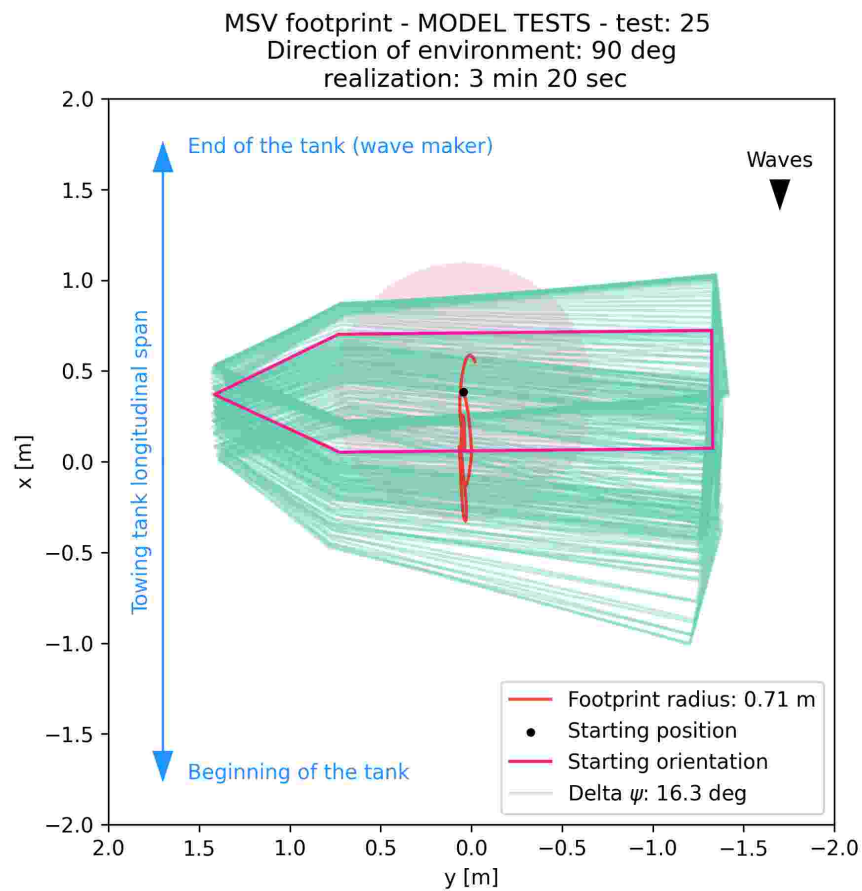


Figure C.7: Footprint of the physical ship model in dynamic positioning under environmental disturbances - test 25

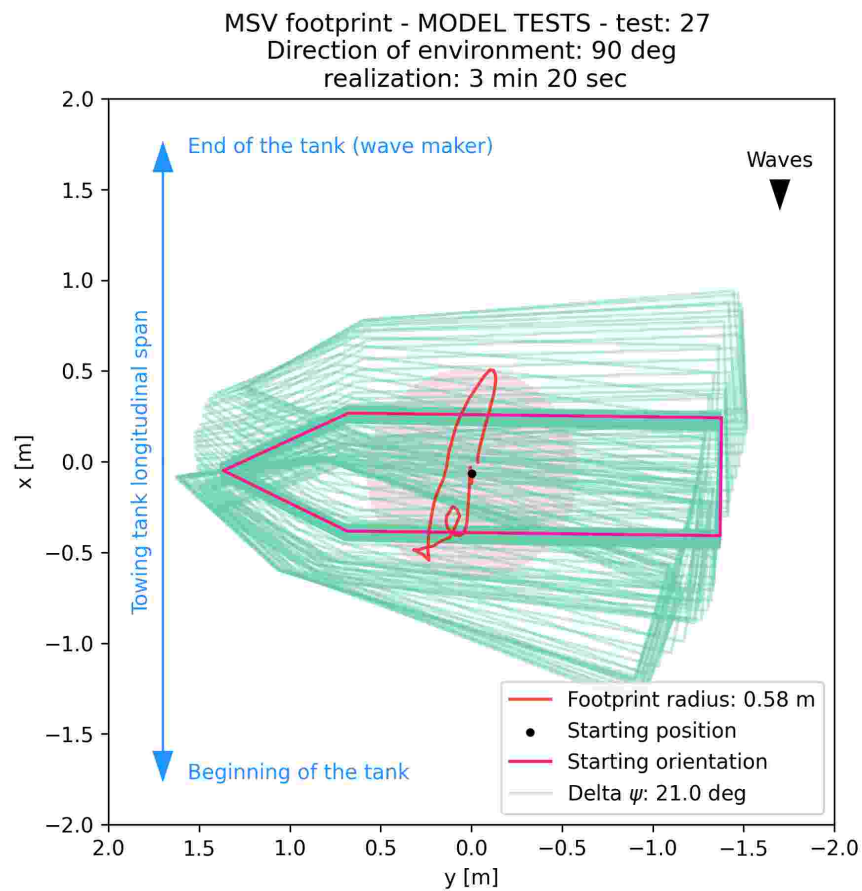


Figure C.8: Footprint of the physical ship model in dynamic positioning under environmental disturbances - test 27

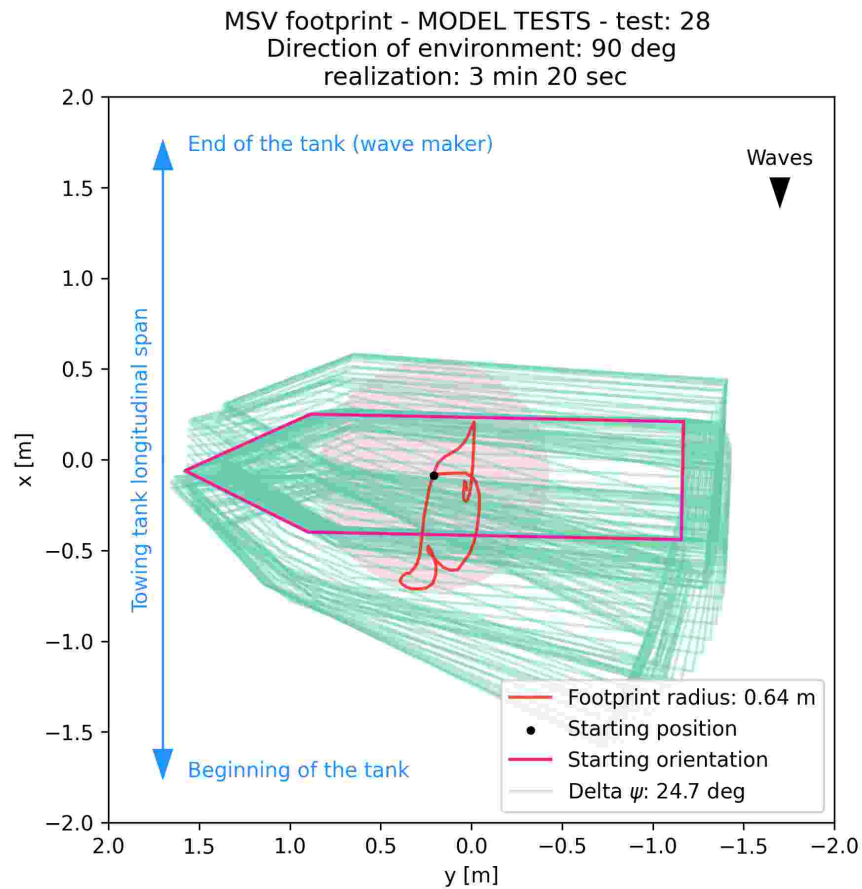


Figure C.9: Footprint of the physical ship model in dynamic positioning under environmental disturbances - test 28

# Bibliography

- ABS (2021). *Guide for Dynamic Positioning Systems*. American Bureau of Shipping.
- Alagili, O., Khan, M., Ahmed, S., Imtiaz, S., Zaman, M., and Islam, M. (2020). Performance assessment of DP control systems for different sea states. pages 1–6.
- Arditti, F., Souza, F., Martins, T., and Tannuri, E. (2015). Thrust allocation algorithm with efficiency function dependent on the azimuth angle of the actuators. *Ocean Engineering*, 105:206–216.
- Arditti, F. and Tannuri, E. A. (2012). Experimental analysis of a thrust allocation algorithm for DP systems considering the interference between thrusters and thruster-hull. *IFAC Proceedings Volumes*, 45(27):43–48. 9th IFAC Conference on Manoeuvring and Control of Marine Craft.
- Aydin, C., Ünal, U. O., and Sariöz, K. (2022). Computation of environmental loads towards an accurate dynamic positioning capability analysis. *Ocean Engineering*, 243:110201.
- Benham, F. A. (1997). *Prediction of wind and current loads on VLCC's*. Oilcompanies International Marine Forum, London, England.
- Blendermann, W. (1994). Parameter identification of wind loads on ships. *Journal of Wind Engineering and Industrial Aerodynamics*, 51(3):339–351.
- Bosland, R., Dijk, J., and Huijsmans, R. (2009). Numerical prediction of thruster-thruster interaction. In *ASME 2009 28th International Conference on Ocean, Offshore and Arctic Engineering*.

- Chen, Y., Bian, Y., Cui, Q., Dong, L., Xu, B., and Hu, M. (2021). LTVMPc for Dynamic Positioning of An Autonomous Underwater Vehicle. In *2021 5th CAA International Conference on Vehicular Control and Intelligence (CVCI)*, pages 1–5.
- Cheng, P., Zhang, C., Xie, W., Zhang, W., and He, S. (2023). Network-based adaptive multievent-triggered fuzzy dynamic positioning controller design for unmanned surface vehicles against denial-of-service attacks. *IEEE Transactions on Control of Network Systems*, 10(2):612–624.
- Dang, X.-K., Do, V.-D., and Nguyen, X.-P. (2020). Robust adaptive fuzzy control using genetic algorithm for dynamic positioning system. *IEEE Access*, 8:222077–222092.
- de Wit, C. (2009). Optimal thrust allocation methods for dynamic positioning of ships. Master’s thesis, Delft University of Technology.
- Deb, K., Pratap, A., Agarwal, S., and Meyarivan, T. (2002). A fast and elitist multiobjective genetic algorithm: Nsga-ii. *IEEE Transactions on Evolutionary Computation*, 6(2):182–197.
- Deng, F., Zhang, H., Ding, Q., Zhang, S., Du, Z., and Yang, H. (2024). PSO and nnpc-based integrative control allocation for dynamic positioning ships with thruster constraints. *Ocean Engineering*, 292:116553.
- Ding, F., Gao, P., Zhang, X., and Wang, Y. (2020). Thrust allocation of dynamic positioning based on improved differential evolution algorithm. In *2020 39th Chinese Control Conference (CCC)*, pages 1368–1373.
- Ding, F., Zhang, J., and Wang, Y. (2021). Fault grouping bias strategy of thrust allocation for dynamic positioning ship. In *2021 IEEE International Conference on Mechatronics and Automation (ICMA)*, pages 548–553.
- DNV (2010). *ENVIRONMENTAL CONDITIONS AND ENVIRONMENTAL LOADS*. Det Norske Veritas.
- DNV (2021). *DNV-ST-0111, Assessment of station keeping capability of dynamic positioning vessels*. Det Norske Veritas.
- Donnarumma, S., Figari, M., Martelli, M., Vignolo, S., and Viviani, M. (2018). Design and validation of dynamic positioning for marine systems: A case study. *IEEE Journal of Oceanic Engineering*, 43(3):677–688.

- el Moctar, O., Lantermann, U., and Chillcce, G. (2022). An efficient and accurate approach for zero-frequency added mass for maneuvering simulations in deep and shallow water. *Applied Ocean Research*, 126:103259.
- English, J. and Wise, D. (1975). *Hydrodynamic Aspects of Dynamic Positionin*. Oilcompanies International Marine Forum, London, England.
- Faltinsen, O. M. (1990). *Sea loads on ships and offshore structures*. Cambridge University Press Cambridge; New York.
- Fossen, T. (2002). *Marine Control Systems: Guidance, Navigation and Control of Ships, Rigs and Underwater Vehicles*. Marine Cybernetics AS, Trondheim.
- Fossen, T. I. (2021). *Handbook of Marine Craft Hydrodynamics and Motion Control*. John Wiley & Sons. Ltd., Chichester, UK, 2nd edition edition.
- Fossen, T. I. and Perez, T. (2009). Kalman filtering for positioning and heading control of ships and offshore rigs. *IEEE Control Systems Magazine*, 29(6):32–46.
- Fu, M., Wang, L., and Yu, L. (2019). A finite-time output feedback control scheme for dynamic positioning system of ships. *IEEE Access*, 7:100638–100648.
- Gao, D., Wang, X., Wang, T., Wang, Y., and Xu, X. (2019). Optimal thrust allocation strategy of electric propulsion ship based on improved non-dominated sorting genetic algorithm II. *IEEE Access*, 7:135247–135255.
- Goldfarb, D. and Idnani, A. (1983). A numerically stable dual method for solving strictly convex quadratic programs,. *Mathematical Programming*, 27:1–33.
- Hao, L.-Y., Wu, Z.-J., Shen, C., Cao, Y., and Wang, R.-Z. (2024). Tube-based model predictive control for constrained unmanned marine vehicles with thruster faults. *IEEE Transactions on Industrial Informatics*, 20(3):4606–4615.
- Hasan, S. M. U. (2018). A procedure for the dynamic positioning estimation in initial ship-design. Master’s thesis, University of Rostock.

- Ihle, I.-A., Skjetne, R., and Fossen, T. I. (2004). Nonlinear formation control of marine craft with experimental results. In *2004 43rd IEEE Conference on Decision and Control (CDC)(IEEE Cat. No. 04CH37601)*, volume 1, pages 680–685. IEEE.
- IMCA (2007). *IMCA M 103 Guidelines for the design and operation of dynamically positioned vessels*. International Marine Contractors Association.
- IMCA (2017). *IMCA M 140, Specification For DP Capability Plots*. International Marine Contractors Association.
- ITTC (2021). *ITTC Quality System Manual, Procedure, Propulsion/Bollard Pull Test*.
- Ji, D., Ogbonnaya, S. G., Hussain, A. F., Hussain, S., Ye, Z., and Wang, X. (2023). Utilizing Lyapunov-Based Model Predictive Control to Achieve Dynamic Positioning for the Haizhe Autonomous Underwater Vehicle. In *2023 2nd International Conference on Automation, Robotics and Computer Engineering (ICARCE)*, pages 1–5.
- Jiao, L. and Wang, X. (2024). Thrust allocation under ship failure based on improved drosophila algorithm. In *2024 5th International Conference on Computer Engineering and Application (ICCEA)*, pages 1607–1613.
- Johansen, T. and Fossen, T. (2013). Control allocation — A survey. *Automatica*, 49(5):1087–1103.
- Johansen, T., Fossen, T., and Berge, S. (2004). Constrained nonlinear control allocation with singularity avoidance using sequential quadratic programming. *IEEE Transactions on Control Systems Technology*, 12(1):211–216.
- Kalikatzarakis, M., Coraddu, A., Oneto, L., and Anguita, D. (2022). Optimizing fuel consumption in thrust allocation for marine dynamic positioning systems. *IEEE Transactions on Automation Science and Engineering*, 19(1):122–142.
- Koop, A., Cozijn, H., Schrijvers, P., and Vaz, G. (2017). Determining thruster-hull interaction for a Drill-Ship using CFD. In *Proceedings of the ASME 2017 36th International Conference on Ocean, Offshore and Arctic Engineering OMAE2017*.

- Kraskowski, M. and Grymajło, P. (2021). Development of the measurement stand for experimental model tests of the dynamically positioned vessels. In *Symposium proceedings*. International symposium of hydrodynamics in ship design, safety, manoeuvring and operation. 22nd HYDRONAV 2021.
- Li, W., Ren, Y., and Lin, S. (2020). Design of dynamic surface controller based on nonlinear observer for ship dynamic positioning system. In *2020 Chinese Automation Congress (CAC)*, pages 836–841.
- Li, W., Xie, H., Dan, Y., Meng, F., and Cui, J. (2024). Multi-thruster unmanned surface vehicle dynamic positioning control based on optimal active disturbance rejection control. In *2024 IEEE 25th China Conference on System Simulation Technology and its Application (CCSSTA)*, pages 47–52.
- Lindegaard, K.-P. (2003). *Acceleration Feedback in Dynamic Positioning*. PhD thesis, Faculty of Information Technology, Mathematics, and Electrical Engineering Department of Engineering Cybernetics, Norwegian University of Science and Technology.
- Liu, C. and Zhang, Y. (2020). Optimal constrained control allocation for multiple thrusters in dynamic positioning system. In *2020 39th Chinese Control Conference (CCC)*, pages 1402–1407.
- Liu, R., Yang, X., and Jia, Y. (2019). Design of nonlinear observer for ship dynamic positioning system. In *2019 IEEE 3rd Information Technology, Networking, Electronic and Automation Control Conference (ITNEC)*, pages 1339–1342.
- Liu, Y., Tuo, Y., Li, J., Wang, S., Gao, S., and Li, M. (2024). Anti-disturbance control for dynamic positioning of vessels based on interval type-2 fuzzy estimator. In *2024 43rd Chinese Control Conference (CCC)*, pages 2679–2684.
- Ljungberg, F., Rastegarpour, S., and Feyzmahdavian, H. R. (2024). Modified neural mpc with guaranteed constraints for dynamic positioning of marine vessels. In *2024 IEEE 29th International Conference on Emerging Technologies and Factory Automation (ETFA)*, pages 1–4.
- Lloyd, A. R. J. M. (1998). *Seakeeping Ship Behavior in Rough Weather*. ARMJ Lloyd.

- Lu, X., Chen, Y., Wang, X., and Zhao, J. (2021). A multi-agent distributed optimization method for thrust allocation. In *2021 China Automation Congress (CAC)*, pages 4725–4730.
- Maciel, P., Koop, A., and Vaz, G. (2013). Modelling thruster-hull interaction with cfd. In *Proceedings of the International Conference on Offshore Mechanics and Arctic Engineering - OMAE*, volume 7.
- Maliky, N., Subarkah, M., Putra, N., and Hidayat, S. (2020). Prediction of vessel dynamic model parameters using computational fluid dynamics simulation. *Advances in Science Technology and Engineering Systems Journal*, 5:926–936.
- Maliky, N. A., Teguh Subarkah, M., and Hidayat, S. (2019). Added mass and drag prediction using CFD fluent simulation for an autonomous barge parameters. In *2019 6th International Conference on Electric Vehicular Technology (ICEVT)*, pages 52–57.
- Martelli, M., Faggioni, N., and S., D. (2022). A time-domain methodology to assess the dynamic positioning performances. *Ocean Engineering*, 247(0029-8018):110668.
- Mauro, F. and Gaudiano, F. (2018). Station-keeping calculations in early design stage: Two possible approaches. In *Technology and Science for the Ships of the Future - Proceedings of NAV 2018*, pages 372 – 379. IOS Press.
- Mehrzadi, M., Terriche, Y., Su, C.-L., Othman, M. B., Vasquez, J. C., and Guerrero, J. M. (2020). Review of dynamic positioning control in maritime microgrid systems. *Energies*, 13(12):3188.
- Meng, Y., Zhang, X., and Zhang, X. (2023). Identification modeling of ship nonlinear motion based on nonlinear innovation. *Ocean Engineering*, 268:113471.
- Øveraas, H., Halvorsen, H. S., Landstad, O., Smånes, V., and Johansen, T. A. (2023). Dynamic positioning using model predictive control with short-term wave prediction. *IEEE Journal of Oceanic Engineering*, 48(4):1065–1077.
- Øvereng, S. S., Nguyen, D. T., and Hamre, G. (2021). Dynamic positioning using deep reinforcement learning. *Ocean Engineering*, 235:109433.

- Piekło, A., Hoffmann, P., Witkowska, A., and Zubowicz, T. (2023). Identification of ship's hull mathematical model with numerical methods. In *Proceedings of the XXI Polish Control Conference*, pages 327–337. Springer.
- Piekło, A., Hoffmann, P., Witkowska, A., and Zubowicz, T. (2024). Thrusters interactions in dynamic positioning operations with numerical methods. International Ocean and Polar Engineering Conference, pages ISOPE-I-24–584.
- Piekło, A., Witkowska, A., and Zubowicz, T. (2022). Power efficient thrust allocation algorithms in design of dynamically positioned ships.
- Piekło, A., Witkowska, A., and Zubowicz, T. (2023a). Dynamic positioning capability assessment based on optimal thrust allocation. *Polish Maritime Research*, 30(2):28–38.
- Piekło, A., Witkowska, A., and Zubowicz, T. (2023b). Dynamic positioning capability assessment for ship design purposes. In Kowalcuk, Z., editor, *Intelligent and Safe Computer Systems in Control and Diagnostics. 15th International Conference on Diagnostics of Processes and Systems, Poland, September 5-7, 2022*, volume 545, pages 386–397, Cham. Springer International Publishing.
- Qiu, C. (2022). Research on optimal design of ship power system based on PID control. In *2022 IEEE International Conference on Advances in Electrical Engineering and Computer Applications (AEECA)*, pages 1434–1439.
- Raghunathan, R. N., Skulstad, R., Li, G., and Zhang, H. (2023). Design of constraints for a neural network based thrust allocator for dynamic ship positioning. In *IECON 2023- 49th Annual Conference of the IEEE Industrial Electronics Society*, pages 1–6.
- Ruth, E. (2008). *Propulsion control and thrust allocation on marine vessels*. PhD thesis, Norwegian University of Science and Technology.
- Selimović, D., Lerga, J., Prpić-Oršić, J., and Kenji, S. (2020). Improving the performance of dynamic ship positioning systems: A review of filtering and estimation techniques. *Journal of marine science and engineering*, 8(4):234.

- Sen, D. T. and Vinh, T. C. (2016). Determination of added mass and inertia moment of marine ships moving in 6 degrees of freedom. *International Journal of Transportation Engineering and Technology*, 2:8–14.
- Serraris, J. W. and Cozijn, J. L. (2017). DP stationkeeping accuracy: a calculation approach, integration in DP plots and results of a case study. In *Dynamic Positioning Conference*.
- Skjetne, R. (2005). *The Maneuvering Problem*. PhD thesis, Faculty of Information Technology Mathematics, and Electrical Engineering, Department of Engineering Cybernetics, Norwegian University of Science and Technology.
- Skjetne, R., Smogeli, Ø., and Fossen, T. I. (2004). Modeling, identification, and adaptive maneuvering of CyberShip II: A complete design with experiments. In *IFAC Proceedings Volumes*, volume 37, pages 203–208. IFAC Conference on Computer Applications in Marine Systems - CAMS 2004, Ancona, Italy, 7-9 July 2004.
- Smierzchalski, R. (2016). The structure of the control system for a dynamically positioned ship. In *2016 21st International Conference on Methods and Models in Automation and Robotics (MMAR)*, pages 641–644.
- Suijkerbuijk, D. (2013). CFD analysis of transient behavior of azimuth thrusters.
- Syntakas, S. and Vlachos, K. (2023). Tube-based nonlinear MPC of an over-actuated marine platform for navigation and obstacle avoidance using control barrier functions. In *2023 31st Mediterranean Conference on Control and Automation (MED)*, pages 704–709.
- Tang, Z., He, H., Wang, L., and Wang, X. (2021). An optimal thrust allocation algorithm with bivariate thrust efficiency function considering hydrodynamic interactions. *Journal of Marine Science and Technology*, 27:52 – 66.
- Tomera, M. (2009). Model matematyczny statku Cybership II. *Scientific Journal of Gdynia Maritime University*, (62):2541–2486.
- Tomera, M. (2012). Dynamic positioning system design for "blue lady". simulation tests. *Polish Maritime Research*, 19:57–65.

- Tomera, M. (2014). Dynamic positioning system for a ship on harbour manoeuvring with different observers. experimental results. *Polish Maritime Research*, 21:13–24.
- Tuo, Y., Zhou, X., and Huang, W. (2021). Thrust allocation based on improved global artificial fish swarm algorithm for the dynamic positioning system of vessels. In *2021 6th International Conference on Automation, Control and Robotics Engineering (CACRE)*, pages 560–566.
- Valčić, M. (2020). *Optimization of thruster allocation for dynamically positioned marine vessels*. PhD thesis, University of Rijeka.
- van 't Klooster, S. J. B. (2018). How good is good enough in DP calculations? a case study into uncertainties involved in the DP capability prediction process. Master's thesis, Delft University of Technology.
- van 't Veer, R. and Gachet, M. (2011). Dynamic positioning - early design, capability and offsets, a novel approach. In *Proceedings of the ASME 2011 30th International Conference on Ocean, Offshore and Arctic Engineering*.
- Veksler, A., Johansen, T. A., Borrelli, F., and Realsen, B. (2016). Dynamic positioning with model predictive control. *IEEE Transactions on Control Systems Technology*, 24(4):1340–1353.
- Værnø, S. A., Skjetne, R., Kjerstad, Ø. K., and Calabrò, V. (2019). Comparison of control design models and observers for dynamic positioning of surface vessels. *Control Engineering Practice*, 85:235–245.
- Wang, A., Xin, M., Lang, X., Cai, M., Ji, W., and Liu, Y. (2024). Dynamic Sliding Mode-based Fault-Tolerant Control for Ship Dynamic Positioning Based on T-S Fuzzy Piecewise Affine Models. In *2024 39th Youth Academic Annual Conference of Chinese Association of Automation (YAC)*, pages 2227–2232.
- Wang, L., Yang, J.-m., and Xu, S.-w. (2018). Dynamic positioning capability analysis for marine vessels based on a dpcap polar plot program. *China Ocean Engineering*, 32(1):2191–8945.
- Wang, W. and Wei, Y. (2021). Research on thrust allocation method of semi-submersible drilling platform based on improved cuckoo search algorithm. In *2021 IEEE 5th Advanced Information Technology, Electronic and Automation Control Conference (IAEAC)*, volume 5, pages 349–356.

- Wang, Y., Jiang, B., Wu, Z.-G., Xie, S., and Peng, Y. (2021). Adaptive sliding mode fault-tolerant fuzzy tracking control with application to unmanned marine vehicles. *IEEE Transactions on Systems, Man, and Cybernetics: Systems*, 51(11):6691–6700.
- Wei, Z., He, Z., Sun, B., and Su, Y. (2024). Research on thrust allocation for power positioning system based on improved sparrow search algorithm with multi-strategy fusion. *IEEE Access*, 12:148434–148449.
- Wen, W., Qu, Y., and Liu, Z. (2023). Wave-filtering observer design in station-keeping control for dynamic positioning ships. In *2023 IEEE 6th International Conference on Automation, Electronics and Electrical Engineering (AUTEEE)*, pages 201–205.
- White, F. M. (2011). *Fluid Mechanics*. McGraw-Hill, New York.
- Witkowska, A., Armiński, K., Zubowicz, T., Ossowski, F., and Śmierzchalski, R. (2020). Autonomous ship utility model parameter estimation utilising Extended Kalman Filter. In Bartoszewicz, A., Kabziński, J., and Kacprzyk, J., editors, *Advanced, Contemporary Control*, pages 1531–1542, Cham. Springer International Publishing.
- Wondergem, M., Lefeber, E., Pettersen, K., and Nijmeijer, H. (2011). Output feedback tracking of ships. 19:442–448.
- Wu, D., Ren, F., and Zhang, W. (2016). An energy optimal thrust allocation method for the marine dynamic positioning system based on adaptive hybrid artificial bee colony algorithm. *Ocean Engineering*, 118:216–226.
- Xia, G., Liu, J., Pang, C., and Xue, J. (2015). Constrained model predictive control design for dynamic positioning of a supply ship. In *OCEANS 2015-MTS/IEEE Washington*, pages 1–6. IEEE.
- Xia, G., Sun, C., Zhao, B., Xue, J., and Xia, X. (2019a). Observer-Based Control for Dynamic Positioning Ships with Input Delay. In *OCEANS 2019 - Marseille*, pages 1–5.
- Xia, G., Sun, X., Zhao, B., and yang, Y. (2019b). Thrust allocation for dynamic positioning vessels with switchboard power limit and diving forbidden sectors. In *2019 Chinese Automation Congress (CAC)*, pages 2677–2682.

- Ya-nan, S., Rong-hua, X., Qin-ruo, W., and Zi-yin, S. (2020). Study on stochastic nonlinear observer in ship dynamic positioning system. In *2020 39th Chinese Control Conference (CCC)*, pages 916–920.
- Yan, X., Chen, C., and Fan, T. (2018). Effects of different wave spectra on dynamic positioning accuracy. *Brodogradnja*, 69:83–92.
- Yang, X., Liu, R., and Guo, L. (2019). A robust sliding mode observer for dynamic positioning system. In *2019 IEEE 3rd Advanced Information Management, Communicates, Electronic and Automation Control Conference (IMCEC)*, pages 85–90.
- Yu, Z. and Du, J. (2024). Nonlinear model predictive dynamic positioning control with nonlinear thrust allocation for fully actuated vessels under thruster magnitude and rate saturations. In *2024 14th Asian Control Conference (ASCC)*, pages 01–06.
- Zalewski, P. (2016). Convex optimization of thrust allocation in a dynamic positioning system. *Sci. J. Mar. Univ. Szczecin* 48(120), 10.17402/176:58–62.
- Zalewski, P. (2017). Constraints in allocation of thrusters in a dp simulator. *Sci. J. Mar. Univ. Szczecin* 52(124), 10.17402/244:40–50.
- Zaman, M. B., Kusuma, I. R., Katilik, A. C., Semin, and Santoso, A. (2019). Design of ship model dynamic positioning system using pid-based microcontroller. In *2019 IEEE Asia-Pacific Conference on Geoscience, Electronics and Remote Sensing Technology (AGERS)*, pages 49–56.
- Zhang, Q. and Jaiman, R. K. (2019). Numerical analysis on the wake dynamics of a ducted propeller. *Ocean Engineering*, 171:202–224.
- Zhang, X. and Xu, Z. (2020). A nonlinear observer for ship dynamic positioning system. In *2020 Chinese Automation Congress (CAC)*, pages 3878–3883.
- Zhao, L. and Roh, M.-I. (2015). A Thrust Allocation Method for Efficient Dynamic Positioning of a Semisubmersible Drilling Rig Based on the Hybrid Optimization Algorithm. *Mathematical Problems in Engineering*, 2015:1–12.

Zheng, M., Yang, S., and Li, L. (2020). Stability Analysis and T-S Fuzzy Dynamic Positioning Controller Design for Autonomous Surface Vehicles Based on Sampled-Data Control. *IEEE Access*, 8:148193–148202.

Zhou, B. and Zhao, M. (2020). Numerical simulation of thruster-thruster interaction for rov with vector layout propulsion system. *Ocean Engineering*, 210:107542.